

**Deanship of Graduate Studies
Al- Quds University**

**A comparison Study between the Observations and the
Simulation Results of Barghouthi Model for O^+ and H^+
Outflows in the Polar Wind**

Sharif Hasan Mahmoud Ghithan

M.Sc. Thesis

Jerusalem-Palestine

1430 / 2009

A comparison Study between the Observations and the
Simulation Results of Barghouthi Model for O^+ and H^+
Outflows in the Polar Wind

Prepared By:
Sharif Hasan Mahmoud Ghithan

B.Sc. physics from Birzeit University, Palestine

Supervisor: Prof. Imad A. Barghouthi

A thesis Submitted in Partial Fulfillment of Requirement for
the Degree of Master of Science in Physics
Department/Physics Master
Faculty of Science/Al- Quds University

1430 / 2009

Al- Quds University
Deanship of Graduate Studies
M. Sc. Physics / Physics Department

Thesis Approval

A comparison Study between the Observations and the Simulation Results of
Barghouthi Model for O^+ and H^+ Outflows in the Polar Wind

Prepared By: Sharif Hasan Mahmoud Ghithan
Registration No: 20611290

Supervisor: Prof. Imad A. Barghouthi

Master thesis submitted and accepted, Date: 28.4.2009

The names and signatures of the examining committee members are as follows:

| | |
|---|----------------|
| 1- Head of committee: Prof.: Imad A. Barghouthi | Signature----- |
| 2- Internal Examiner: Dr.: Khawla Qamhieh | Signature----- |
| 3- External Examiner: Dr.: Abdel-Rahman M. Abu-labdeh | Signature----- |

Jerusalem-Palestine

1430 / 2009

Dedication

I wish to dedicate this thesis to
My Family, for encouragement and trust

Sharif Hasan Mahmoud Ghithan

Declaration

I certify that this thesis submitted for the degree of Master of Science of physics, is the result of my own research, except where otherwise acknowledged, and that this thesis (or any part of the same) has not been submitted for a higher degree to any other university or institution.

Signed:.....

Sharif Hasan Mahmoud Ghithan

Date: 28.4.2009

Mobile: +972598599159

Email: Ghithan53@yahoo.com

Acknowledgements

After thanking God the Merciful the Graceful, who granted me the capability to complete this study, I would like to present my warm appreciation and thanks for every person, who assisted me to accomplish this work: my research advisor, Prof. Imad A. Barghouthi for his guidance and patience to empower me with vital skills, and continuous support through all stages of this study. Staff of physics department, who afford all necessary facilities. Mr. Samer Hajiji for his help and unlimited assistance through this work. Mr. Sae'd Shahin for his help and encouragement. Family members, who tolerated my absence from the family activities and they supported and encouraged during my graduate work, my mother, father, brothers, and sisters Mahmoud, Mohammed, Shereen, Shadia, Nadia, Khadiga, Fadia, and Fida'a. Also my heart prays humbly to God to bless my grandmother.

Last, but not least, my deep thanks go to those helping me directly and indirectly from my friends and colleagues during my work in this thesis.

Abstract

The continuous outflow of thermal plasma escaping from the polar ionosphere at high latitudes to the magnetosphere along "open" geomagnetic field lines is called the polar wind, [Axford, 1968]. This plays an important role in the ionosphere-magnetosphere coupling.

The heating of ions (i.e., acceleration of ions, which means, increases of velocity with altitude), owing to the interaction with electromagnetic turbulence (i.e., wave particle interactions), plays an important role in the outflow of the polar wind ions (i.e., O^+ and H^+) in the polar wind region. The effect of wave particle interaction (WPI) on H^+ and O^+ ions outflows in the polar wind region were investigated by using Monte Carlo Simulation.

The Monte Carlo simulation is a simple concept, goes straight forward algorithms, and was developed to include the effects of altitude and velocity dependent wave particle interactions, gravitational force, polarization electrostatic field, and the divergence geomagnetic field, within the simulation tube (1.7 to 13.7 R_E).

As a result of the effect WPI (i.e. the perpendicular heating), the temperature anisotropy ($T_{\perp} / T_{\parallel}$) for H^+ ions is reduced at low altitudes, but it is reversed ($T_{\perp}(H^+) > T_{\parallel}(H^+)$) at higher altitudes. On the other hand, the temperature anisotropy ($T_{\perp} / T_{\parallel}$) for O^+ ions increases with altitude at low altitude and at high altitude its average value is (~ 53), where ($T_{\perp}(O^+) > T_{\parallel}(O^+)$) for all altitudes, where the perpendicular heating makes the O^+ and H^+ velocity distribution functions developed a conic shape at high altitudes.

When an ion is heated and moves upward along the geomagnetic field lines, the Larmor radius (a_L) of that ion increases and it may become comparable to or greater than the wavelength electromagnetic turbulence (λ_{\perp}), then the ratio (a_L / λ_{\perp}) exceeds unity, therefore, the perpendicular diffusion coefficient (D_{\perp}) becomes velocity dependent, consequently, the heating of the ions becomes self-limiting and the velocity distribution function of ions exhibits toroidal features. This result is consistent with the observation of both H^+ and O^+ toroidal distributions at high altitudes. The toroidal features of O^+ ions

appear at lower altitudes compared with H^+ ions (i.e. the saturation point of H^+ ions occurred at higher altitudes than those for O^+ ions).

The most important result in this study is that, the wavelength of the electromagnetic turbulence equal 8km, (i.e., $\lambda_{\perp} = 8km$), since the simulation results of Barghouthi model represent the closest results to the observations, which obtained from different satellites.

Finally, we can conclude that Barghouthi model is an excellent model in the polar wind region, since it produce acceptable simulation results when compared quantitatively and qualitatively to the corresponding observations. This close agreement between the simulation results and observations provides evidence that Barghouthi model described in this thesis is appropriate to be used, when modeling the heating of ions through the wave particle interaction in the polar wind region.

Table of Contents

| Content Title | Page |
|---|-----------|
| DECLARATION..... | i |
| ADNOWLEDGEMENTS..... | ii |
| ABSTRAC..... | iii |
| TABLE OF CONTENTS..... | v |
| LIST OF TABLES..... | vii |
| LIST OF FIGURES..... | viii |
| LIST OF PHOTOS..... | xi |
| LIST OF APPENDICES..... | xii |
| LIST OF ABBREVIATIONS..... | xiii |
| CHAPTER ONE: Introduction..... | 1 |
| 1.1 Introduction..... | 1 |
| 1.2 The polar wind..... | 3 |
| 1.3 The sources of the polar wind..... | 9 |
| 1.4 Statement of the problem..... | 18 |
| CHAPTER TWO: Theoretical Formulations..... | 19 |
| 2.1 Boltzmann Equation..... | 19 |
| 2.2 Wave Particle Interaction (WPI)..... | 22 |
| 2.3 Barghouthi model..... | 26 |
| 2.4 Monte Carlo method (MC method)..... | 27 |
| CHAPTER THREE: The Results..... | 32 |
| 3.1 Introduction..... | 32 |
| 3.2 O ⁺ ions..... | 33 |
| 3.3 H ⁺ ions..... | 40 |

| | |
|---|-----------|
| | |
| CHAPTER FOUR: Quantitative comparison..... | 48 |
| 4.1 Introduction..... | 48 |
| 4.2 Quantitative comparison..... | 50 |
| CHAPTER FIVE: Qualitative comparison..... | 59 |
| 5.1 Qualitative comparison..... | 59 |
| 5.2 Summary and conclusion..... | 82 |
| REFERENCES..... | 86 |
| APPENDICES..... | 93 |
| ARABIC ABSRTAC..... | 109 |

List of Tables

| Table Title | Page |
|-------------|------|
|-------------|------|

| | |
|---|----|
| Table 4.1: summarizes the properties of some polar wind satellites..... | 49 |
| Table 4.2: Comparison between the observations and simulation results of Barghouthi model for H^+ ions..... | 57 |
| Table 4.3: Comparison between the observations and simulation results of Barghouthi model for O^+ ions..... | 58 |
| Table 5.1-A: Barghouthi Model Predictions and Experimental Verification..... | 74 |
| Table 5.1-B: Barghouthi Model Predictions and Experimental Verification..... | 75 |
| Table 5.1-C: Barghouthi Model Predictions and Experimental Verification..... | 76 |
| Table 5.1-D: Barghouthi Model Predictions and Experimental Verification..... | 77 |
| Table 5.1-E: Barghouthi Model Predictions and Experimental Verification..... | 78 |
| Table 5.1-F: Barghouthi Model Predictions and Experimental Verification..... | 79 |
| Table 5.2-A: Barghouthi Model Predictions and simulation results Verification..... | 80 |
| Table 5.2-B: Barghouthi Model Predictions and simulation results Verification..... | 81 |

List of Figures

Figure Title

Page

| | |
|---|----|
| Figure 1.1: The shape of geomagnetic field lines that is compressed from the sun side and elongated from the opposite side because of solar wind outflow..... | 3 |
| Figure 1.2: Schematic diagram of polar wind flow in the polar cap in the northern hemisphere..... | 4 |
| Figure 1.3: Solar wind enters the atmosphere according the polar Funnel Region..... | 5 |
| Figure 1.4: The interaction of electrons from the sun with earth's magnetic shield cause the beautiful auroras we see in the sky..... | 6 |
| Figure 1.5: Schematic diagram of polar wind flow in the polar ionosphere..... | 7 |
| Figure 1.6: A schematic diagram for the different regions of the ion flow along diverging geomagnetic field lines, and the transition region embedded in between Barosphere and Exosphere..... | 9 |
| Figure 1.7: The orbit of the DE-1, it gives excellent coverage of the polar cap, the auroral field lines and the equatorial region at radial distances extending out to $4.65R_E$ | 11 |
| Figure 2.1: Schematic diagram showing the causes of ion outflow from the Earths ionosphere..... | 24 |
| Figure 2.2: Schematic diagram that illustrates the gyrating motion of a single ion across electromagnetic turbulence perpendicular to the geomagnetic field..... | 27 |
| Figure 2.3: A schematic representation of the model considered by the Monte Carlo method..... | 29 |
| Figure 3.1: O^+ ions velocity distribution functions at different geocentric distances (1.71, 4.27, 5.29, 5.97, 6.66, 7.0, 7.34 and $8.69R_E$) for different electromagnetic turbulence wavelengths (λ_{\perp})..... | 34 |
| Figure 3.2: Altitude profiles of the lower order O^+ moment for different | |

| | |
|--|----|
| electromagnetic turbulence wavelengths (λ_{\perp})..... | 37 |
| Figure 3.3: H^+ ions velocity distribution functions at different geocentric distances (1.7, 5.29, 8.19, 9.39, 11.1, 12.8, and 13.7 R_E) for different electromagnetic turbulence wavelengths (λ_{\perp})..... | 42 |
| Figure 3.4: Altitude profiles of the lower order H^+ moment for different electromagnetic turbulence wavelengths (λ_{\perp})..... | 44 |
| Figure 4.1: Altitude profiles of the lower order moment for the electromagnetic turbulence wavelength ($\lambda_{\perp} = 8km$), for O^+ ions (solid line) and H^+ ions (dashed line)..... | 53 |
| Figure 4.2: Altitude profile of ions temperatures, for O^+ ions (solid line) and H^+ ions (dashed line), according to Barghouthi model and for the electromagnetic turbulence wavelength ($\lambda_{\perp} = 8km$)..... | 54 |
| Figure 4.3: Altitude profile of ions velocity, for O^+ ions (solid line) and H^+ ions (dashed line), according to Barghouthi model and for the electromagnetic turbulence wavelength ($\lambda_{\perp} = 8km$)..... | 55 |
| Figure 4.4: Altitude profile of ions parallel velocity, for O^+ ions (solid line) and H^+ ions (dashed line), according to Barghouthi model and for the electromagnetic turbulence wavelength ($\lambda_{\perp} = 8km$)..... | 56 |
| Figure 5.1: Altitude profile of ions potential energy (ϕ) due to the body force, for O^+ ions (solid line) and H^+ ions (dashed line), according to Barghouthi model..... | 60 |
| Figure 5.2: Altitude profile of ions temperature anisotropy ($T_{\perp} / T_{\parallel}$), for O^+ ions (solid line) and H^+ ions (dashed line), according to Barghouthi model..... | 60 |
| Figure 5.3: Altitude profile of ions temperature anisotropy ($T_{\parallel} / T_{\perp}$), for O^+ ions (solid line) and H^+ ions (dashed line), according to Barghouthi model..... | 61 |
| Figure 5.4: Altitude profile of ions energy, for O^+ ions (solid line) and H^+ ions (dashed line), according to Barghouthi model..... | 62 |
| Figure C.1: Spiral motion of a charged particle in a uniform magnetic field..... | 96 |

| | |
|---|-----|
| Figure C.2: Magnetic bottles for plasma particles..... | 97 |
| Figure E.1: The ratio (R) given in equation (E.1) versus the argument ($k_{\perp} v_{\perp} / \Omega_i$) | 101 |

List of Photos

| Photo Title | Page |
|---|-------------|
| <hr/> | |
| Photo 1.1: A view of the entire auroral oval taken by satellite on October 2007 from high above the North Polar Region..... | 1 |

List of Appendices

| Appendix Title | Page |
|--|------|
| Appendix A: Gravitational Force..... | 93 |
| Appendix B: Polarization Electrostatic Field..... | 94 |
| Appendix C: Charged Particles in a Magnetic Field..... | 95 |
| Appendix D: Wave Particle Interaction (WPI)..... | 97 |
| Appendix E: Barghouthi model..... | 99 |
| Appendix F: Monte Carlo method..... | 101 |
| F.1 Generation of ions velocity..... | 101 |
| F.2 Generation of $v_{\perp s}$ | 102 |
| F.3 Generation of $v_{\parallel s}$ | 103 |
| F.4 Distribution Function..... | 104 |
| F.5 Moments of the distribution function..... | 106 |
| F.5.1. Density..... | 106 |
| F.5.2. Drift velocity..... | 107 |
| F.5.3. Perpendicular temperature..... | 107 |
| F.5.4. Parallel temperature..... | 108 |

List of Abbreviations

- ❖ **DE-1**: Dynamic Explorer 1 satellite.
- ❖ **Fig.** : Figure.
- ❖ **MC**: Monte Carlo.
- ❖ **PW**: Polar wind.
- ❖ **PWI**: Plasma Wave Instrument.
- ❖ **WPI**: Wave Particle Interaction.

Chapter One

Introduction

1.1 Introduction

The polar wind is an ambipolar outflow of thermal plasma (i.e. mainly H^+ , O^+ , He^+ ions, and electrons) from the terrestrial ionosphere at high latitudes to the magnetosphere along the magnetic field lines of the Earth. The polar wind occurs inside the region of aurora ovals; which is a beautiful natural phenomenon, occurs most often in the polar region of the Earth, in the form of majestic, colorful, and irregular lights in the night sky, as shown in photo (1.1).

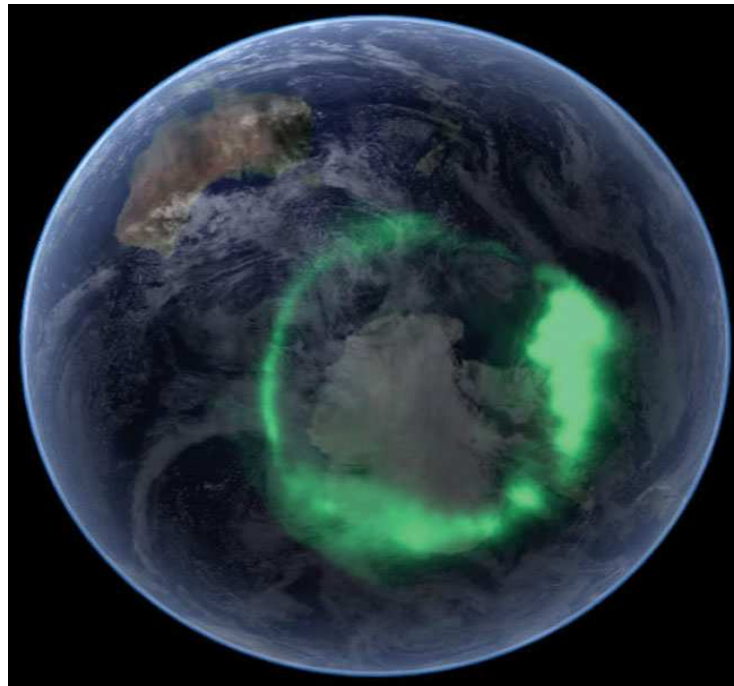


Photo 1.1: A view of the entire auroral oval taken by satellite on October 2007 from high above the North Polar Region.

<http://earthobservatory.nasa.gov/IOTD/view.php?id=6226> (9/11/2008)

The Aurora oval takes a shape in the form of rough ring, whose radius about (2252.6 - 2494km) around the Earth's magnetic poles. In addition, the ring generally located between 65 and 75 degrees latitude in both poles of the Earth and its height from the surface of the Earth is about 96.5 km. However, the aurora can occur in both poles of the earth; the aurora that occurs in the northern pole is named Aurora Borealis but the aurora that occurs in the southern pole is named Aurora Australis.

[Axford, 1968], coined the term "polar wind" to describe the continuous flow of thermal plasma escaping from the polar ionosphere at high latitudes to the magnetosphere along "open" geomagnetic field lines (i.e. the supersonic nature of thermal plasma expansion and outflows), in analogy to the supersonic expansion of the solar wind from the sun. As the polar wind expansion and flows, it undergoes four major transitions: from chemical to diffusion dominance, from subsonic to supersonic, from collision-dominated to collisionless regimes, and transition from heavy to light ions. Also, the polar wind plasma outflows change with geomagnetic activity, seasons, and solar cycles.

The cloud of gas and suspended solids extending from the Earth surface out many thousands of kilometers is called the atmosphere of the Earth, which is varied in density and composition as altitude increases above the surface of the Earth. On the other hand, the name of the layer of the Earth's atmosphere, above around 80km that is ionized by solar radiation, is called the ionosphere, which is a mixture of charged particles (i.e. ions and electrons). The ionosphere considers the main source of the plasma (i.e. ions, electrons, and neutral atoms) which is supplied to the magnetosphere of the Earth, [Shelley et al., 1972].

The magnetosphere is the region surrounding the Earth where the geomagnetic field is stronger than the interplanetary field, and in which appears the effect of the geomagnetic force on the ions and electrons. The magnetosphere is a dynamic region of flowing plasma controlled by the geomagnetic field, and it is contain cold plasma from the Earth's ionosphere and hot plasma from solar wind, which comes from the sun. The Earth's magnetic field extends far out into space for thousands of kilometers and it is like a dipole magnet near the surface of the Earth.

1.2 The polar wind

The Earth is one of the planets that have a strong magnetic field. To describe the shape of the Earth magnetosphere, we must first discuss phenomena caused by the sun. The sun emits charged particles continuously from its extremely hot atmosphere. These charged particles are mostly electrons and protons, that are produced from the thermonuclear reactions inside the sun. Solar streams radiate into space in all directions at high speed, and pull the sun magnetic field with it. The energetic particles and the sun magnetic field that they pull into space are called the solar wind. The solar wind spreads in all directions in the space around the sun at velocities of 450 km/s or more, and collides with the planets, comets, moons, etc.

The magnetosphere is the place of dynamic interactions between the solar wind and the Earth plasma. The solar wind plays an important role in the shape of the magnetosphere. Therefore, the magnetic field lines of the Earth that are facing the sun (sunward side) will be compressed. On the other hand, the magnetic field lines on the opposite direction (anti sunward side) will be dragged "elongated" into a magnetotail. The shape of the magnetosphere is illustrated in Fig.(1.1).

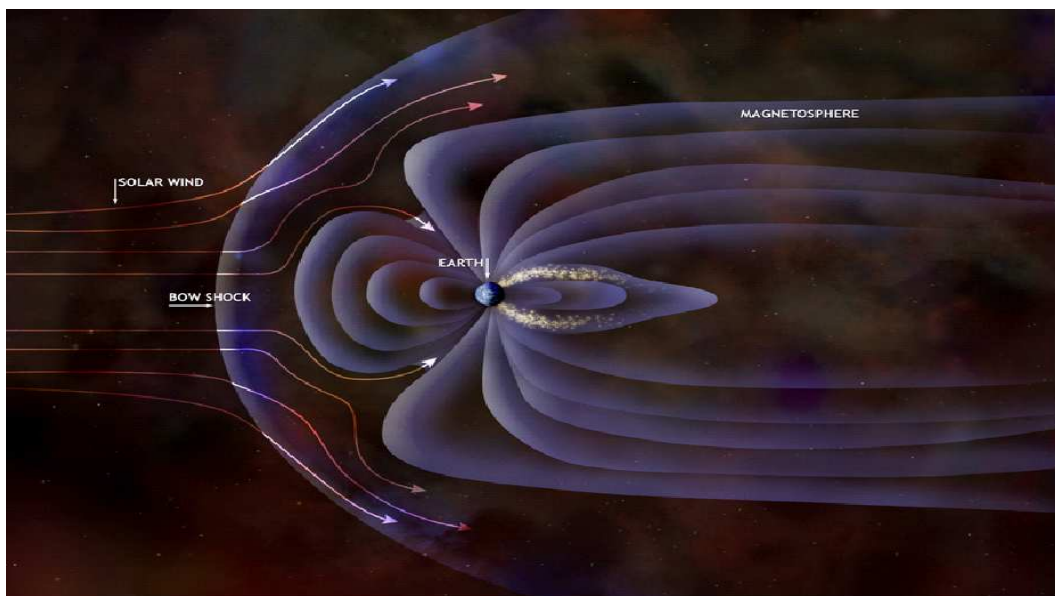


Figure 1.1: The shape of geomagnetic field lines that is compressed from the sun side and elongated from the opposite side because of solar wind outflow.

http://chandra.harvard.edu/photo/2005/earth/earth_mag_auro_illustration_label.jpg
(15/10/2008)

The magnetopause is the boundary between the confined planetary magnetic field and the solar wind plasma in the magnetosheath. The long tail-like structure on the anti sunward side seen in Fig.(1.1) allows thermal plasma (O^+ , H^+ , He^+ ions, and electrons) to escape along these fields lines in the tail, since the pressure in the ionosphere is much greater than that in the magnetospheric tail, [Dessler and Michel,1966; Bauter,1966]. This continuous outflow of thermal plasma escaping from the polar ionosphere to the magnetosphere along open (more generally tail-like) magnetic field lines is called the polar wind, [Axford, 1968], as shown in Fig.(1.2).

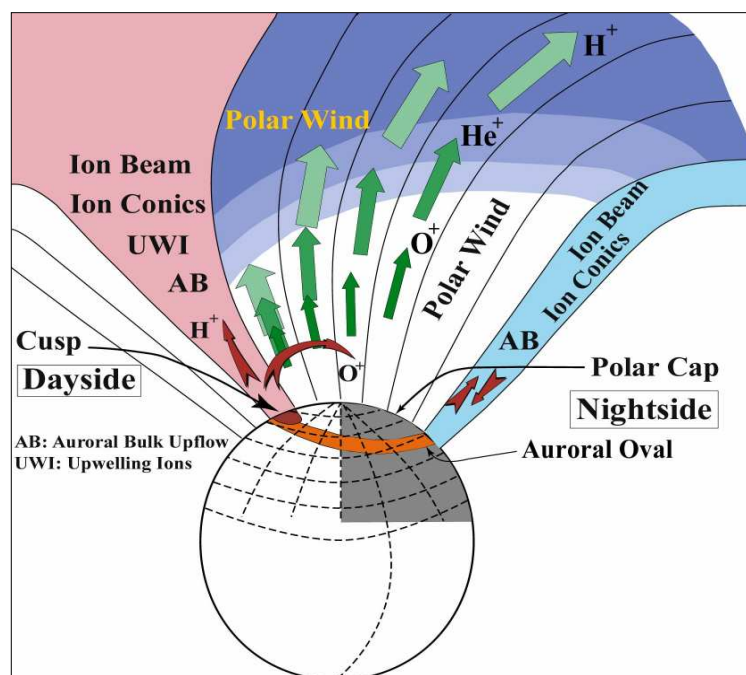


Figure (1.2): Schematic diagram of polar wind flow in the polar cap in the northern hemisphere.

<http://ssdoo.gsfc.nasa.gov/education/lectures/fig12.gif> (12/4/2008)

When the charged particles of the solar wind approach to the Earth's magnetic field, they are forced to change their path, and begin a spiral motion along the magnetic field lines. Therefore, this spiral motion leads the charged particles to the northern and southern hemisphere of the Earth. At this region the Earth's magnetic field lines converge to form a shape of magnetic tube, which is called Polar Funnel. Therefore, the trapped charged

particles can be channeled into the polar funnel, and then enter the upper atmosphere of the earth as shown in Fig.(1.3).

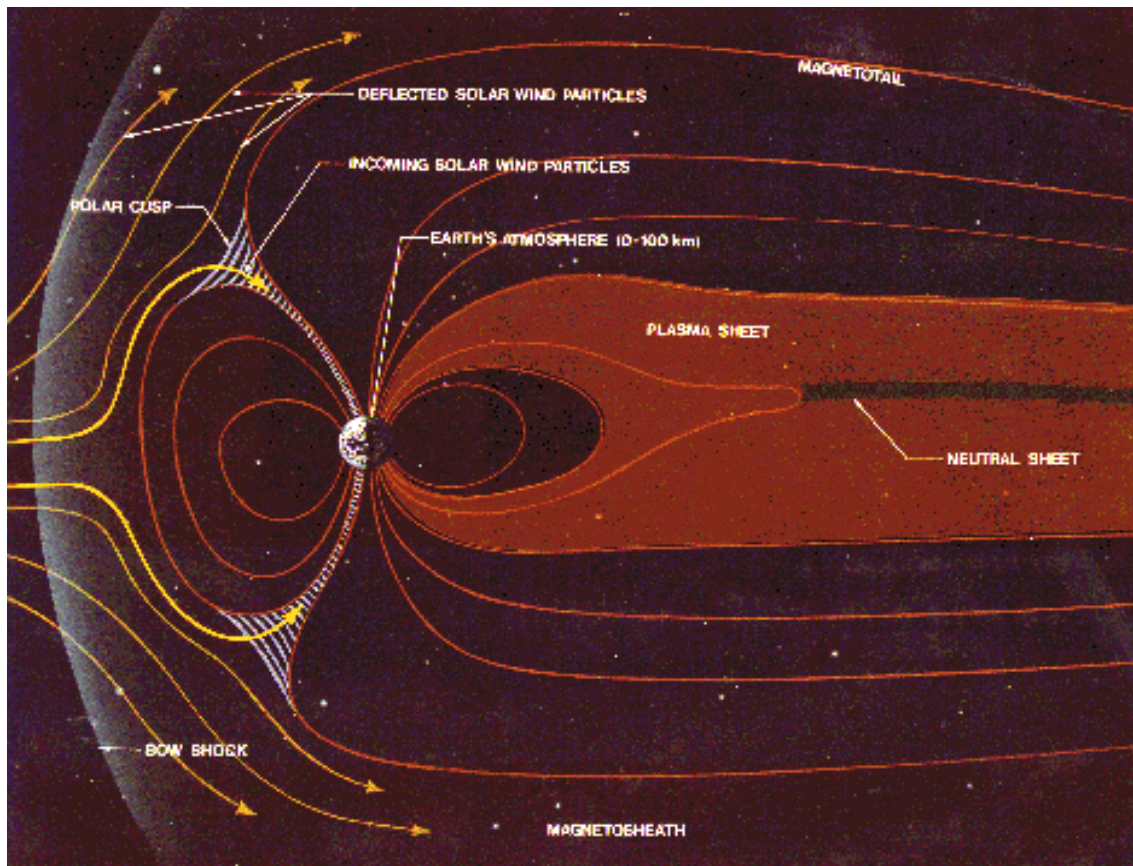


Figure 1.3: Solar wind enters the atmosphere according the polar funnel Region.
http://en.wikipedia.org/wiki/Image:Magnetosphere_schematic.jpg (5/3/2008)

Solar wind has a large kinetic energy due to a high speed. Therefore, they enter the upper atmosphere, and collide with the atoms of the atmospheric gas. Because of these collisions, the electrons of atmospheric gas will be excited to higher states, when excited electrons return back to their original states in their atoms; they will emit energy in the form of light, this light which forms Aurora, as shown in Fig.(1.4). [Therodore p. Snow, The Dynamic universe, fourth Edition, 1993].

Also, when the solar wind hits the magnetic field of the Earth, a shock wave is form, known as the bow shock. Because the solar wind is supersonic, therefore, the charged particles of the solar wind are slowed down to be subsonic and large amount of the kinetic energy is converted to thermal energy.

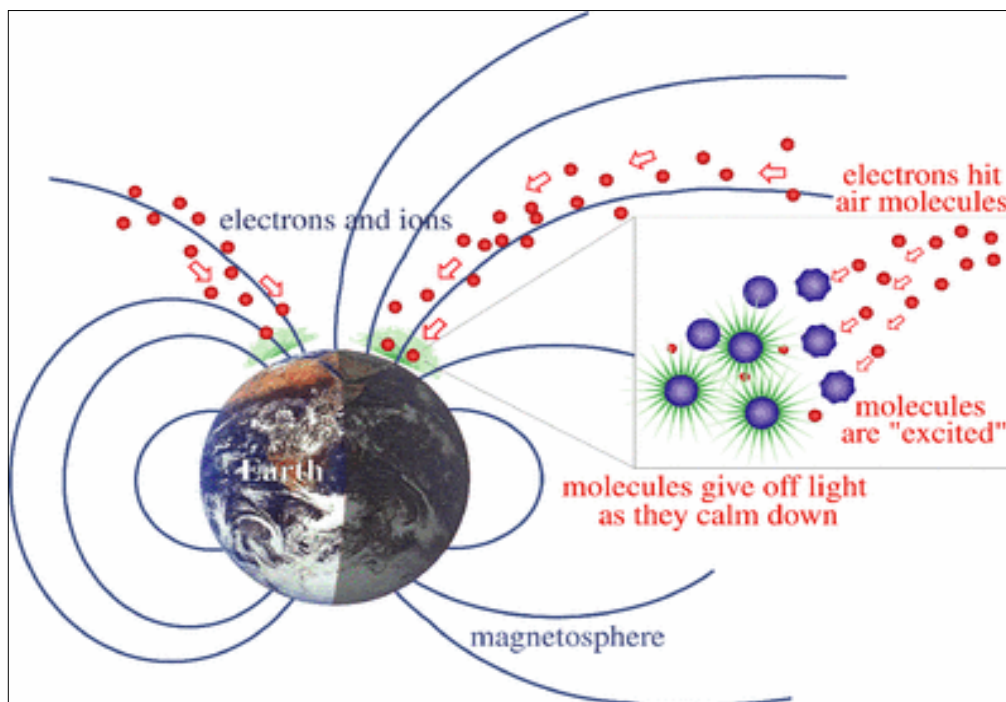


Figure 1.4: The interaction of electrons from the sun with earth's magnetic shield cause the beautiful auroras we see in the sky

http://z.about.com/d/weather/1/0/q/-/-/What_causes_aurora.gif (4/2/2009).

The region between the bow shock and the magnetopause is called the magnetosheath; the particles in this region originate from the shocked [solar wind](#). The magnetosheath plasma is thermalized subsonic and the density of the magnetosheath plasma is greater than the solar wind plasma. Also, the magnetic field is stronger in the magnetosheath region compared to out in the solar wind, in addition, the magnetosheath plasma is deflected around the Earth magnetic field. The magnetosheath region can be shown in Fig.(1.3).

The classical polar wind is an outflow of thermal plasma in the polar cap region from the high latitude ionosphere to the magnetosphere as shown in Fig.(1.5).

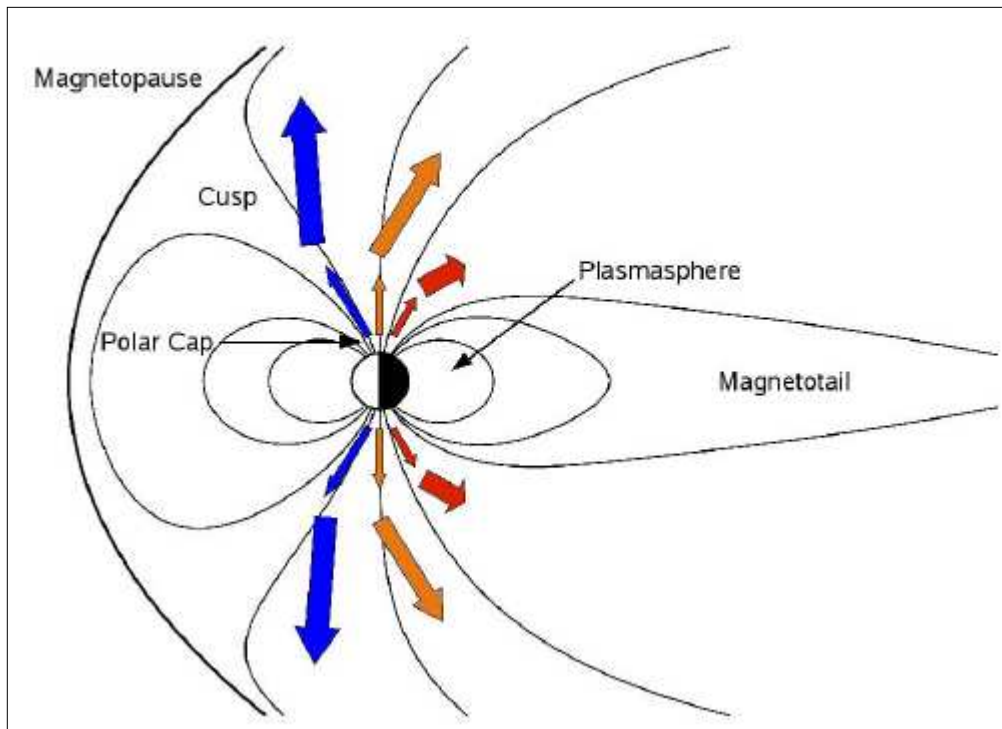


Figure 1.5: Schematic diagram of polar wind flow in the polar ionosphere. The classical polar wind occurs in the polar cap region, [Yau et al., 2007].

The polar cap is the area around the geomagnetic pole bounded by the aurora ovals, as shown in Fig.(1.2). Polar caps are high latitude regions on both hemispheres with open magnetic field lines connecting directly to the [interplanetary magnetic field](#). In addition, [polar caps](#) form one of the [ionospheric sources](#) of [magnetospheric plasma](#). This is due to the so-called polar wind, first suggested from theoretical arguments [Banks and Holzer, 1968; Axford, 1968]. The defining classical polar wind characteristics are that it is cold, field-aligned (out of the ionosphere), and the velocities are inversely correlated with ion mass, favoring lighter ions, (i.e. H^+ and He^+), [Banks and Holzer, 1969]. Later observations have revealed some new features in the polar wind. For example, there is clear day-night asymmetries in the ion and electron features, the ions velocity increases monotonically with altitude, and they become supersonic at high altitudes, [Abe et al., 1993].

The outflow consists of light thermal ions (H^+ , He^+) and heavy energized ions (O^+ , N^+ , O_2^+ , N_2^+ , NO^+) and electrons. As shown in Fig.(1.5), as the polar wind ions flow

upward along “open” geomagnetic field lines and undergo anti-sunward convection in the polar cap, they generally increase in both drift speed and temperature.

Since the ion is much more massive than electrons, so it experience a much larger gravitational force compared with electron. Therefore, spatial separation between the two is formed, this slight charge separation in quasi-neutral plasma forms an ambipolar electric field, were the polar wind plasma outflow results by accelerate the ions by the ambipolar electric field in order to achieve charge neutrality with fast upflowing electrons. Therefore, the polar wind outflow occur. Besides the ambipolar electric field there are another forces that affect in the polar wind plasma outflow such as, pressure gradient force (up ward), since the pressure in the ionosphere is greater than that in the magnetosphere tail, gravity (down ward), magnetic mirror force (upward), this force results from the motion of an ions in a medium which the magnetic field changes in it, and effect of the wave particle interaction (upward), this result from the interaction between ion and the electromagnetic turbulence.

As the polar wind outflow it undergoes four major transitions: the transition from chemical to diffusion dominance, transition from subsonic to supersonic, transition from collision-dominated to collision less regimes, and transition from heavy to light ions [Schunk, 1988]. But the most important transition is a transition from collision-dominated to collisionless region. Since these two regions are the most important regions in the polar wind. First, collision-dominated region which called ion-barosphere, the ions in this region behaves like fluid. Second, the collisionless regimes, which called exosphere, where each particle in this region is characteristics dominate the ion motion. These two regions are separated from each other by a transition layer, where the ions of the plasma change their behavior rabidly from collision-dominated to collisionless, as shown in Fig.(1.6).

Over the past 40 years, since the papers of [Axford1968, Banks and Holzer1968, Marubashi 1970], observation from different polar-orbiting satellites (i.e. ISIS-2, DE-1, Akebono, and POLAR satellites over the altitude range from 1.16 to $9R_E$) have confirmed the existence of the polar wind and emerges its basic characteristics.

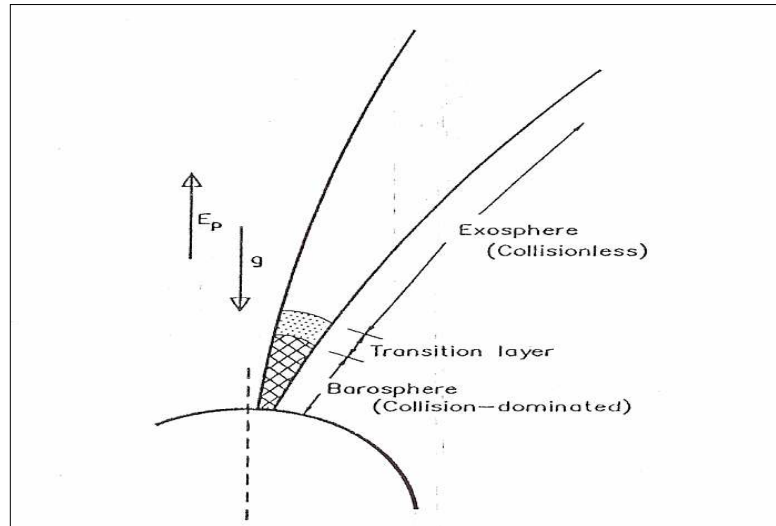


Figure 1.6: A schematic diagram for the different regions of the ion flow along diverging geomagnetic field lines, and the transition region embedded in between Barosphere and Exosphere, [Barghouthi et al., 1993].

The velocity of the polar wind ions increases with increasing altitude, also the electron temperature play important role in the ion outflow. When the electron temperature increased the velocity of the polar wind ions increased. In addition, the velocity of the polar wind ions in the dayside is higher than that on the nightside, owing to the increase of the ambipolar electric field or due to the presence of additional acceleration mechanisms, especially escaping atmospheric photoelectrons. In addition, the rate of the increase of velocity of the polar wind ions with altitude is greatest at low altitude on both dayside and nightside. Since the velocity of the polar wind ions increases with altitude, therefore by the time they reach $2.1R_E$ all polar wind ions are supersonic. The temperature of the polar wind ions is generally low, and less than that of the electrons polar wind, [Yau et al., 2007].

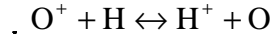
1.3 The sources of the polar wind

The polar ionosphere plasma, which has a maximum density at around 300km altitude from the surface of the Earth, is a significant and at times dominant source of plasma to the magnetosphere, in addition to the direct or indirect entry of the solar wind plasma. The outflow of polar wind plasma is limited by the rate of production of the outflowing ions

and the effect of their Coulomb collisions with the other ions. Oxygen ions results from the photoionization reaction, which is given by:

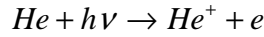


where $h\nu$ is the photon energy that interacts with the O atom, λ is the wavelength of the photon in Angstrom ($\text{\AA} = 10^{-10} \text{ m}$), which is in the ultraviolet range. On the other hand, at low altitudes, the dominant source of polar wind H^+ ion is the accidental-resonant charge exchange reaction between hydrogen atoms and oxygen ions, which is given by:

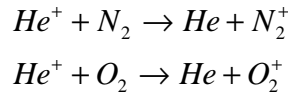


Therefore, the amount of H^+ ions that outflow away from the Earth depends on the density of O^+ ions in the polar ionosphere [Sojka et al., 1979].

The He^+ ions are produced by photo-ionization of neutral helium, which is given by:



where $h\nu$ the photon energy that interacts with the He atom and e is the electron. The density of He^+ ions is decreased by the charge exchange between He^+ and the molecules N_2 and O_2 , that given by:



Therefore, the above equations produce N_2^+ and O_2^+ ions from the accidental-resonant charge exchange reaction.

The polar wind plasma contains suprathermal components of both light (i.e. H^+) and heavy ions (i.e. O^+). It was believed that O^+ ions are exist at low altitude only, since it is relatively heavy ions and experience large gravitational force compared to the light ions, but the observations assure that there is suprathermal and energetic O^+ ions are present at high altitude ($1.8 - 2.58R_E$) together with H^+ and He^+ ions [Abe et al., 1993a,b].

The studies proved that the polar wind plays an important role in the ionosphere-magnetosphere coupling, by transfer the mass, momentum, and energy between the different regions in the solar –terrestrial environment. Also there are three main ion sources of magnetosphere plasma; these are the polar cap, the aurora region, and the cusp.

The polar wind plasma outflow changes with the geomagnetic activity, season, and solar cycles. For example, the O^+ ions flux reaches maximum in the summer, while the H^+ ions flux exhibits a spring maximum. Also, the He^+ ions flux reaches maximum in the winter, which increases by a factor of 25 from summer to winter and it increases by a factor of two from solar maximum to solar minimum [Raitt and Schunk, 1983]. The activity of the sun changes periodically, which it takes 11-years for the sun to change from its low activity (Solar Minima) to its high activity (Solar Maxima), and then back to its Solar Minima, this phenomena is called 11-year solar cycle.

In addition, the H^+ ions flux is largest in the noon sector and smallest in the midnight sector. As the polar wind plasma outflow, a mixing of cold polar wind plasma with hot magnetospheric plasma result in stabilities, which increases the polar wind plasma outflow to higher altitude. In the high geomagnetic activity, a large amount of superthermal and energetic O^+ ions are present in the magnetosphere [Yau et al., 1985; Moore et al., 1986a; Chappell et al., 1987]. The DE-1 satellite as shown in Fig.(1.7), and Akebono observations provide data, that explain how the polar wind velocity, temperature, flux, ion distribution, and ionospheric conditions changes with altitude, season, solar cycle, and geomagnetic activity. Also the data obtained by the PWI instrument on DE-1 space craft are help us to known the form of the diffusion coefficient (D_{\perp}).

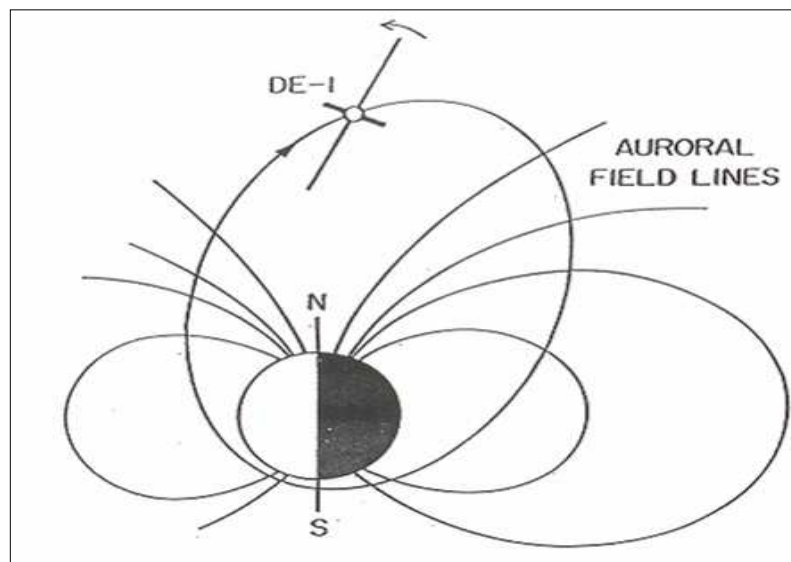


Figure 1.7: The orbit of the DE-1, it gives excellent coverage of the polar cap, the auroral field lines and the equatorial region at radial distances extending out to $4.65R_E$ [Gurnett et al., 1988].

A well-known mechanism of the coupling between the ionosphere and the magnetosphere is the outflow of plasma along the magnetic field lines of the Earth at high latitudes from the ionosphere to the magnetosphere. The ion acceleration through wave particle interaction with electromagnetic turbulence at high latitudes can be accepted to explain the existence of ions at altitudes ranging from a few hundred kilometers to several Earth radii in the polar wind region.

The plasma outflow from the polar ionosphere was first proposed by [Axford, 1968; Banks and Holzer, 1968; Marubashi, 1970]. This outflow was termed the "polar wind" in analogy with the solar wind, which had just been theorized and observed by [Parker, 1958; Bonetti et al., 1962, 1963; Neugebauer and Snyder, 1962; Snyder et al., 1963].

After few years, Observations from several polar orbiting satellites have confirmed the existence of the polar wind and established its basic characteristics (i.e. density, velocity, temperature, etc.). Therefore, there are several models were developed to study the behavior of the polar wind plasma (i.e. the ion outflow) and to explain the non-Maxwellian features of H^+ and O^+ ion velocity distribution at high latitudes, these models including: Hydrodynamics [Bank and Holzer 1968, 1969a, b], Hydromagnetic [Holzer et al., 1971], Generalized transport [Schunk and Watkins 1981, 1982], kinetic [Lemaire 1972, Lemaire and Scherer 1970, 1973], and Semi-kinetic [Barakat and Schunk 1983, 1984]. Some times many models are confused with each other to form new model such as, Monte Carlo and macroscopic PIC (Particle-In-Cell).

[Schunk, 1988] made a detailed review for these models and the classical picture of the polar wind. However, it is worthwhile to distinguish among four types of models (i.e. kinetic, semi-kinetic, Monte Carlo, and macroscopic PIC) because these models are some times confused with each other.

The kinetic models used the collisionless Boltzmann equations to describe species of plasma (ions and electrons) and solve them by Liouville theorem, [Lemaire and Scherer, 1971]. On the other hand, semi-kinetic models used collisionless Boltzmann equations (Vlasov equation) to describe the ions behavior and Boltzmann relation to describe the electron behavior, [Barakat and Schunk, 1983, 1984]. Monte Carlo approach is used to include the effect of collisions in the Boltzmann relation, [Barakat and Lemaire, 1990; Barghouthi et al., 1993]. The PIC model used the simulation domain which is divided into

cells, and small steps of time (Δt) are used in order to do the simulation. In this simulation domain (magnetic tube) the ions are allowed to move under the effect of body forces (i.e. gravity and electrostatic field) and collisions. As a result we can compute the ion density, after (Δt) the new body force is computed and do simulation again.

The previous studies on the polar wind results in a classical picture of plasma, where the O^+ ions are gravitationally bound, since it is a relatively heavy ion, but the H^+ ions escape to higher altitude where they become supersonic and develop temperature anisotropy ($T_{||} > T_{\perp}$), [Barakat and Schunk, 1983]. By using the semi-kinetic model [Barakat and Schunk, 1983] showed that H^+ distribution close to Maxwellian distribution at low altitudes ($\sim 1.7R_E$). The outflow of O^+ ions was found to be improved due to the effect of high electron temperature, [Barakat and Schunk, 1983], high ion temperature, [Li et al., 1988], and energetic magnetospheric electrons, [Barakat and Schunk, 1984]. In the model of [Lemaire and Scherer, 1972a], a monotonic potential energy altitude profile was assumed for each polar wind ion species. The species are divided into four trajectory types: ballistic, escaping, trapped, and incoming. All four trajectory types are allowed for particles such as O^+ ions that have positive potential energies (i.e. electric plus gravitational) above the baropause, but only escaping and incoming trajectories are possible for particles such as H^+ ions that have monotonically decreasing potential energy.

The escape of O^+ ions has a special importance due to elevated plasma temperature and increase the energy of the magnetospheric electrons, [Barakat and Schunk 1983, 1984; Li et al., 1988]. Furthermore, [Wu et al., 1992 and Belety et al., 1992] studied the escape of O^+ and H^+ ions in the vertical directions in the topside high-latitude ionosphere by using European Incoherent Scatter (EISCAT) VHF radar. They were able to estimate vertical velocities and fluxes of H^+ and O^+ ions, and to determine the properties of polar wind plasma outflow, and hence the structure of that region can be described.

In a series of studies, [Barakat and Schunk, 1987, 1989; Chen and Ashour-Abdalla, 1990] concluded that the polar wind could become unstable. By using plasma wave instrument (PWI) aboard on the DE-1 satellite significant levels of electromagnetic turbulence were observed at high altitude. This electromagnetic turbulence has an important effect on the

escape of heavy ionospheric ions (i.e. O^+ ions) into magnetosphere by heating these ions due to cyclotron resonance with the electromagnetic turbulence.

Several studies have been conducted of the effects that WPI have on ion outflow. The effects of WPI were first studied in the auroral region, because the observed levels of wave turbulence there are several orders of magnitude larger than those measured in the polar cap [Gurnett et al., 1984]. [Chang et al., 1986] and [Retterer et al., 1987] used a Monte Carlo simulation to study the perpendicular heating of O^+ due to a cyclotron resonance with broadband electromagnetic turbulence (i.e. wave particle interaction). An imposed wave spectral density was used that was constant with altitude, and O^+ conics were formed that had characteristics which were in agreement with the measurements. In addition, they studied the effect of wave particle interaction (WPI) on the outflow of O^+ and H^+ ions in the polar wind and aurora region, where they described the ion velocity by a quasi-linear diffusion equation that can be solved by using Monte Carlo simulation, and also adopted altitude-independent diffusion coefficient (D_{\perp}).

The studies of the effects of WPI in the polar wind region were motivated by measurements of electromagnetic wave turbulence above the polar cap, [Gurnett and Inan, 1988; Ludin et al., 1990]. In the polar cap, the electromagnetic turbulence levels are much smaller than those in the aurora region. [Barakat and Barghouthi, 1994] incorporated the effect of WPI on the polar wind ions into their steady-state collisionless kinetic calculations. They adopted an iterative approach in order to reach a self-consistent solution that accounted for both the WPI and the ions kinetic behavior. These initial studies were subsequently improved by allowing for an altitude variation of the electromagnetic turbulence level, which was guided by measurements, [Barghouthi, 1997]. The results indicated that, as expected, the effects of WPI are larger in the auroral region than in the polar cap, but they are important in both domains, where the WPI energize the ions and enhance their escape rates.

Similar to an earlier study of the resonant interaction between electromagnetic turbulence and the O^+ ions through wave particle interaction [Retterer et al., 1987], the effect of the WPI in the polar wind study was expressed in the form of an operator for perpendicular diffusion coefficient, and was taken into account by Monte Carlo simulations. The

perpendicular heating lead to parallel acceleration as the ions escape upward, because of the mirror force transferring their perpendicular energy to the field-aligned direction (i.e. in the parallel direction), [Retterer et al., 1987]. The results of the polar wind study indicated that both the density and outflow velocity of the O^+ ions are strongly related to the level of the electromagnetic turbulence; the escape flux of these heavy ions (i.e. O^+ ions) could be enhanced by a factor of 10^5 with strong WPI. In addition, [Pierrard and Barghouthi, 2006] have studied the effects of the WPI on the double-hump H^+ ion velocity distribution function in the polar wind.

The 16-moment models of [Ganguli et al., 1987] and [Demars and Schunk, 1989] predicted that, the velocity of the H^+ polar wind ions was as large as 16 –20 km/s, at high altitudes and the parallel H^+ ion temperature was greater than the perpendicular temperature between 2.7 and $6.6R_E$ (i.e. above the collision dominated region; above $1.7R_E$). Also, [Ganguli, 1996] reviewed the various theoretical models and observations from different satellites of the polar wind in details. In addition, he survey the sources and characteristics of the polar wind.

In the classical polar wind models, it was believed that O^+ ions are exist at low altitude only, since it is considered too heavy to overcome their gravitational potential barrier and experience large gravitational force compared to the light ions. In contrast, significant acceleration of O^+ ions is theoretically possible in the non-classical polar wind models and this consistent with observations, were suprathermal O^+ ions with supersonic speed were observed in the polar cap magnetosphere by the DE-1 satellite [Gurgiolo and Burch, 1982; Waite et al., 1985]. Also, [Abe et al., 1993a, b] confirmed that there is suprathermal and energetic O^+ ions are presented at high altitude ($1.8 - 2.58R_E$) together with H^+ and He^+ ions There are a number of the non-classical polar wind ion acceleration (increase of velocity with altitude) models, which include centrifugal acceleration, enhanced electron temperature, enhanced ion temperature, strong ionosphere convection, escaping atmospheric photoelectrons, external ion heating, and wave particle interaction (WPI) [Yau et al, 2007], where we will use Barghouthi model to study the effect of velocity and altitude dependent WPI on O^+ and H^+ ions outflows in the polar wind region.

In the Tam et al., [1995] model; they predicted that the perpendicular temperature comparable to the parallel temperature at high altitudes. Also, [Schunk and Watkins, 1982;

Demars and Schunk, 1987a, 1995] models predicted that the temperature anisotropy increases with altitude at high altitudes for the polar wind ions.

Another series of studies, [Barakat and Barghouthi, 1994a, b], [Barghouthi and Barakat, 1995], [Barghouthi, (1997), Barghouthi et al., (1998), and Barghouthi and Atout, (2006)], used Monte Carlo approach, in which the effect of body forces included, to investigate the effect of wave particle interaction on the H^+ and O^+ ions outflow in the polar wind region. They conclude that the effect of finite gyroradius is the reason for produce of the H^+ and O^+ ions toroids at high altitudes above the polar cap, that are observed by TIDE and TIMAS ion instruments on board the polar spacecraft. In addition, they found that, the O^+ ions are preferentially heated because of higher mass and owing to the pressure cooker effect. Furthermore, they conclude that the effect of the body forces is more important in the polar wind region than their effect in the auroral region on ions, and also, the effect of the body forces on O^+ ions is more important than that on H^+ ions. Furthermore, they found that the ions are more energetic in the auroral region than in the polar wind region. In addition, they modified the formula for diffusion coefficient (D_{\perp}) to take into account the effect of finite Larmor radius and used it to study the H^+ and O^+ ions outflow in the polar wind. At higher altitudes in the polar cap ($\sim 1.95R_E$), electromagnetic wave turbulence can significantly affect the ion outflow through the perpendicular ion heating that occurs as a result of wave particle interactions (Ludin et al., 1990; Barghouthi, 1997).

[Su et al., 1998] reported the characteristics (i.e. velocity, density, parallel temperature, perpendicular temperature, parallel heat flux, and perpendicular heat flux) of H^+ , He^+ , and O^+ ions on POLAR Satellite at both $1.8 R_E$ and $8 R_E$ altitude over the polar cap. In addition, they concluded the large velocities of the polar wind at very high altitudes reflect to the continuing acceleration due to a number of mechanisms, were there is a perpendicular ion heating of the polar wind plasma in the topside ionosphere.

[Lemaire et al., 2007] review the history of development of polar wind models and theories and they account the early polar wind measurement, non-Maxwellian distribution of ion species, and account for collision processes. The most important and generally accepted mechanism for the non-Maxwellian distribution features is the wave particle interactions. In this mechanism, as the ions (i.e. H^+ and O^+ ions) drift upward along the magnetic field

lines of the earth, they interact with the electromagnetic turbulence, that observed at high altitude, and consequently, give the ions heat in the direction perpendicular to the magnetic field of the earth. In addition, the mirror force converts some of the gained ion energy in the perpendicular direction into kinetic energy in the parallel direction; therefore these effects combine to form a well known ion-conic distribution. In addition, to [Lemaire et al., 2007], [Tam et al., 2007] reviewed the various collisional and collisionless kinetic models of the polar wind in details. Therefore, theoretical studies and observation conclude that, the wave particle interaction mechanism is generally accepted and play an important role in determines the behavior of H^+ and O^+ ion outflow.

Recently, [yau et al., 2007] reviewed the history of development of polar wind models and theories, and they offered Statistical studies or surveys of polar wind ion observations using data from ten or more satellite orbit passes. These observations were made from the ISIS-2, DE-1, Akebono, and POLAR satellites over the altitude range of 1,000 to 50,500 km, and spanned different phases of solar cycle, and they form a composite picture of the polar wind.

This study is very important, since it is given theoretical explain for the existing of O^+ ions (which is a heavy ions and gravitationally bound) at high altitude from the Earth ($1.7 - 13.7R_E$), and to collect information about the environmental space, in order to know how we will deal with environmental space when we send space craft. In addition, this study has important applications in space communications, Also, it provides addition knowledge to science of space physics.

We can conclude that [Barghouthi, 1997] obtained an altitude diffusion coefficient and [Barghouthi et al., 1998] obtained a diffusion coefficient, which is velocity dependent. In this study we will use the form of diffusion coefficient that depends on altitude from [Barghouthi, 1997] and that depends on velocity from [Barghouthi et al., 1998] to investigate the H^+ and O^+ ions outflow in the polar wind region, especially we will use this developed model (Barghouthi model) to study the effect of velocity and altitude dependent wave particle interactions on H^+ and O^+ ions in the polar wind region, and we will compare between the simulation results wave-particle interaction model (Barghouthi model) with observations.

1.4 Statement of the problem

Several wave particle interaction models (i.e. Barghouthi model, Bouharm model, and RCC model) have been suggested for investigating the energization of H^+ and O^+ ions in polar wind region and to explain the non-Maxwellian features of ions outflows in the polar wind region.

In this thesis, we are interested to compare between the simulation results of Barghouthi model with observations (i.e. quantitative and qualitative comparison). Also we are going to explain the reason why the O^+ ions (which is a heavy ions) are exist at high altitude from the Earth ($1.7 - 13.7R_E$).

This thesis is organized as follows: theoretical formulation for Boltzmann equation, wave-particle interaction, Barghouthi model, and Monte Carlo model that takes into account, polarization electrostatic field, diverging geomagnetic field, and the effects of velocity- and altitude-dependent wave-particle interactions are presented in chapter 2. We present the simulation results of Barghouthi model in chapter 3. In chapters 4 and 5, we compare between the simulation results for both O^+ and H^+ ions to the corresponding observations. Chapter 4 presents a quantitative comparison and chapter 5 presents qualitative comparison.

Chapter Two

Theoretical Formulations

2.1 Boltzmann Equation

Plasma is the fourth state of matter in addition to gas, liquid, and solid, which consist of free charges (i.e. ions, electrons, and neutral atoms). The polar wind plasma consists of several species (i.e. H^+ , O^+ , He^+ , and electrons), where the flow of these species occurs under the effect of external forces (gravitational, magnetic, and polarization electrostatic) and the net collisions of species.

Since we deal with polar wind plasma in the Barghouthi model, it is convenient to describe each species in polar wind plasma by a separate velocity distribution function $f_s(v_s, r_s, t)$. The velocity distribution function is defined such that $f_s(v_s, r_s, t)dv_s dr_s$ which represents the number of particles of species s which at time t have velocities between v_s and $v_s + dv_s$, and positions between r_s and $r_s + dr_s$. The evolution in time changes the distribution function (i.e. change of v_s, r_s) because of the net effect of many external forces and the net collisions of species, which can be described by Boltzmann equation, [Schunk, R. W., Rev. Geophysics, 15, 429, 1977]

$$\frac{\partial f_s}{\partial t} + \mathbf{v}_s \cdot \nabla f_s + [\mathbf{g} + \frac{e_s}{m_s}(\mathbf{E} + \frac{1}{c} \mathbf{v}_s \times \mathbf{B})] \cdot \nabla_{v_s} f_s = \frac{\delta f_s}{\delta t} \quad (2.1)$$

where (\mathbf{g}) is the acceleration of gravity, (\mathbf{E}) is the electric field, (\mathbf{B}) is the magnetic field, (e_s, m_s) are the charge and the mass of the species s respectively, (c) is the speed of light, ($\frac{\partial}{\partial t}$) is the time derivatives, (∇) is the coordinate space gradient, and (∇_{v_s}) is the velocity

space gradient. The right hand side of Boltzmann equation ($\frac{\partial f_s}{\partial t}$) represents the rate of change of $f_s(v_s, r_s, t)$ in a given region of phase space (v_s, r_s) as a result of collisions.

The solution of Boltzmann equation given the individual velocity distribution functions of the different species of the plasma, but the Boltzmann equation is not easy to solve. Therefore, different approaches are used to find closed-form solutions to Boltzmann equation. These mathematical approaches are used, because the plasma flow conditions can change obviously within a given region or from one region to another. These mathematical approaches include: Hydrodynamics [Bank and Holzer 1968, 1969a, b], Hydromagnetic [Holzer et al., 1971], Generalized transport [Schunk and Watkins 1981, 1982], kinetic [Lemaire 1972, Lemaire and Scherer 1970, 1973], and Semi-kinetic [Barakat and Schunk 1983, 1984], Monte Carlo [Barakat and Lemaire, 1990; Barghouthi et al., 1993, 2003a], and hybrid particle in cell (PIC) models [Demars and Schunk, 1987; Ganguli and Palmadesso, 1987; Wilson et al., 1990].

In this study we work in a collisionless region ($1.7-13.7R_E$). Therefore, we concentrate on the effect of velocity and altitude dependent wave particle interaction, and neglect the collisions in this region. In addition, the flow of species not only under the effect of the influence of external forces (gravitational, magnetic, and polarization electrostatic), but there exist electromagnetic ion cyclotron waves (i.e. wave particle interaction), so the ions move in the collisionless region under the effects of these forces and the effect of wave particle interaction.

In this thesis we will study the outflow of thermal plasma (i.e. O^+ , H^+ , and electrons) from the polar ionosphere to the magnetosphere along the geomagnetic field lines in the polar cap (i.e., polar wind). Also, we consider that the ions move under the effect of body forces (gravitational and polarization electrostatic), geomagnetic force, and the affect of wave particle interaction.

The gravitational potential energy $\phi_g(r)$ for the polar wind ions is given by the following formula:

$$\phi_g(r) = GM_E m \left(\frac{1}{1.7R_E} - \frac{1}{r} \right) \quad (2.2)$$

where G is the universal gravitational constant, M_E is the Earth mass, m is the ion mass, r is the distance between the ion and the Earth, and $1.7R_E$ is the lower boundary for Barghouthi model in the polar wind, where $r > 1.7R_E > R_E$, for more details see Appendix A.

In the geocentric altitude which extend from 1.7 to $13.7R_E$ (i.e. simulation region for Barghouthi model), the polar wind plasma considered to be collisionless. Since the electrons are very light in the ionosphere, therefore the electron escape away from the ionosphere along the geomagnetic field lines by electrons pressure gradient force, but the heavier ions are bound by gravity and they can not move with the electrons. Therefore, when the electrons start to move away along the magnetic field lines, the ions and electrons are slightly charge separated and a polarization electrostatic field is occurred, due to a slight separation of charges. The polarization electrostatic field pulls back the electrons and pulls up the ions with equal force.

The polarization electrostatic potential energy $\phi_E(r)$ is given by:

$$\phi_E(r) = kT_e \ln \left(\frac{n_e}{(n_e)_o} \right) \quad (2.3)$$

where k is the Boltzmann constant, T_e is the electron temperature, which is constant, n_e is electrons density, and $(n_e)_o$ is the equilibrium electron density (i.e., the density at $1.7R_E$), for more details see Appendix B.

Finally, the final potential energy profile $\phi(r)$ owing to body forces (i.e. gravitational and polarization electrostatic) is given by [Barakat and Schunk, 1983]:

$$\phi(r) = kT_e \ln \left(\frac{n_e}{(n_e)_o} \right) + GM_E m \left(\frac{1}{1.7R_E} - \frac{1}{r} \right) \quad (2.4)$$

where k is Boltzmann's constant, T_e is the electron temperature, n_e and $(n_e)_o$ are the electron densities at r and $1.7R_E$, respectively, which can be calculated from the quasi-neutrality condition $[n_e = n(O^+) + n(H^+)]$, G is the gravitational constant, M_E is the mass of the Earth, and m is the ions mass.

When a charged particle moves in a magnetic field it will be affected by magnetic force which known as the Lorentz force, that given as:

$$\mathbf{F} = \frac{q}{c} \mathbf{v} \times \mathbf{B} \quad (2.5)$$

where (q) is the charge of the particle, (\mathbf{v}) is the velocity of the charged particle, (c) is the speed of light, and (\mathbf{B}) is the magnetic field. The Lorentz force changes only the direction of ions velocity, but the amount of velocity do not changes. Therefore, the ion will move in a circular motion about the magnetic field, due to magnetic force. The radius of the circular path is called Larmor radius a_L , which it can be obtained by equating between the magnetic force and the centrifugal force.

$$a_L = \frac{mc}{q} \frac{v_{\perp}}{B} \quad (2.6)$$

where m is the mass of the ion and v_{\perp} the perpendicular component velocity.

The quantity $\left(\frac{qB}{mc} \right)$ is called the gyrofrequency denoted by:

$$\Omega_c = \frac{qB}{mc} \quad (2.7)$$

Since the Lorentz force operates in the direction perpendicular to velocity vector v_{\perp} , therefore there is no work done on the ion and the total energy of the ion remains constant, for more details see Appendix C.

On the other hand, the geomagnetic field is taken to be proportional to r^{-3} where (r) is the geocentric distance ($B \propto \frac{1}{r^3}$). Therefore:

$$B = \frac{B_0}{r^3} \quad (2.8)$$

where B_0 is the magnetic field of the Earth at the surface of the Earth.

2.2 Wave Particle Interaction (WPI)

The flow of plasma from the ionosphere toward the magnetosphere a long the geomagnetic field lines known as the polar wind. This indicates that the ionosphere is the major source of ions provided to the magnetosphere. Several models were developed to study the

outflow of ions in the polar cap region (i.e. centrifugal acceleration, enhanced electron temperature, enhanced ion temperature, strong ionosphere convection, escaping atmospheric photoelectrons, external ion heating, and wave particle interaction, [Yau et al., 2007]. In our study we use the wave particle interaction model to investigate the outflow of the polar wind plasma.

Many theoretical investigations studied the polar wind plasma using WPI. [Ludin et al., 1990; Barghouthi, 1997], concluded that, at high altitudes in the polar cap ($\sim 1.95R_E$), the electromagnetic turbulence can significantly affect the ion outflow through the perpendicular ion heating that occurs as a result of WPI. WPI are known to play an important role in energizing polar wind ions comes from the ionosphere. This process is effective over a wide range of altitudes and is particularly important in polar cap. The WPI act to preferentially heat the ions in a direction perpendicular to magnetic field lines of the Earth, and then the ions are expelled via the mirror force, which yields from the gradient of the magnetic field with altitude. The heated ions are then driven upwards by the mirror force.

The effects of WPI were first studied in the auroral region, since the observed levels of electromagnetic turbulence in the auroral region greater than that in the polar wind region. Therefore, the effect of WPI in the auroral region is more obviously, [Gurnett et al., 1984]. In addition, [Chang et al., 1986] and [Retterer et al., 1987] used a Monte Carlo technique to study the perpendicular heating of O^+ due to a cyclotron resonance with the electromagnetic turbulence. As a result of WPI, the ions heated and energized to levels much higher than the gravitational and polarization potential energies and the result obtained a conic for O^+ ions distribution, which in agreement with observations taken by (DE-1) satellite, [Barakat and Barghouthi, 1994b]. Therefore the effect of WPI is effective at high altitudes, where the ions gain more and more energy due to the effect of WPI. Since, it takes along time for the ion to reach high altitudes, the rate of perpendicular adiabatic cooling decreases because of the decreasing in magnetic field at high altitudes.

The early studies of the effects of WPI that have done on the polar wind were based on the Monte Carlo technique, where the diffusion coefficient is altitude independent (i.e. the effect of WPI is altitude independent), [Barakat and Barghouthi, 1994]. On the other hand, [Barghouthi, 1997] improved the expression of WPI to be altitude dependent by allowing

the electromagnetic turbulence level to be variable with altitude. The results indicated that, as expected, the effects of WPI are larger in the auroral region than in the polar cap, but they are important in both regions, where the WPI energize the ions and drift them upwards.

Theoretical studies and observations show that the WPI plays an important role in determining the behavior of escaping of plasma (i.e. O^+ , H^+ , He^+ ions, and electrons) and the strength of the effect of WPI are significant in comparison to other forces such as electrostatic, gravitational, and geomagnetic forces. As a result, the effect of WPI should be included in the models, as shown in Fig.(2.1).

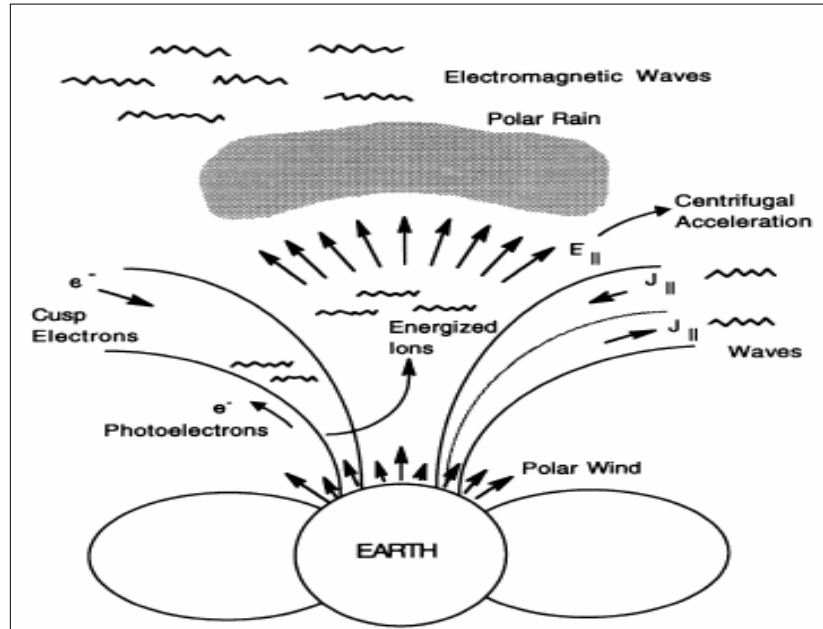


Figure 2.1: Schematic diagram showing the causes of ion outflow from the Earth's ionosphere, [Schunk and Sojka, 1997].

To include the effect of the WPI in a collisionless region replace the collision term in Boltzmann equation by the term that represents the interaction between ions and the electromagnetic turbulence, which is represented by particle diffusion in the velocity space such that [Retterer et al., 1987a]:

$$\left[\frac{\partial f_j}{\partial t} \right]_{WPI} = \left(\frac{1}{v_{\perp}} \right) \frac{\partial}{\partial v_{\perp}} \left[D_{\perp j} v_{\perp} \frac{\partial f_j}{\partial v_{\perp}} \right] \quad (2.9)$$

where D_{\perp} is the quasi-linear velocity diffusion coefficient rate perpendicular to geomagnetic field lines.

The influence of WPI on the ion species during Δt under the effect of the gravitational, electrostatic, and geomagnetic forces, is taking into consideration by incrementing the ions perpendicular velocity by randomly increment Δv_{\perp} such that:

$$\langle (\Delta v_{\perp})^2 \rangle = 4D_{\perp} \Delta t \quad (2.10)$$

where Δt is the time interval chosen randomly and D_{\perp} is the perpendicular diffusion coefficient rate.

To study the effect of WPI, we need to know the expression for the diffusion coefficient D_{\perp} . [Barghouthi, (1997) and Barghouthi et al., (1998)] computed the altitude dependence of D_{\perp} by analyzing experimental data obtained by PWI on board the DE-1 satellite. They obtained the following expression for the perpendicular diffusion coefficient rate D_{\perp} in the polar wind plasma:

$$D_{\perp}(r) = \begin{cases} 5.77 \times 10^3 (r/R_E)^{7.95} \text{ cm}^2 \text{ sec}^{-3}, & \text{for } H^+ \\ 9.55 \times 10^2 (r/R_E)^{13.3} \text{ cm}^2 \text{ sec}^{-3}, & \text{for } O^+ \end{cases} \quad (2.11)$$

This expression for the altitude dependent diffusion coefficient did not produce results that agree with the observations. To producing these observations requires a velocity dependent diffusion rate as suggested by [Retterer et al., 1994], for more details see Appendix D.

To model the heating process (i.e. wave-particle interactions), we specify a model for the diffusion coefficient D_{\perp} as a function of perpendicular velocity v_{\perp} and position r/R_E along magnetic field lines of the Earth. For the spatial variation, (i.e. the altitude dependence) we choose the form obtained by [Barghouthi, 1997], equation (2.11), while for the velocity dependence, we choose the form obtained by [Barghouthi et al., 1998].

2.3 Barghouthi model

[Retterer et al., 1987b]; assumed the wavelength (λ_{\perp}) of the electromagnetic turbulence to be much greater than the ions Larmor radius $a_L \left(i.e., \frac{k_{\perp} v_{\perp}}{\Omega_i} \right)$. However, the ions of the polar wind plasma are accelerated owing to the WPI. So, they are escape upward along the magnetic field lines of the Earth, but the magnetic field intensity (\mathbf{B}) of the Earth decreasing when the altitude increasing, where the geomagnetic field is taken to be proportional to r^{-3} (where r is the geocentric distance and $B \propto \frac{1}{r^3}$). However, the ions Larmor radius (a_L) inversely proportional to the magnetic field intensity (\mathbf{B}) as shown in equation (2.6). Therefore, the ions Larmor radius (a_L) increasing rapidly with altitude. As a result, at high altitudes, the ions Larmor radius (a_L) may become comparable to or even more than the perpendicular electromagnetic turbulence (λ_{\perp}) as shown in Fig.(2.2), and consequently the quantity $\frac{k_{\perp} v_{\perp}}{\Omega}$ becomes greater than one. As a result, the assumption made by [Retterer et al., 1987b] and the diffusion coefficient expression (D_{\perp}) which is velocity independent becomes inaccurate.

[Barghouthi, 1997 and Barghouthi et al., 1998] obtained a new form for diffusion coefficient (D_{\perp}) for the case the ions Larmor radius (a_L) is comparable or larger than the perpendicular electromagnetic turbulence (λ_{\perp}), which is altitude and velocity dependent:

$$D_{\perp}(r, v_{\perp}) = D_{\perp}(r) \begin{cases} 1 & \text{for } \left(\frac{k_{\perp} v_{\perp}}{\Omega_i} \right) < 1 \\ \left(\frac{k_{\perp} v_{\perp}}{\Omega_i} \right)^{-3} & \text{for } \left(\frac{k_{\perp} v_{\perp}}{\Omega_i} \right) \geq 1 \end{cases} \quad (2.12)$$

where the diffusion coefficient $D_{\perp}(r)$ is given in equation (2.11). This form of the diffusion coefficient (D_{\perp}) (i.e., altitude and velocity dependent) is the solution of equation (2.9), for more details see Appendix E.

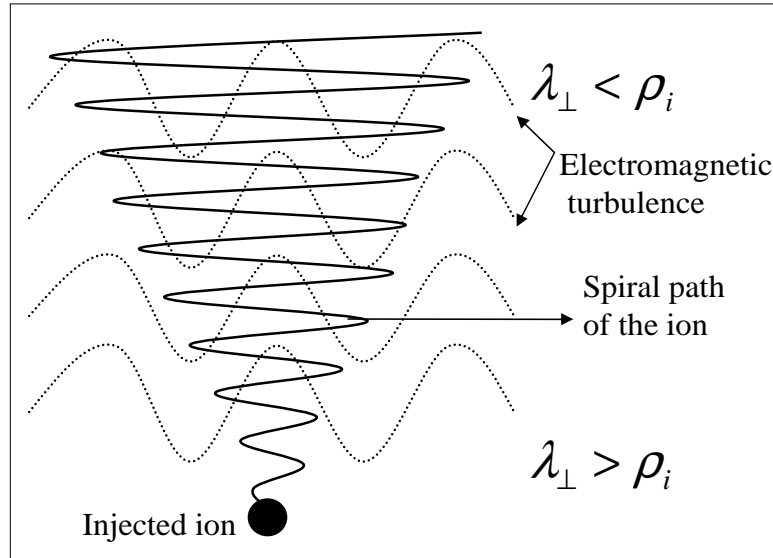


Figure 2.2: Schematic diagram that illustrates the gyrating motion of a single ion across electromagnetic turbulence perpendicular to the geomagnetic field [Barghouthi and Atout, 2006].

2.4 Monte Carlo method (MC method)

The expression "Monte Carlo method" is actually very general. Monte Carlo (MC) method based on the use of random numbers and probability statistics to investigate problems. The beginning of Monte Carlo method as a highly universal numerical technique became applicable just with appearance of computers (i.e.1949) and its name refers to a city in Monaco in Canada, [Belotserkovskii and Khlopkov, 2006].

The use of Monte Carlo method to model physical problems allows us to examine more complex systems by solving equations which describe the interactions between hundreds or thousands of ions. Therefore, with Monte Carlo method we can use Monte Carlo technique to solve Boltzmann's equation, which described in the section (2.1)

Monte Carlo simulation is a simple concept compared with the other simulation models. It goes straight forward algorithms, and it is a powerful technique to solve Boltzmann's equation by a particle simulation, in order to find the velocity distribution function and its moments (i.e. density, drift velocity, parallel temperature, and perpendicular temperature).

MC simulation developed to include the effect of body forces (i.e. gravitational and polarization electrostatic), geomagnetic force, and the effect of WPI, which make it the best technique, are used in the space plasma physics. Therefore, we use it to solve Boltzmann's equation to find the velocity distribution function and the moments of the ions. In other words, we will use the MC technique to solve equation (2.9) to obtain the ion velocity distribution and its moments.

In the MC method we can follow the motion of the individual particles such as O^+ or H^+ ion and to continually monitor its velocity. We can simulate the motion of an ion in the polar wind region at high altitude and high latitude, which is collisionless regime. We deal the polar wind plasma as a steady state flow of the three main component of the polar wind plasma (i.e. H^+ , O^+ , and electrons). Hence, the simulation region is a geomagnetic tube extending from $r = 1.7R_E$ to $r = 13.7R_E$, as shown in Fig.(2.3).

The ion is injected into the simulation region from the lower boundary (i.e. $1.7R_E$) with a random initial velocity that corresponds to the ion distribution function immediately below the lower boundary. The test ion moves under the influence of body forces (gravitational and polarization electric field), magnetic mirror force, and the effect of WPI.

The influence of WPI on the tested ion during short time interval (Δt) under the effect of the gravitational force, electrostatic force, and geomagnetic force, is taking into consideration by incrementing the ions perpendicular velocity by randomly increment (Δv_{\perp}) such that, $\langle (\Delta v_{\perp})^2 \rangle = 4D_{\perp}\Delta t$, where Δt is the time interval chosen randomly and D_{\perp} is the perpendicular diffusion coefficient rate, which is given in equation (2.12). The behavior of the ion during short time interval (Δt) is determined by the conservation of energy, and the conservation of the first adiabatic invariant μ , where $\mu = \frac{mv_{\perp}^2}{2B}$.

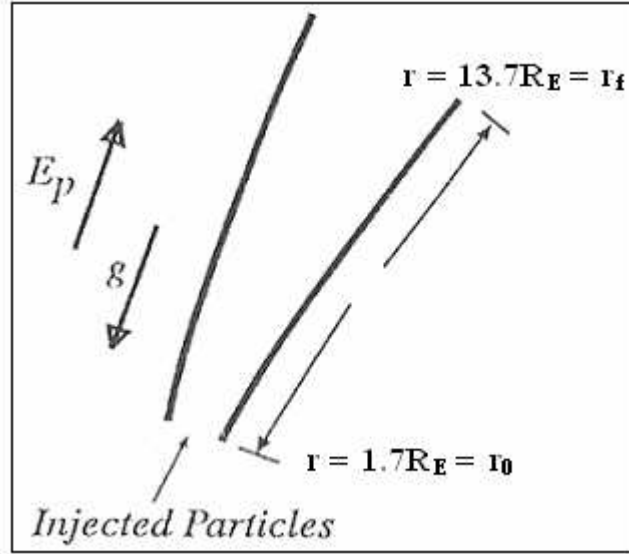


Figure 2.3: A schematic representation of the model considered by the Monte Carlo method [Barakat and Barghouthi, 1994a, b].

The above procedures are repeated until the tested ion exits the simulation region at either boundary (i.e. lower boundary($1.7R_E$) or higher boundary ($13.7R_E$)). After that, another test ion is initiated at the starting point (i.e. $1.7R_E$). In the simulation process we need to inject 10^7 ions from the starting point, in order to get a complete picture on the behavior of the ions, also, since the O^+ ions are gravitationally bound, so not all O^+ ions that enter the simulation region can escape to high altitude, since the potential energy of O^+ ions is positive and increases with altitude. These ions will be monitored until they escape from the simulation region which extends from $r = 1.7 R_E$ to $r = 13.7R_E$, and at each altitude the behavior of these ions is registered by a two dimensional grid in velocity space (i.e. parallel and perpendicular velocities to the geomagnetic field lines).

The velocities of the tested ions, that they cross one of the monitoring altitude, can be used to compute the moments of the distribution function at that altitude. Also, the time that an ion spends in each bin divided by the bin's volume is taken to be proportional to the ion velocity distribution function at the center of the bin, [Barghouthi et al. 2003a].

The moments of the distribution function are given by the following expressions:

$$n_s = \int f_s(v_s) d^3v_s \quad (2.13)$$

$$u_s = \frac{\int v_{lls} f_s(v_s) d^3 v_s}{\int f_s(v_s) d^3 v_s} \quad (2.14)$$

$$T_{lls} = \frac{\frac{m_s}{k} \int (v_{lls} - u_s)^2 f_s(v_s) d^3 v_s}{\int f_s(v_s) d^3 v_s} \quad (2.15)$$

$$T_{\perp s} = \frac{\frac{m_s}{2k} \int v_{\perp s}^2 f_s(v_s) d^3 v_s}{\int f_s(v_s) d^3 v_s} \quad (2.16)$$

The above equations (2.13) – (2.16) are the ion density, drift velocity, parallel temperature, perpendicular temperature, respectively, and s denotes the type of the ion (i.e. H^+ or O^+), for more details see Appendix F.

In this study, the Monte Carlo simulation was run for Barghouthi model, where the perpendicular diffusion coefficient $D_{\perp}(r, v_{\perp})$ is given in equation (2.12), and in each simulation we used 10^7 tested ions, in order to get a complete picture on the behavior of the ions, also, since the O^+ ions are gravitationally bound, so not all O^+ ions that enter the simulation region can escape to high altitude, since the potential energy of O^+ ions is positive and increases with altitude. As a result, we can compute the ion distribution function and also the profiles of its velocity moments (i.e. density, drift velocity, parallel temperature, and perpendicular temperature) for both H^+ and O^+ ions. The boundary conditions selected for polar wind region are similar to those of [Barghouthi et al., 1998].

The effects of WPI were introduced via a Monte Carlo technique by using Compaq Visual Fortran programming language, and an iterative approach was used in order to converge to self-consistent results. In practice, an iterative approach was used to find the electrostatic potential. The model was run to solve the case of altitude dependent and velocity independent WPI as a starting point. The resulting electrostatic potential and consequently, the potential energy due to body force (i.e. equation (2.4)), was then used in the model to find $n(O^+)$ and $n(H^+)$ with altitude and velocity dependent wave-particle interactions, which were substituted in $[n_e = n(O^+) + n(H^+)]$ and in equation (2.4) in order to compute and improved value of $\phi(r)$. The new profile of $\phi(r)$ was then used to compute new

density profile. The iteration process was continued until convergence was reached, which happened to occur in few (3–4) steps.

Chapter Three

The results

3.1 Introduction

The energization of charged particles, due to the interaction with electromagnetic turbulence (i.e. wave particle interaction) has a significant influence on ions transport in space. The effects of altitude and velocity dependent wave particle interactions on H^+ and O^+ ions outflow in the polar wind region have been investigated by using Monte Carlo simulation.

To model the heating process, (i.e. wave particle interactions), we specify a model for the velocity diffusion coefficient (D_{\perp}) as a function of perpendicular velocity (v_{\perp}) and position (r/R_E) along geomagnetic field line. For the spatial variation, (i.e. the altitude dependence) we chose the form obtained by [Barghouthi, 1997], while for the velocity dependence, we chose the form obtained by [Barghouthi et al., 1998]. The final expression is called the Barghouthi model, which is given in equation (2.12).

The boundary conditions selected for the polar wind region are similar to those of [Barghouthi et al., 1998], at lower boundary (i.e. $1.7 R_E$). We set the O^+ ion drift velocity at 0 cmsec^{-1} , the oxygen ion density at 100 cm^{-3} , and the O^+ ion temperature at 3000°K . In addition, the boundary condition for the H^+ polar wind ion, we set at the lower boundary (i.e. $1.7 R_E$) the H^+ ion drift velocity at 11 kms^{-1} , the hydrogen ion density at 200 cm^{-3} , and the H^+ ion temperature at 3000°K . Also, the electron temperature was kept constant at 1000°K along the entire simulation tube ($1.7 - 13.7 R_E$). In addition, the velocity distribution function for both H^+ and O^+ ions is supposed to be Maxwellian (i.e. the

perpendicular temperature equal the parallel temperature, in other words, there is no temperature anisotropy) at the lower boundary (i.e. at $1.7R_E$).

We considered a wide range of characteristic wavelengths for the waves (electromagnetic turbulence) [$\lambda_{\perp} = \infty, 50, 20, 8$, and 1km] that covers the circumstances expected to occur in the polar wind region, since the data obtained by the Plasma Wave Instrument (PWI) on Dynamic Explorer-1(DE-1) satellite do not include information about (λ_{\perp}), (i.e. perpendicular wavelength of the electromagnetic turbulence). In addition, there is no detailed information about the spectrum of the electromagnetic turbulence.

In previous studies, the ions Larmor radius (a_L) is assumed to be less than the wavelength of the electromagnetic turbulence (λ_{\perp}). However, the ions of the polar wind plasma is accelerated owing to the WPI. So, they are escape upward along the geomagnetic field lines. As a result, the ions Larmor radius (a_L) increasing rapidly with altitude. Therefore, at high altitudes, the ions Larmor radius (a_L) will be comparable to or exceeds the wavelength of the electromagnetic turbulence (λ_{\perp}). As a result, [Barghouthi, 1997 and Barghouthi et al., 1998] obtained a new forms for diffusion coefficient (D_{\perp}) for the case the ions Larmor radius (a_L) is comparable or exceeds the perpendicular electromagnetic turbulence (λ_{\perp}), which called the Barghouthi model, which is include the effects of altitude and velocity dependent WPI.

3.2 O^+ ions

To study the effect of altitude and velocity dependence WPI on the O^+ ions, we computed the distribution function $f(O^+)$ at several altitudes extended from 1.7 to $13.7R_E$ for different values of the perpendicular electromagnetic turbulence (λ_{\perp}), which are [$\lambda_{\perp} = \infty, 50, 20, 8$, and 1km]. The Barghouthi model simulation results of the O^+ ions velocity distribution function $f(O^+)$ are shown in Fig.(3.1). We supposed wide range of (λ_{\perp}) in the O^+ ions case, where (1st panel) $\lambda_{\perp} \rightarrow \infty$, (2nd panel) $\lambda_{\perp} = 50\text{ km}$, (3rd panel) $\lambda_{\perp} = 20\text{ km}$, (4th panel) $\lambda_{\perp} = 8\text{ km}$, and (5th panel) $\lambda_{\perp} = 1\text{ km}$.

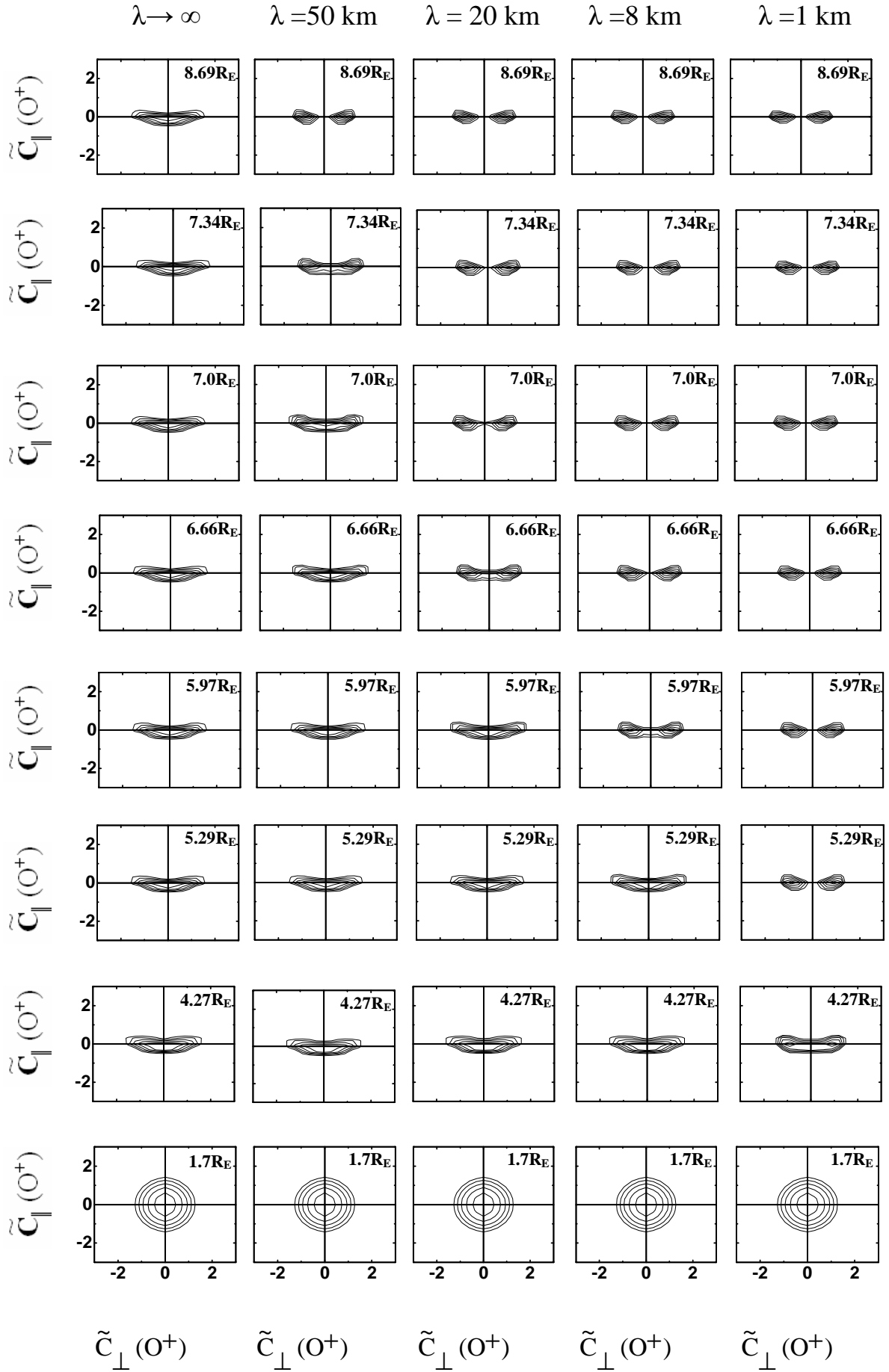


Figure 3.1: O^+ ions velocity distribution functions at different geocentric distances (1.7, 4.27, 5.29, 5.97, 6.66, 7.0, 7.34 and $8.69R_E$) for different electromagnetic turbulence wavelengths (λ_\perp), the wavelengths considered here are $\lambda_\perp \rightarrow \infty$ (1st panel), $\lambda_\perp = 50 \text{ km}$ (2nd panel), $\lambda_\perp = 20 \text{ km}$ (3rd panel), $\lambda_\perp = 8 \text{ km}$ (4th panel), and $\lambda_\perp = 1 \text{ km}$ (5th panel). $f(O^+)$ is represented by equal values contours in the normalized velocity ($\tilde{c}_\parallel, \tilde{c}_\perp$) plane, where $\tilde{c} = [\mathbf{v} \cdot \mathbf{u}(O^+)] / [2kT(O^+)/m(O^+)]^{1/2}$. The contour levels decrease successively by a factor $e^{1/2}$ from the maximum.

For the case ($\lambda_\perp \rightarrow \infty$), the diffusion coefficient (D_\perp) become altitude dependent and velocity independent, since the perpendicular wave vector $k_\perp = \frac{2\pi}{\lambda_\perp}$. So, the perpendicular wave vector $k_\perp \rightarrow 0$, since $\lambda_\perp \rightarrow \infty$. As a result, from Barghouthi model expression (i.e. equation (2.12)), the effect of WPI become velocity independent (i.e. the effect of WPI is altitude dependent only). From Barghouthi model, simulation results for the case $\lambda_\perp \rightarrow \infty$ (1st panel of Fig.(3.1)) we see that at the exobase (i.e. $1.7R_E$) in the 1st panel the distribution function $f(O^+)$ shows Maxwellian features, because the perpendicular diffusion coefficient $D_\perp(O^+)$ is very small at low altitude, so the effect of WPI is negligible. As the geocentric altitude increases, the diffusion coefficient $D_\perp(O^+)$ increases, as shown in equation (2.11), then the role of WPI becomes more significant in heating the ions in the perpendicular direction (i.e. the strength of WPI increases). As a result, the distribution function $f(O^+)$ develops large temperature anisotropy, [i.e. $T_\perp(O^+) > T_\parallel(O^+)$], which forming "pancake-like" distributions that folds into O^+ conics due to the effect of mirror force (i.e. diverging magnetic field), as shown in (1st panel of Fig.(3.1)) at geocentric altitudes start from $4.27R_E$ to high altitudes.

But for the case ($\lambda_\perp = 50 \text{ km}$), the behavior of ions remains the same as the case of $\lambda_\perp \rightarrow \infty$ up to altitude $\sim 7.0R_E$, where the toroidal features starts to appear at altitude $\sim 7.34R_E$ and become obvious at altitude $\sim 8.69R_E$, and saturated above this level (1st and 2nd panels of Fig.(3.1)). This means that, the general shape of $f(O^+)$ becomes invariable with altitude. For the case $\lambda_\perp = 20 \text{ km}$ the distribution functions behaves as in the case of

$\lambda_{\perp} \rightarrow \infty$ and $\lambda_{\perp} = 50 \text{ km}$ up to $\sim 5.97R_E$, but the toroidal distribution appears at lower altitude (i.e. $\sim 6.66R_E$), which form completely at $\sim 7.43R_E$, and saturated above this level (3rd panels of Fig.(3.1)). However, for $\lambda_{\perp} = 8 \text{ km}$, the toroidal shape appears at lower altitudes. It starts to appear at altitude $\sim 5.97R_E$ and becomes well established at altitude $\sim 6.66R_E$ (4th panel of Fig.(3.1)). Moreover, for the case $\lambda_{\perp} = 1 \text{ km}$ the toroidal features appear at a lower altitude $\sim 4.27R_E$, which become obvious at geocentric altitude $\sim 5.29R_E$ (5th panel of Fig.(3.1)), and the distribution function $f(O^+)$ becomes saturated above that level (i.e. above $5.29R_E$).

The formation of ion toroids can be explained if we return back to equation (2.12), which represent the expression of Barghouthi model, the diffusion coefficient (D_{\perp}) has maximum value near zero perpendicular velocity (i.e. $k_{\perp}v_{\perp}/\Omega < 1$), and decreases rapidly for large values of (v_{\perp}) (i.e. $k_{\perp}v_{\perp}/\Omega \geq 1$). Therefore, the ions (H^+ or O^+) tend to move out of the region of large diffusion coefficient (D_{\perp}) (i.e. $k_{\perp}v_{\perp}/\Omega < 1$) and accumulate in the region of relatively low diffusion coefficient (D_{\perp}) (i.e. $k_{\perp}v_{\perp}/\Omega \geq 1$) forming the aforementioned toroidal distribution.

For the cases $\lambda_{\perp} = 50 \text{ km}$, $\lambda_{\perp} = 20 \text{ km}$, $\lambda_{\perp} = 8 \text{ km}$, and $\lambda_{\perp} = 1 \text{ km}$, the O^+ velocity distribution function $f(O^+)$ saturates after forming the toroidal shape (i.e. the general shape of the distribution function $f(O^+)$ becomes invariable with altitude), because the perpendicular heating becomes invariable (i.e. the perpendicular heating become self-limiting). We also notice that as electromagnetic turbulence (λ_{\perp}) decreases, the argument

$\frac{a_L}{\lambda_{\perp}}$ approaches one at low altitudes, and consequently the toroidal distribution appears at

lower altitudes, namely for the case $\lambda_{\perp} = 1 \text{ km}$ the toroidal become to appear at altitude $\sim 4.27R_E$. The toroidal features become completely at altitude $\sim 5.29R_E$ (5th panel of Fig.(3.1)).

In addition we see in Fig.(3.2) the altitude profiles of lower order moments of O^+ ions, which include; density $n(O^+)$, drift velocity $u(O^+)$, parallel temperature $T_{\parallel}(O^+)$, and perpendicular temperature $T_{\perp}(O^+)$ for wide range of the electromagnetic turbulence (λ_{\perp}). [$\lambda_{\perp} \rightarrow \infty$ (double-dotted dashed), $\lambda_{\perp} = 50 \text{ km}$ (dotted dashed), $\lambda_{\perp} = 20 \text{ km}$ (dotted), $\lambda_{\perp} = 8 \text{ km}$ (dashed) and $\lambda_{\perp} = 1 \text{ km}$ (solid)].

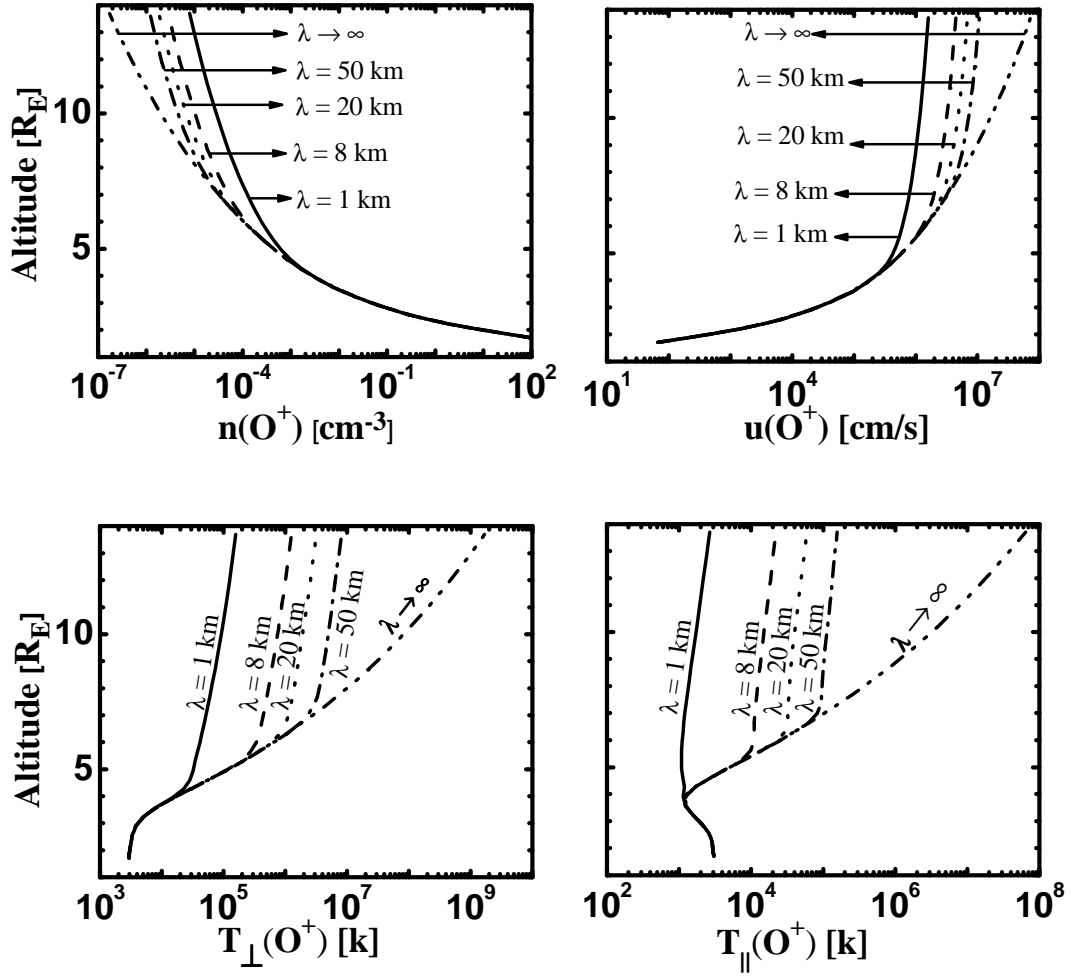


Figure 3.2: Altitude profiles of the lower order O^+ moment for different electromagnetic turbulence wavelengths (λ_{\perp}). The wavelengths considered here are $\lambda_{\perp} \rightarrow \infty$ (double-dotted dashed line), $\lambda_{\perp} = 50 \text{ km}$ (dotted dashed line), $\lambda_{\perp} = 20 \text{ km}$ (dotted line), $\lambda_{\perp} = 8 \text{ km}$ (dashed line), $\lambda_{\perp} = 1 \text{ km}$ (solid line). The O^+ moments considered here are: density $n(O^+)$ (top left), drift velocity $u(O^+)$ (top right), perpendicular temperature $T_{\perp}(O^+)$ (bottom left), and parallel temperature $T_{\parallel}(O^+)$ (bottom right).

The drift velocity of O^+ ions $u(O^+)$ (top right panel of Fig.(3.2)) increases with altitude, which can be explained as follow: the effect of WPI heating the ions in the perpendicular direction, which increases the upward mirror force, and so increases the acceleration of the ions in the upward direction, (i.e. increases of drift velocity with altitude). However, we note that, the drift velocities at low altitudes (i.e. below $4.5R_E$) are coincided for different values of the perpendicular electromagnetic turbulence (λ_\perp), which are [$\lambda_\perp = \infty, 50, 20, 8$, and 1km], since the argument ($\frac{a_L}{\lambda_\perp}$) is less than unity (i.e. the behavior of O^+ ions below the saturation point is the same for all values (λ_\perp), that is, the ion self-limiting is negligible. For the case $\lambda_\perp = 50\text{ km}$, the acceleration rate decreases, and so $u(O^+)$ decreases above the saturation point which occurs at altitude $\sim 7.5 R_E$ in comparison with the case $\lambda_\perp \rightarrow \infty$, and this is obvious result of the energization self-limiting nature, which occurs when $\frac{a_L}{\lambda_\perp}$ exceeds unity (i.e. above saturation point). For the case $\lambda_\perp = 20\text{ km}$, we see that the saturation level appears earlier $\sim 6.5R_E$, as λ_\perp decreases more (i.e. $\lambda_\perp = 8\text{ km}$). The saturation level appears at lower altitude $\sim 6.0R_E$, for smaller values λ_\perp (i.e. $\lambda_\perp = 1\text{ km}$). $u(O^+)$ is reduced and the saturation level appears at lower altitude $\sim 4.5R_E$. These results have a close agreement with the distribution function results displayed in Fig.(3.1).

The drift velocity of O^+ ions $u(O^+)$ (top right panel of Fig.(3.2)) decreases as electromagnetic turbulence wavelength (λ_\perp) decreases, because of the reduction of the heating rate, this can be explained as follow: the expression for the diffusion coefficient (D_\perp) is a function of altitude and velocity as shown in equation (2.12). As electromagnetic turbulence wavelength (λ_\perp) decreases therefore, the wave vector $\left(k_\perp = \frac{2\pi}{\lambda_\perp}\right)$ increases. So the argument $\left(\frac{k_\perp v_\perp}{\Omega}\right)$ increases, and hence the expression $\left(\frac{k_\perp v_\perp}{\Omega}\right)^{-3}$ decreases, so the diffusion coefficient (D_\perp) decreases. As a result, the strength of WPI decreases and reduction the heating rate.

To study the effect of finite electromagnetic turbulence wavelength (λ_{\perp}) on the O^+ density $n(O^+)$, we first set the following argument. For the range of ($\lambda_{\perp} \geq 1\text{km}$) considered here, the finite electromagnetic turbulence wavelength (λ_{\perp}) effect occurs at relatively high altitude ($\geq 4.5R_E$) where the kinetic energy of the ion becomes more than the energy needed to escape and cross the potential barrier. Therefore, the drift velocity $u(O^+)$ is trans-sonic, and since the O^+ ions are in the flux-limiting flow condition [Barakat and Schunk, 1983], a corresponding increases in the ions drift velocity (top right panel of Fig.(3.2)) is expected to compensate in the decreases in the ions density (top left panel of Fig.(3.2)), and hence to keep the net escape flux constant, where in the steady-state polar wind ion flow, the continuity equation required that: $F_i = n_i v_i$, where F, n_i , and v_i are the flux, density, and velocity of the polar wind ions. As electromagnetic turbulence wavelength (λ_{\perp}) decreases the increased scale height starts at lower altitudes, which consistent with the drift velocity $u(O^+)$.

The WPI (i.e. perpendicular heating) has two opposing effects on the O^+ ions density $n(O^+)$. It increases the number of O^+ ions that can escape and crossing the potential barrier and reach to higher altitudes, this slightly dominates at low altitudes. In contrast, WPI increases the drift velocity of O^+ ions, which reduce the density of O^+ ions, this effect dominates at high altitudes. This explains the slight increase in density at low altitudes and large increases in it at high altitudes, due to WPI effects.

The behavior of O^+ ions temperature (perpendicular or parallel) is a result of balance between WPI heating affect in the perpendicular direction and perpendicular adiabatic cooling (i.e. $\mu = \frac{mv_{\perp}^2}{2B}$); but the O^+ ions perpendicular temperature $T_{\perp}(O^+)$ is increasing monotonically with altitude; which means that at all altitudes the effect WPI is greater (i.e. WPI is dominant) than that of perpendicular adiabatic cooling. At lower altitudes the heating is enhanced owing to the "pressure cooker effect", which results from the temporary trapping of O^+ ions between the lower magnetic deflection point and the upper gravitational point, when an ion bounces between these deflection points, it is accelerated in the perpendicular direction (i.e. the ion energized to higher perpendicular temperature).

The profiles of O^+ ions parallel temperature $T_{\parallel}(O^+)$ (right bottom panel of Fig.(3.2)) is influenced by WPI, where as O^+ ions perpendicular heating increases, part of this energy is transfer from the perpendicular direction to the parallel direction, and consequently, the parallel temperature increases at high altitude, but at low altitude O^+ ions parallel temperature $T_{\parallel}(O^+)$ decreases with altitude, owing to parallel adiabatic cooling. However, as $T_{\perp}(O^+)$ decreases due to the effect of finite Larmor radius this on the other hand decreases the O^+ parallel temperature $T_{\parallel}(O^+)$. In general, we see that perpendicular temperature $T_{\perp}(O^+)$ and parallel temperature $T_{\parallel}(O^+)$ display much more changes (several orders of magnitude) with electromagnetic turbulence wavelength (λ_{\perp}) than density $n(O^+)$ and drift velocity $u(O^+)$.

Finally, from the profiles of lower order moments of O^+ ions are shown in Fig.(3.2), we note that the behavior of O^+ ions for each profile at low altitudes (i.e. below $4.3R_E$) coincide for all the values of λ_{\perp} , that is because the argument $\frac{a_L}{\lambda_{\perp}}$ is less than unity. For instance, the drift velocity of O^+ ions $u(O^+)$ (top right panel of Fig.(3.2)) decreases as electromagnetic turbulence wavelength (λ_{\perp}) decreases, because of the reduction of the heating rate, and the density of O^+ ions $n(O^+)$ (top left panel of Fig.(3.2)) increases as electromagnetic turbulence wavelength (λ_{\perp}) decreases to keep the escape flux constant. Also as electromagnetic turbulence wavelength (λ_{\perp}) decreases, the growth rate of $T_{\perp}(O^+)$ (bottom left panel of Fig.(3.2)) and so $T_{\parallel}(O^+)$ (bottom right panel of Fig.(3.2)) is reduced owing to the significant reduction in the heating rate above the saturation levels. Generally, the saturation level appears at low altitudes for small values of electromagnetic turbulence wavelength (λ_{\perp}) as discussed above.

3.3 H^+ ions

To study the effect of the wave particle interaction on the H^+ ions, we calculated velocity distribution function $f(H^+)$ at different altitudes extended from 1.7 to $13.7R_E$ and for different values of the perpendicular electromagnetic turbulence (λ_{\perp}), which are $\lambda_{\perp} = \infty$,

50, 20, 8, and 1km. The Barghouthi model simulation results of the H^+ ions velocity distribution function $f(H^+)$ are shown in Fig.(3.3). we supposed a wide range of λ_{\perp} as in the O^+ ions case (1st panel) $\lambda_{\perp} \rightarrow \infty$, (2nd panel) $\lambda_{\perp} = 50 \text{ km}$, (3rd panel) $\lambda_{\perp} = 20 \text{ km}$, (4th panel) $\lambda_{\perp} = 8 \text{ km}$, and (5th panel) $\lambda_{\perp} = 1 \text{ km}$.

For the case $\lambda_{\perp} \rightarrow \infty$, the diffusion coefficient (D_{\perp}) become altitude dependent and velocity independent as shown in section (3.2) for the O^+ ions case. From the simulation results for the case $\lambda_{\perp} \rightarrow \infty$ (left panel of Fig.(3.3)), we note that at the exobase (i.e. $1.7R_E$), the distribution function shows Maxwellian features, because the perpendicular diffusion coefficient $D_{\perp}(H^+)$ is very small at low altitude. As the geocentric altitude increases, the diffusion coefficient $D_{\perp}(H^+)$ increases, as shown in equation (2.11), and then the strength of WPI increases. As result, the distribution function $f(H^+)$ develops large temperature anisotropy. For example, at $5.29R_E$ there are temperature anisotropy where $T_{\parallel}(H^+) > T_{\perp}(H^+)$, but at $8.19R_E$ the temperature anisotropy inverted [i.e. $T_{\perp}(H^+) > T_{\parallel}(H^+)$]. This is because the effect of WPI increases with altitude, so as the ions drift upward the WPI heat the ions in the perpendicular direction, which yields an increasing of the perpendicular ions temperature $T_{\perp}(H^+)$ as shown in Fig.(3.4). At high altitudes, the role of the WPI become significant in heating the ions in the perpendicular directions. This causes the forming "pancake-like" distributions $T_{\perp}(H^+) > T_{\parallel}(H^+)$, that folds into H^+ conics due to the effect of mirror force (i.e. diverging magnetic field), as shown in (1st panel of Fig.(3.3)) at geocentric altitude ($\sim 8.19R_E$), which become obvious at altitude ($\sim 11.1R_E$) and above this level the conics features is saturates. This means that the general shape of the distribution function $f(H^+)$ becomes invariable with altitude.

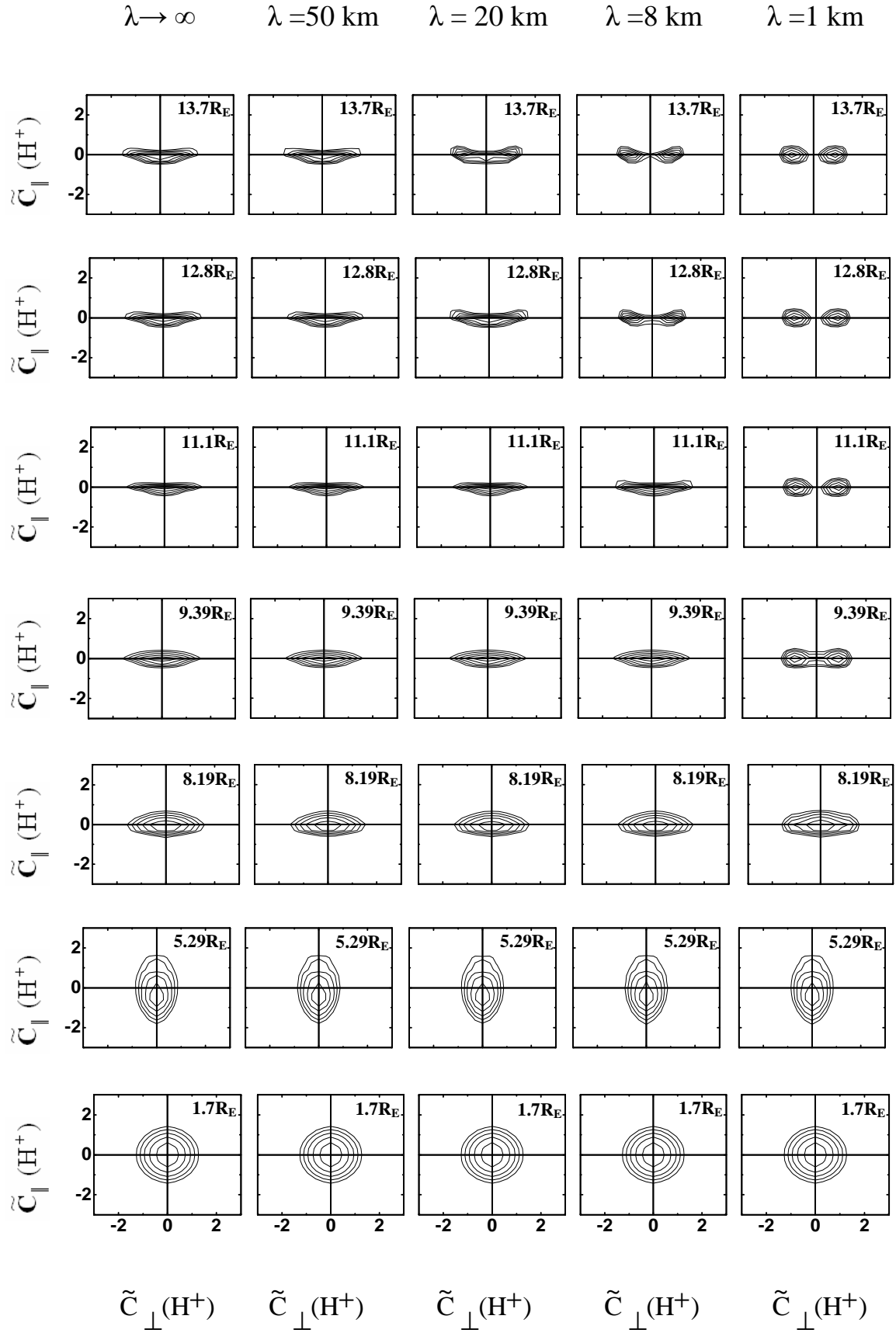


Figure 3.3: H^+ ions velocity distribution functions at different geocentric distances (1.7, 5.29, 8.19, 9.39, 11.1, 12.8, and $13.7R_E$) for different electromagnetic turbulence wavelengths (λ_\perp). The wavelengths considered here are $\lambda_\perp \rightarrow \infty$ (1st panel), $\lambda_\perp = 50 \text{ km}$ (2nd panel), $\lambda_\perp = 20 \text{ km}$ (3rd panel), $\lambda_\perp = 8 \text{ km}$ (4th panel), and $\lambda_\perp = 1 \text{ km}$ (5th panel). $f(H^+)$ is represented by equal values contours in the normalized velocity ($\tilde{c}_\parallel, \tilde{c}_\perp$) plane, where $\tilde{c} = [\mathbf{v} \cdot \mathbf{u}(H^+)] / [2kT(H^+)/m(H^+)]^{1/2}$. The contour levels decrease successively by a factor $e^{1/2}$ from the maximum.

We also note that for the case $\lambda_\perp = 50 \text{ km}$ the distribution function remains the same as the case $\lambda_\perp \rightarrow \infty$ at all geocentric altitudes (1st and 2nd panels of Fig.(3.3)). Furthermore, for the case ($\lambda_\perp = 20 \text{ km}$) the distribution function remains the same as the cases $\lambda_\perp \rightarrow \infty$ and $\lambda_\perp = 50 \text{ km}$ up to $12.8 R_E$ (1st, 2nd, and 3rd panels of Fig.(3.3)), but at high altitudes $\sim 13.7 R_E$ the distribution function begins to display toroidal features. In addition, the case $\lambda_\perp = 8 \text{ km}$ the distribution function remains the same as the cases $\lambda_\perp \rightarrow \infty$, $\lambda_\perp = 50 \text{ km}$, and $\lambda_\perp = 20 \text{ km}$ up to $\sim 11.1 R_E$ (1st, 2nd, 3rd, and 4th panels of Fig.(3.3)), but at high altitudes ($\sim 12.8 R_E$) the distribution function starts to display toroidal features, which becomes obvious at ($13.7 R_E$).

As previously discussed, at high altitudes, the ions Larmor radius (a_L) will be comparable to or exceeds the wavelength of the electromagnetic turbulence (λ_\perp). Also, as electromagnetic turbulence λ_\perp decreases, the argument $\frac{\bar{a}}{\lambda_\perp}$ approaches one at lower altitudes, and consequently the toroidal distribution appears at lower altitudes, namely for the case $\lambda_\perp = 8 \text{ km}$ at altitude $\sim 12.8 R_E$. The toroidal features become more obvious at altitude $\sim 13.7 R_E$ (4th panel of Fig.(3.3)). Moreover, for the case $\lambda_\perp = 1 \text{ km}$ the toroidal features appear at a lower altitude $\sim 9.39 R_E$, and become more pronounced at geocentric altitude $\sim 11.1 R_E$ (5th panel of Fig.(3.3)).

After forming the toroidal shape of distribution function $f(H^+)$, it becomes saturates as shown in (5th panel of Fig.(3.3)) at high altitude (i.e. $12.8R_E$ and $13.7R_E$), since the perpendicular heating becomes self-limiting.

Fig.(3.4) shows the altitude profiles for H^+ lower order moments (i.e. density $n(H^+)$, drift velocity $u(H^+)$, parallel temperature $T_{\parallel}(H^+)$, and perpendicular temperature $T_{\perp}(H^+)$) for wide range of the electromagnetic turbulence (λ_{\perp}), [$\lambda_{\perp} \rightarrow \infty$ (double-dotted dashed line), $\lambda_{\perp} = 50 \text{ km}$ (dotted dashed line), $\lambda_{\perp} = 20 \text{ km}$ (dotted line), $\lambda_{\perp} = 8 \text{ km}$ (dashed line) and $\lambda_{\perp} = 1 \text{ km}$ (solid line)].

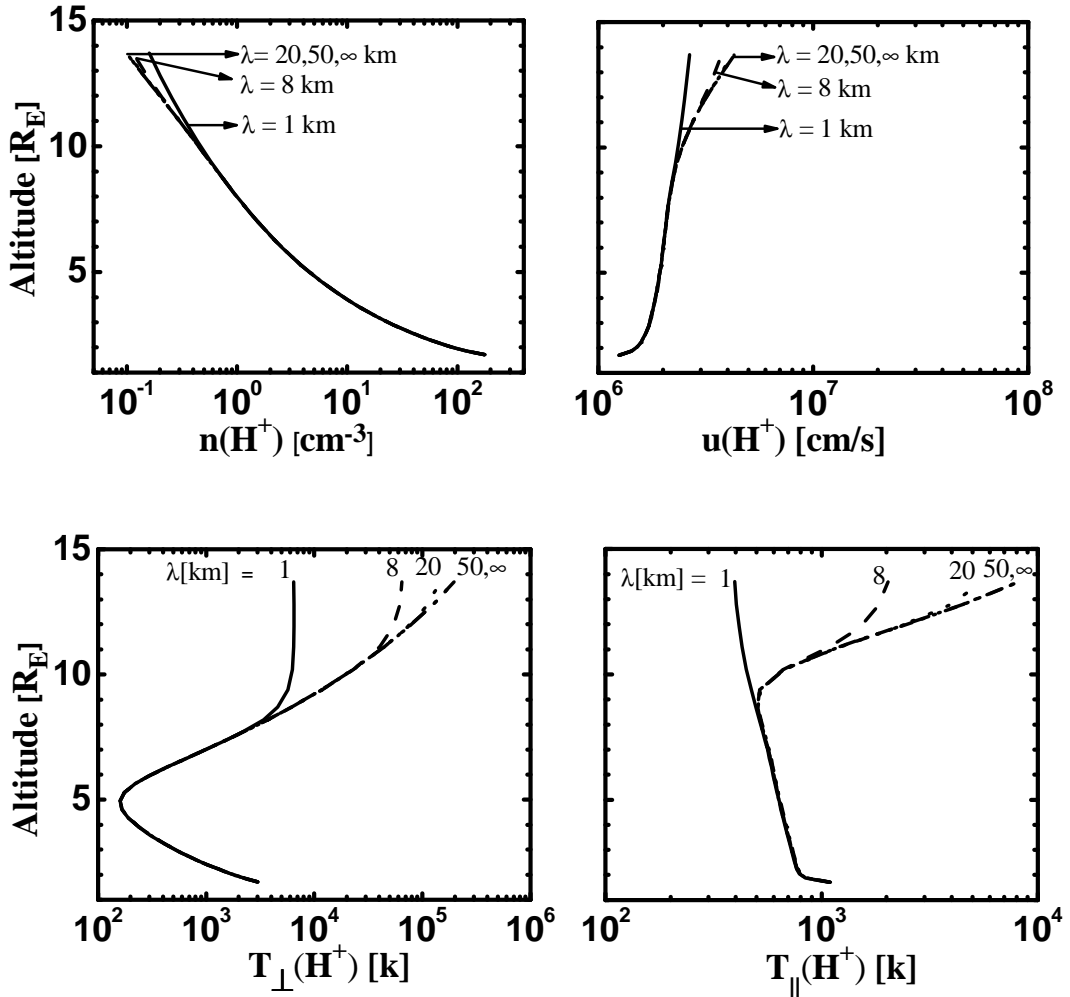


Figure 3.4: Altitude profiles of the lower order H^+ moment for different electromagnetic turbulence wavelengths (λ_{\perp}). The wavelengths considered here are $\lambda_{\perp} \rightarrow \infty$ (double-dotted dashed line), $\lambda_{\perp} = 50 \text{ km}$ (dotted dashed line), $\lambda_{\perp} = 20 \text{ km}$ (dotted line), $\lambda_{\perp} = 8 \text{ km}$ (dashed line) and $\lambda_{\perp} = 1 \text{ km}$ (solid line).

$\lambda_{\perp} = 8 \text{ km}$ (dashed line), $\lambda_{\perp} = 1 \text{ km}$ (solid line). The H^+ moments considered here are: density $n(H^+)$ (top left), drift velocity $u(H^+)$ (top right), perpendicular temperature $T_{\perp}(H^+)$ (bottom left), and parallel temperature $T_{\parallel}(H^+)$ (bottom right).

The drift velocity of H^+ ions $u(H^+)$ (top right panel of Fig.(3.4)) increases with altitude, owing to the effect of WPI and heating in the perpendicular direction, which increases the upward mirror force, and hence, accelerate the H^+ ions in the upward direction.

However, we note that, the lower order H^+ moment at low altitudes are superimposed for different values of the perpendicular electromagnetic turbulence (λ_{\perp}), which are [$\lambda_{\perp} = \infty$, 50, 20, 8, and 1km], because the argument $\frac{a_L}{\lambda_{\perp}}$ is less than unity (i.e. the behavior of H^+ ions below the saturation point is the same for all values λ_{\perp}), that is, the ion self-limiting is negligible. The cases $\lambda_{\perp} = 20, 50$, and $\infty \text{ km}$ are same as $\lambda_{\perp} \rightarrow \infty$, where the two cases are coincide for all altitudes in the simulation tube. But for the case $\lambda_{\perp} = 20 \text{ km}$, the acceleration rate decreases, and so drift velocity $u(H^+)$ decreases above the saturation point which occurs at altitude $12.0R_E$ in comparison with the case $\lambda_{\perp} \rightarrow \infty$, where the two cases are coincide for all altitude below $12.0R_E$. This is more obvious if we look at the perpendicular and parallel temperature. This is an obvious result of the energization self-limiting nature which occurs when $\frac{a_L}{\lambda_{\perp}}$ exceeds unity (i.e. above saturation point). For the case $\lambda_{\perp} = 8 \text{ km}$, we note that the saturation point appears earlier $\sim 10.5R_E$. For smaller values of electromagnetic turbulence (λ_{\perp}) (i.e. $\lambda_{\perp} = 1 \text{ km}$), $u(H^+)$ is reduced more and more and the saturation point occurs at lower altitude $\sim 7.8R_E$. These results have a close agreement with the distribution function results displayed in Fig.(3.3).

The drift velocity of H^+ ions $u(H^+)$ (top right panel of Fig.(3.4)) decreases as electromagnetic turbulence wavelength λ_{\perp} decreases, because of the reduction of the heating rate. This can be explained as follows. The expression for the diffusion coefficient D_{\perp} is a function of altitude and velocity as shown in equation (2.12). As electromagnetic

turbulence wavelength λ_{\perp} decreases. The expression $\left(\frac{k_{\perp} v_{\perp}}{\Omega}\right)^{-3}$ decreases, so the diffusion coefficient D_{\perp} decreases. As a result, the strength of WPI decreases, which means, reduction the heating rate. The density of H^+ ions $n(H^+)$ (top left panel of Fig.(3.4)) increases as electromagnetic turbulence wavelength (λ_{\perp}) decreases to keep the escape flux constant, since the H^+ ions are in the flux-limiting flow condition [Barakat and Schunk, 1983]. A corresponding increases in the ions drift velocity (top right panel of Fig.(3.4)) is expected to compensate for the decreases in the ions density (top left panel of Fig.(3.4)), and hence to keep the net escape flux constant.

Also, as electromagnetic turbulence wavelength (λ_{\perp}) decreases, the growth rate of $T_{\perp}(H^+)$ (bottom left panel of Fig.(3.4)) and so $T_{\parallel}(H^+)$ (bottom right panel of Fig.(3.4)) is reduced, owing to the significant reduction in the heating rate above the saturation levels. Generally, the saturation level appears at low altitudes for smaller values of electromagnetic turbulence wavelength (λ_{\perp}).

The behavior of H^+ ions perpendicular temperature $T_{\perp}(H^+)$ is a result of balance between WPI heating affecting in the perpendicular direction and perpendicular adiabatic cooling (i.e. $\mu = \frac{mv_{\perp}^2}{2B}$); but the H^+ ions perpendicular temperature $T_{\perp}(H^+)$ is increasing monotonically with altitude at high altitude, since the effect WPI is greater than that of perpendicular adiabatic cooling (i.e. WPI is dominant). But at low altitude the H^+ ions perpendicular temperature $T_{\perp}(H^+)$ is decreasing with altitude, since the adiabatic cooling is greater than that of the effect of WPI in the perpendicular direction.

The profiles of parallel temperature $T_{\parallel}(H^+)$ (right bottom panel of Fig.(3.4)) is influenced by WPI, where the effect of WPI have a three-fold effect on parallel temperature $T_{\parallel}(H^+)$: First, the perpendicular heating enhances the upward mirror force and consequently, the parallel adiabatic cooling is strengthened. Second, as the ions move upward along the divergent magnetic field lines, result in parallel temperature $T_{\parallel}(H^+)$ increases due to the energy transfer from the perpendicular to the parallel directions. Third,

the effect of velocity dependent diffusion coefficient, which decreases the heating in perpendicular direction, the net result of these effects determines the behavior of parallel temperature $T_{\parallel}(H^+)$.

Since H^+ ions perpendicular heating increases at high altitude, since the WPI is the dominant, which causes heating in the perpendicular directions, part of this energy is transferred from the perpendicular direction to the parallel direction, and consequently, the parallel temperature increases at high altitude, but at lower altitude H^+ ions parallel temperature $T_{\parallel}(H^+)$ decreases with altitude, since the parallel adiabatic cooling is the dominant and the effect of WPI is too weak. On the other hand, at relatively higher altitude the effect of WPI is strengthened, but parallel adiabatic cooling is still the dominant, therefore H^+ ions parallel temperature $T_{\parallel}(H^+)$ decreases slowly with altitude. However, as $T_{\perp}(H^+)$ decreases due to the effect of finite Larmor radius this also decreases the H^+ parallel temperature $T_{\parallel}(H^+)$. In general, we see that perpendicular temperature $T_{\perp}(H^+)$ and parallel temperature $T_{\parallel}(H^+)$ display much more changes (several orders of magnitude) with electromagnetic turbulence wavelength (λ_{\perp}) than density $n(H^+)$ and drift velocity $u(H^+)$.

The behavior of O^+ ions different from that of H^+ ions, under the effect of WPI. This is due to two reasons: First, the potential energy of the H^+ ions is negative and decreasing with altitude, while the potential energy for O^+ ions is positive and monotonically increasing with altitude, as we well show in chapter five, second, the diffusion coefficient of O^+ ions $D_{\perp}(O^+)$ greater than the diffusion coefficient of H^+ ions $D_{\perp}(H^+)$, and so O^+ ions is preferentially heated compared with H^+ ions.

Also, the differences between the behavior of H^+ and O^+ under the effect of finite Larmor radius can be owing to two factors: First, the mass of O^+ ion is much large comparable to that of H^+ ion [$m(O^+) = 16 \times m(H^+)$]. Second, the preferential heating of O^+ ion seemed at lower altitudes, and so the saturation levels occur earlier because of the self-limiting heating.

Chapter Four

Quantitative Comparison

4.1 Introduction

The Monte Carlo (MC) simulation was used in order to study the effect of wave particle interaction on H^+ and O^+ outflow at high altitudes and high latitudes in the polar wind region. The MC technique considered WPI in addition to the mechanisms included in the classical polar wind studies such as gravity, polarization electrostatic field, and divergence of magnetic field of the Earth. In this study the Monte Carlo simulation was run for Barghouthi model, where the perpendicular diffusion coefficient $D_{\perp}(r, v_{\perp})$ is given in equation (2.12), and in each simulation we used 10^7 tested ions in order to compute the ion distribution function and also compute the profiles of its velocity moments (i.e. density, drift velocity, parallel temperature, and perpendicular temperature) for both H^+ and O^+ ions. The boundary conditions selected for polar wind region are similar to those of [Barghouthi et al., 1998].

From the year of 1968 (i.e. over the past 40 years), since the seminal papers of Nishida, [1966] and others Axford, [1968], Banks and Holzer, [1968], and Marubashi, [1970], observations from several polar orbiting satellites have confirmed the existence of the polar wind and established its basic characteristics (i.e. density, velocity, temperature).

Statistical studies or surveys of polar wind ion observations using data from ten or more satellite orbit passes, these observations were made from the ISIS-2, DE-1, Akebono, and POLAR satellites over the altitude range of 1,000 to 50,500 km (i.e. 1.16 to $9R_E$) and spanned different phases of solar cycle. The polar wind ion observations made on all four satellites, the ISIS-2 and DE-1 observations covered the 1,000 – 4,000 km altitude range, but the POLAR observations were made at solar minimum, and were made over one year

period. Also, it focused on the altitude ranges 5,000 – 6,000 km and 29,000 – 50,500 km altitude (i.e. near the POLAR perigee and apogee) region, respectively. The Akebono observations were made over a 10-year period spanning two 11-year solar cycles, and focused on the altitude range 1,000 –10,000 km. Table (4.1) summarizes the properties of some polar wind satellites.

Table 4.1: summarizes the properties of some polar wind satellites

| Altitude(km) | Satellite | Epoch | Observed Species | Reference |
|----------------|-----------|-----------|-----------------------|-------------------------------|
| 1,400 | ISIS-2 | 1971–1972 | H^+, He^+, O^+ | Hoffman,1980 |
| 1,000 – 4,000 | DE-1 | 1981–1983 | H^+, He^+, O^+ | Chandler,1991, 1995 |
| 1,000 – 10,000 | Akebono | 1989–1998 | H^+, He^+, O^+, e^- | Abe, 1993, 2004; Yau, 1995 |
| 5,000 – 6,000 | POLAR | 1996 | H^+, O^+ | Su, 1998; Huddleston, 2005 |
| 7,000 – 23,300 | DE-1 | 1981–1982 | e^- | Persoon 1983 |
| 50,500 | POLAR | 1996 | H^+, He^+, O^+ | Su, 1998; Elliott, 2001 |

In this thesis, we focus on the observations over the altitude range of 4,438 to 80,518 km (i.e. from $1.7R_E$ to $13.7R_E$), which is the simulation tube in the Monte Carlo technique. For the sake of comparison, we chose to present the simulation results of Barghouthi model for the perpendicular electromagnetic turbulence wave length ($\lambda_{\perp} = 8km$), since these simulation results represent the closest to the observations, which obtained from different satellites.

In this study, we compared between the simulation results of Barghouthi model to the corresponding observations from different satellites and simulation result from previous models. Also, we classify our comparison into two chapters: Chapter four presents quantitative comparison (section 4.2), and chapter five presents qualitative comparison (section 5.1).

4.2 Quantitative comparison

In this section, we present the quantitative characteristics of the polar wind ions (i.e. O^+ and H^+ ions) from different satellite observations and some simulation results from previous models.

Nagai et al. [1984] observed cold (i.e. <1 eV temperature) H^+ polar wind ions in the nightside polar cap near $2R_E$ altitude using DE-1 satellite. This study confirmed the supersonic nature of the H^+ polar wind at high altitudes, and motivated the survey of Chandler et al. [1991] using DE-1 data and that of Abe et al. [1993a, 2004] using Akebono data.

At high ($\sim 2 R_E$) altitude outside the plasmasphere, where the polar wind ions density was typically less than 10^3 cm^{-3} and the DE-1 spacecraft was often charged to a few positive volts, and this causes the lowest energy polar wind ions to be repelled by the spacecraft potential. But Nagai et al. [1984] used a negative bias aperture in the DE-1 RIMS instrument to partially overcome the positive spacecraft potential, and successfully detected both H^+ and He^+ polar wind ions down to about zero eV. As a result, the velocity of H^+ ions ranges from 16 to 25 km/s and their temperature ranges from 0.12 to 0.2 eV. Chandler et al. [1991] concluded that, the averaged H^+ polar wind velocity observed on DE-1 increased with altitude, from about ~ 3.5 km/s below $1.32R_E$ to ~ 11 km/s above $1.5R_E$.

The data collected from Akebono satellite used by Abe et al. [1993a], and they concluded that the dayside and nightside profiles were qualitatively similar for all three polar wind species (i.e. H^+ , He^+ , and O^+ ions); approximately monotonic increase in velocity with altitude and the velocity of these ions dependent on their masses. The H^+ velocity typically reached 1 km/s near $1.32R_E$ and the O^+ velocities near $1.95R_E$. This means that the O^+ ions attain significant average upward velocity at higher altitudes compared with H^+ ions. Also they concluded that, for all three polar wind ions, the velocity on the dayside was significantly larger than that on the nightside. In addition, they obtained the H^+ and O^+ velocity at $2.58R_E$ to be about 12 and 3 km/s, respectively.

The survey of Abe et al. [1993a] found the observed ion velocity of all polar wind species to be highly variable, and the O^+ polar wind ions above $1.79R_E$ to have upward velocity up to 4km/s.

Drakou et al. [1997] observed downward flowing He^+ and O^+ ions with a net downward velocity less than 1.5 km/s below $2.1R_E$ on the nightside, the contribution of the perpendicular ion velocity component, downward flowing He^+ and O^+ ions were clearly present in the polar cap, but were less frequent with increasing altitude compared with their upward flowing counterparts.

Su et al. [1998] used data from POLAR satellite at 5,000km (i.e. $1.79R_E$) altitude and they found the following characteristics of the H^+ polar wind ion at this altitude: Its density ranged from less than 0.1 to 100cm^{-3} , and its average was 10cm^{-3} ; the parallel velocity ranged from 10 to 21km/s, and its average was $\sim 15\text{km/s}$; and the averaged parallel and perpendicular temperature was ~ 0.12 and $\sim 0.23\text{eV}$, respectively.

In addition, to properties H^+ ions, Su et al. [1998] obtained the following characteristics of the O^+ ions at 5000km. The O^+ density ranged from 0.1 to 100cm^{-3} , and its average was 7.7cm^{-3} ; its parallel velocity ranged from -3 to 2km/s and its average was -0.9km/s , which means that the ions moving downward, were both upward and downward velocities are observed; finally, its averaged parallel and perpendicular temperature was ~ 0.34 and $\sim 0.61\text{eV}$, respectively.

Furthermore, Su et al. [1998] used data from POLAR satellite at 50,500 km (i.e. $9R_E$) altitude and they obtained the following characteristics of the H^+ and O^+ polar wind ion at this altitude. First, for H^+ ions, the H^+ density ranged from 0.01 to 2cm^{-3} and its average was $\sim 0.3\text{cm}^{-3}$; its parallel velocity ranged from 20 to 110 km/s and its average was ~ 45 km/s; and its averaged perpendicular temperature was ~ 1.1 eV. Second, for O^+ ions, the O^+ parallel velocity ranged from 8 to 32 km/s, and its average was ~ 17 km/s, which means that all observed velocities were upward at the POLAR apogee.

Su et al. [1998] surveyed the characteristics of H^+ and O^+ polar wind ions on POLAR satellite at 44,380km (i.e. $8 R_E$) altitude over the polar cap, and found the averaged O^+

velocities to be ~ 27 km/s. This large velocities reflect the continuing acceleration of the polar wind at very high altitudes due to a number of mechanisms.

The major polar wind ions consist primarily from H^+ , He^+ , and O^+ ions and have a significant drift velocity component in the upward direction (opposite to the magnetic field in the northern hemisphere), the averaged parallel velocity at high altitude for H^+ ion is 14km/s at altitude range $2.26-2.42R_E$, Drakou et al. [1997].

Yau et al. [2007] reviewed the polar wind models and observations, and they conclude that the generalized transport equations based models predict that the supersonic H^+ ions flow at high altitudes at velocity as large as 16-20km/s at or below $2.9R_E$. In addition, Drakou et al. [1997] and Su et al. [1998] observed from satellites that the temperature of polar wind ions (i.e. H^+ and O^+ ions) is generally low, and is in the range of 0.05–0.35 eV between 2.1 and $2.58R_E$.

Recently, Nilsson et al. [2008] demonstrated that, the velocity of O^+ ion at $5R_E$ is about 20km/s; they used this value as an initial value of the O^+ ion velocity in their model.

Finally, we compared between the above observations and simulation results of Barghouthi model, for both H^+ ion observations and O^+ ion observations. The comparison is summarized in the following two tables; Table (4.2) shows the comparison for H^+ ions, and Table (4.3) shows the comparison for O^+ ions.

The simulation results of Barghouthi model are obtained from; the profiles of the distribution function velocity moments (i.e. density, drift velocity, parallel temperature, and perpendicular temperature) for both H^+ and O^+ ions (i.e. Fig.(4.1)), the altitude profile of ions temperatures (i.e. Fig.(4.2) for both H^+ and O^+ ions), the altitude profile of ions velocity for both H^+ and O^+ ions (i.e. Fig.(4.3)), and altitude profile of ions parallel velocity for both H^+ and O^+ ions (i.e. Fig.(4.4)).

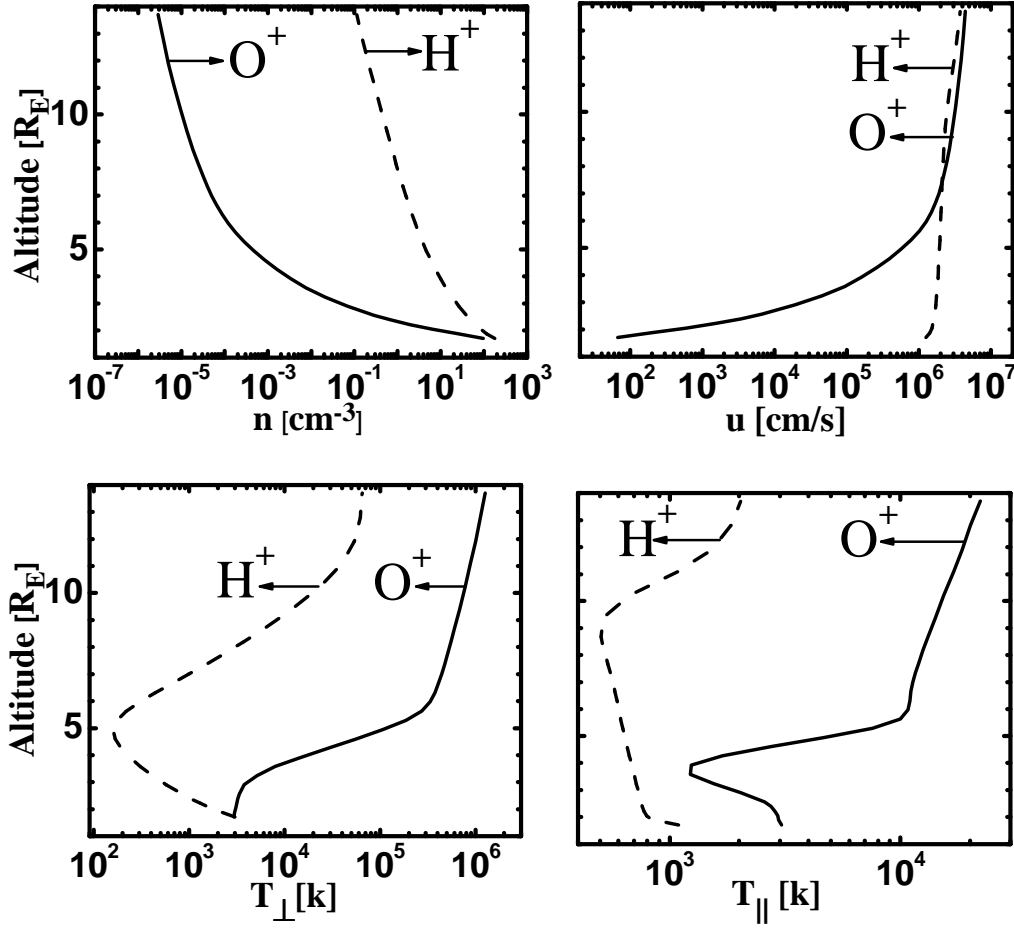


Figure 4.1: Altitude profiles of the lower order moment for the electromagnetic turbulence wavelength $\lambda_{\perp} = 8km$, for O^+ ions (solid line) and H^+ ions (dashed line). The moments considered here are: density $n[cm^{-3}]$ (top left), drift velocity $u[cm/s]$ (top right), perpendicular temperature $T_{\perp}[k]$ (bottom left), and parallel temperature $T_{\parallel}[k]$ (bottom right).

The ion velocity vector can be analyzed into two orthogonal components, with respect to the direction of the magnetic field (\mathbf{B}_o), these two components are: one parallel to (\mathbf{B}_o), which represented by (\mathbf{v}_{\parallel}) and the other perpendicular to (\mathbf{B}_o) which represented by (\mathbf{v}_{\perp}).

Therefore, it is recommended to write:

$$\mathbf{v} = \mathbf{v}_{\parallel} + \mathbf{v}_{\perp} \quad (4.1)$$

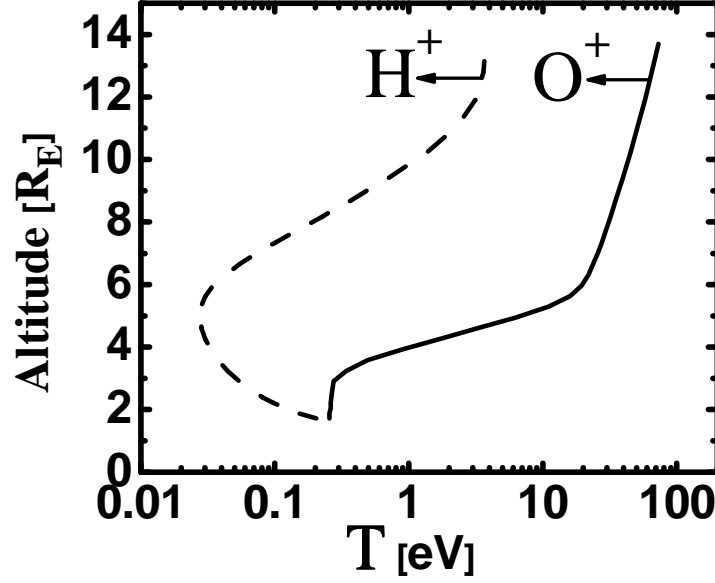


Figure 4.2: Altitude profile of ions temperatures for O^+ ions (solid line) and H^+ ions (dashed line), according to Barghouthi model and for the electromagnetic turbulence wavelength $\lambda_{\perp} = 8km$.

The random thermal velocity is defined as $\mathbf{c}_s = \mathbf{v}_s - \mathbf{u}_s$. From the expectation value of the kinetic energy ($\frac{1}{2}mc_s^2$), we can obtain the thermal energy ($\frac{3}{2}kT_s$), [Barghouthi et al., 2003]

$$\frac{3}{2}kT_s = \frac{\int \frac{1}{2}m_s \left[(v_{\parallel s} - u_s)^2 + v_{\perp s}^2 \right] f_s(v_s) d^3v_s}{\int f_s(v_s) d^3v_s} \quad (4.2)$$

from the above equation (i.e. equation (4.2)), we can simplify it to obtain equation (4.3):

$$\frac{3}{2}kT = \frac{1}{2}m(v^2 - u^2) \quad (4.3)$$

Therefore, the velocity of the ions is given by:

$$v = \sqrt{\frac{3kT + mu^2}{m}} \quad (4.4)$$

In addition, to derive the parallel velocity of the ions, equation (4.2) can be written as [Barghouthi et al., 2003]:

$$\frac{1}{2}kT_{\parallel s} + kT_{\perp s} = \frac{\int \frac{1}{2}m_s(v_{\parallel s} - u_s)^2 f_s(v_s) d^3v_s}{\int f_s(v_s) d^3v_s} + \frac{\int \frac{1}{2}m_s v_{\perp s}^2 f_s(v_s) d^3v_s}{\int f_s(v_s) d^3v_s} \quad (4.5)$$

From equation (4.5), we can write the following equation:

$$\frac{1}{2}kT_{\parallel s} = \frac{\int \frac{1}{2}m_s(v_{\parallel s} - u_s)^2 f_s(v_s) d^3v_s}{\int f_s(v_s) d^3v_s}, \quad (4.6)$$

and the above equation can be simplified to obtain equation (4.7)

$$\frac{1}{2}kT_{\parallel s} = \frac{1}{2}m \mathbf{v}_{\parallel}^2 - \frac{1}{2}mu^2 \quad (4.7)$$

Therefore, the parallel velocity of the ions is given by:

$$\mathbf{v}_{\parallel} = [(kT_{\parallel s} + m u^2)/m]^{1/2} \quad (4.8)$$

Finally, we calculated the velocity and parallel velocity for both H^+ and O^+ ions at all geocentric altitude in the simulation tube. After that we plot the altitude profile of the ions velocity as shown in Fig.(4.3), and the altitude profile of the ions parallel velocity as shown in Fig.(4.4).

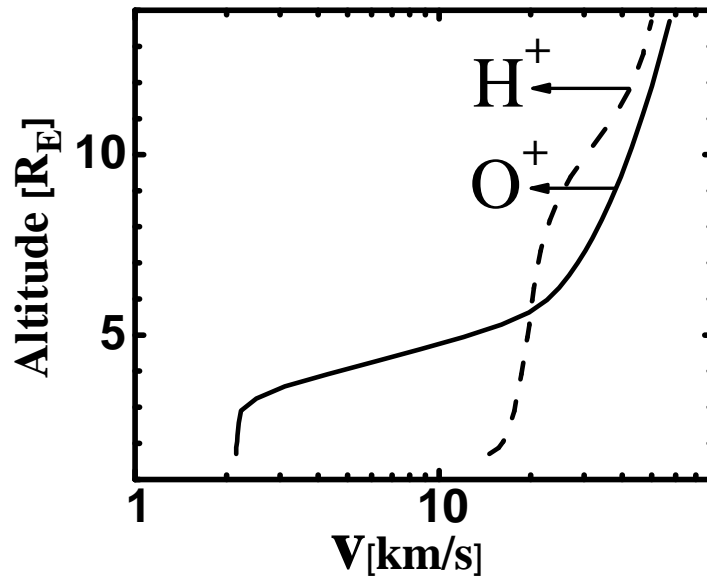


Figure 4.3: Altitude profile of ions velocity, for O^+ ions (solid line) and H^+ ions (dashed line), according to Barghouthi model and for the electromagnetic turbulence wavelength $\lambda_{\perp} = 8km$.

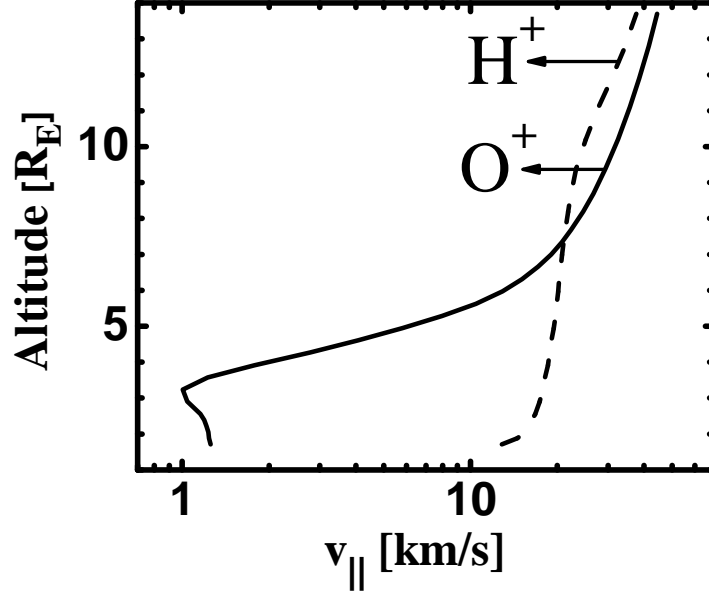


Figure 4.4: Altitude profile of ions parallel velocity, for O^+ ions (solid line) and H^+ ions (dashed line), according to Barghouthi model and for the electromagnetic turbulence wavelength $\lambda_{\perp} = 8km$.

The following two tables summarize the quantitative comparison between the observations and the simulation results of Barghouthi model for both H^+ ions (i.e. Table (4.2)) and O^+ ions (i.e. Table (4.3)), which gives evidence for Barghouthi model.

We can see from these two tables that the simulation results of Barghouthi model in an excellent agreement with observations from different satellites for both O^+ and H^+ ions for the following quantity: density, velocity, parallel velocity, parallel temperature, perpendicular temperature, temperature, and temperature anisotropy at different altitudes. As an example, Su et al. [1998] obtained the temperature of H^+ ions at $4.2R_E$ to be 0.02eV from observations. To be specific, Barghouthi model produced similar results to the observations of Su et al. [1998], where the temperature of H^+ ions at $4.2R_E$ is 0.03eV as obtained from Barghouthi model. Another example, Su et al. [1998] found that, the parallel velocity of O^+ ions at $9R_E$ in the range (8 – 32km/s), this is consistent with the simulation results of Barghouthi model, where the parallel velocity equal to 27.5km/s at $9R_E$. Therefore, Barghouthi model produce acceptable simulation results when compared quantitatively to the corresponding observations for both O^+ and H^+ ions when $\lambda_{\perp} = 8km$.

Table 4.2: Comparison between the observations and simulation results of Barghouthi model for H^+ ions.

| Altitude (R_E) H^+ ions | Characteristics | Observations | Barghouthi model |
|----------------------------------|--|---|---------------------|
| $1.79R_E$ | Density n (cm^{-3}) | (0.1 - 100), [Su et al., 1998] | 100 |
| $9.0R_E$ | Density n (cm^{-3}) | (0.01 - 2), [Su et al., 1998] | 0.7 |
| $1.7R_E$ | Velocity v (km/s) | 11, [Chandler et al., 1991] | 15.2 |
| $2.0R_E$ | Velocity v (km/s) | (16 – 25), [Nagai et al., 1984] | 16.1 |
| $2.58R_E$ | Velocity v (km/s) | 12, [Abe et al., 1993a] | 17.2 |
| $2.89R_E$ | Velocity v (km/s) | (16 – 20), [Generalized transport models] | 17.8 |
| $1.79R_E$ | Parallel velocity v_{\parallel} (km/s) | (10 – 21), [Su et al., 1998] | 13.4 |
| $2.26R_E - 2.42R_E$ | Parallel velocity v_{\parallel} (km/s) | 14 [Drakou et al., 1997] | 16.1 |
| $9.0R_E$ | Parallel velocity v_{\parallel} (km/s) | (20 – 110), [Su et al., 1998] | 22.8 |
| $1.79R_E$ | Perpendicular Temperature (eV) T_{\perp} | 0.23, [Su et al., 1998] | 0.22 |
| $9.0R_E$ | Perpendicular Temperature (eV) T_{\perp} | 1.1, [Su et al., 1998] | 0.7 |
| $1.79R_E$ | Parallel Temperature (eV) T_{\parallel} | 0.12, [Su et al., 1998] | 0.082 |
| $2.0R_E$ | Temperature T (eV) | <1, [Nagai et al., 1984] | 0.15 |
| $2.0R_E$ | Temperature T (eV) | 0.12 – 0.2), [Nagai et al., 1984] | 0.15 |
| $2.1R_E - 2.58R_E$ | Temperature T (eV) | (0.05 – 0.35), [Drakou et al., 1997 and Su et al., 1998] | (0.11-0.07) |
| $4.2R_E$ | Temperature T (eV) | 0.02, [Su et al., 1998] | 0.03 |
| $1.78R_E$ | $(T_{\parallel} / T_{\perp})$ | 0.52, [Su et al., 1998] | 0.37 |

Table 4.3: Comparison between the observations and simulation results of Barghouthi model for O^+ ions.

| Altitude (R_E) O^+ ions | Characteristics | Observations | Barghouthi model |
|----------------------------------|--|--|---------------------|
| $1.79R_E$ | Density n (cm^{-3}) | (0.1-100), [Su et al., 1998] | 30 |
| $1.79R_E$ | Velocity v (km/s) | 4, [Abe et al., 1993a] | 2.15 |
| $1.95R_E$ | Velocity v (km/s) | 1, [Su et al., 1998] | 2.2 |
| $2.1R_E$ | Velocity v (km/s) | 1.5, [Drakou et al., 1997] | 2.2 |
| $2.58R_E$ | Velocity v (km/s) | 3, [Abe et al., 1993a] | 2.3 |
| $5.0R_E$ | Velocity v (km/s) | 20, [Nilsson et al., 2008] | 14 |
| $8.0R_E$ | Velocity v (km/s) | 27, [Su et al., 1998] | 33 |
| $1.79R_E$ | Parallel velocity v_{\parallel} (km/s) | (-3 – 2), [Su et al., 1998] | 1.3 |
| $9.0R_E$ | Parallel velocity v_{\parallel} (km/s) | (8 – 32), [Su et al., 1998] | 27.5 |
| $1.79R_E$ | Perpendicular Temperature (eV) T_{\perp} | 0.61, [Su et al., 1998] | 0.28 |
| $1.79R_E$ | Parallel Temperature (eV) T_{\parallel} | 0.34, [Su et al., 1998] | 0.28 |
| $2.1R_E - 2.58R_E$ | Temperature T (eV) | (0.05 – 0.35), [Drakou et al., 1997 and Su et al., 1998] | 0.25 |
| $1.78R_E$ | $(T_{\parallel} / T_{\perp})$ | 0.55, [Su et al., 1998] | 0.95 |

Chapter Five

Qualitative Comparison

5.1 Qualitative comparison

In this section, we present the qualitative characteristics of the polar wind ions (i.e. O^+ and H^+ ions) from various satellite observations and simulation results from previous models. Also, the qualitative comparison between the simulation results of Barghouthi model from one hand and observations and simulation results on the other hand has been investigated.

The simulation results of Barghouthi model are obtained from: the profiles of the distribution function moments (i.e. density, drift velocity, parallel temperature, and perpendicular temperature) for both H^+ and O^+ ions (i.e. Fig.(4.1)), altitude profile of ions temperatures for both H^+ and O^+ ions (i.e. Fig.(4.2)), altitude profile of ions velocity for both H^+ and O^+ ions (i.e. Fig.(4.3)), altitude profile of ions parallel velocity for both H^+ and O^+ ions (i.e. Fig.(4.4)), altitude profile of ions potential energy for both H^+ and O^+ ions (i.e. Fig.(5.1)), altitude profile of ions temperature anisotropy ($T_{\perp} / T_{\parallel}$) for both H^+ and O^+ ions (i.e. Fig.(5.2)), altitude profile of ions temperature anisotropy ($T_{\parallel} / T_{\perp}$) for both H^+ and O^+ ions (i.e. Fig.(5.3)), and altitude profile of ions energy for both H^+ and O^+ ions (i.e. Fig.(5.4)).

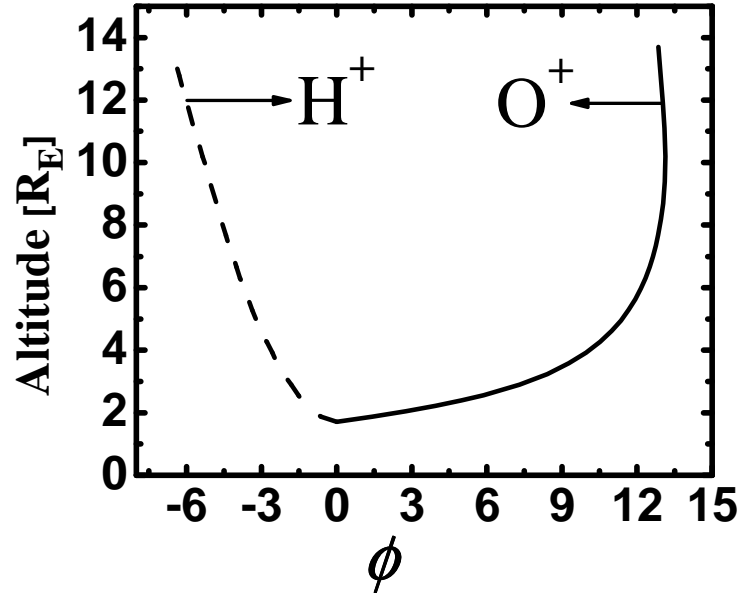


Figure 5.1: Altitude profile of ions potential energy (ϕ) due to the body force for O^+ ions (solid line) and H^+ ions (dashed line), according to Barghouthi model and for the electromagnetic turbulence wavelength $\lambda_{\perp} = 8km$.

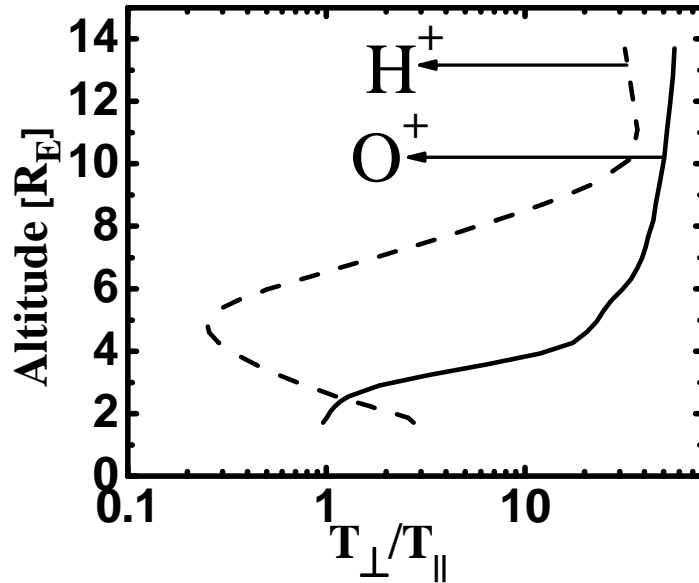


Figure 5.2: Altitude profile of ions temperature anisotropy (T_{\perp}/T_{\parallel}) for O^+ ions (solid line) and H^+ ions (dashed line), according to Barghouthi model and for the electromagnetic turbulence wavelength $\lambda_{\perp} = 8km$.

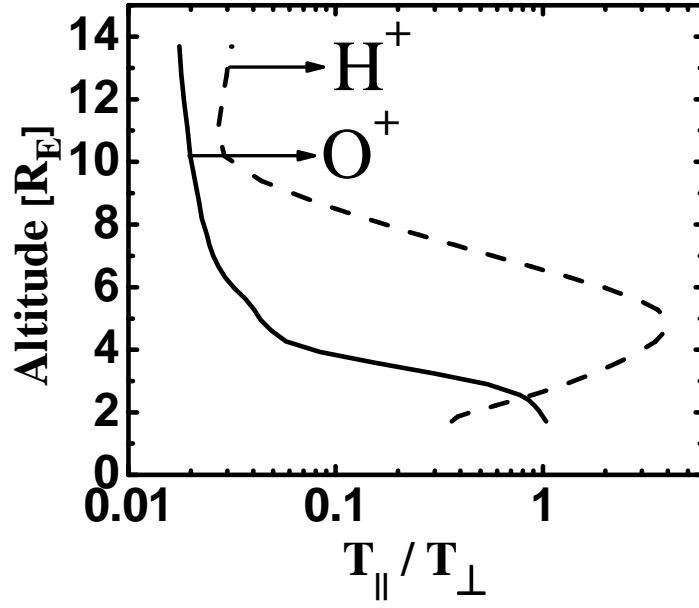


Figure 5.3: Altitude profile of ions temperature anisotropy ($T_{\parallel} / T_{\perp}$), for O^+ ions (solid line) and H^+ ions (dashed line), according to Barghouthi model and for the electromagnetic turbulence wavelength $\lambda_{\perp} = 8km$.

Since the Lorentz force operates in the direction perpendicular to velocity vector (v_{\perp}), therefore there is no work done on the ion and the total energy of the ion that is moving along the magnetic field lines remains constant, [Tsurutani and Lakhina, 1997].

$$E_T = \frac{1}{2}mv^2 = \frac{1}{2}mv_{\parallel}^2 + \frac{1}{2}mv_{\perp}^2 = E_{\parallel} + E_{\perp} \quad (5.1)$$

where E_T , E_{\parallel} and E_{\perp} are the total, parallel, and perpendicular kinetic energy of the ion respectively. On the other hand, the total energy of the ion is given by:

$$E_T = \frac{1}{2}mv^2 = \frac{3}{2}kT \quad (5.2)$$

where m , v , and T are the mass, velocity, and temperature of the ions, respectively, and k is the Boltzmann's constant. Therefore, we find the energy of the polar wind ions (i.e. O^+ and H^+) at different altitudes in the simulation region, after that we plot altitude profile of ions energy for both H^+ and O^+ ions (i.e. Fig.(5.4)).

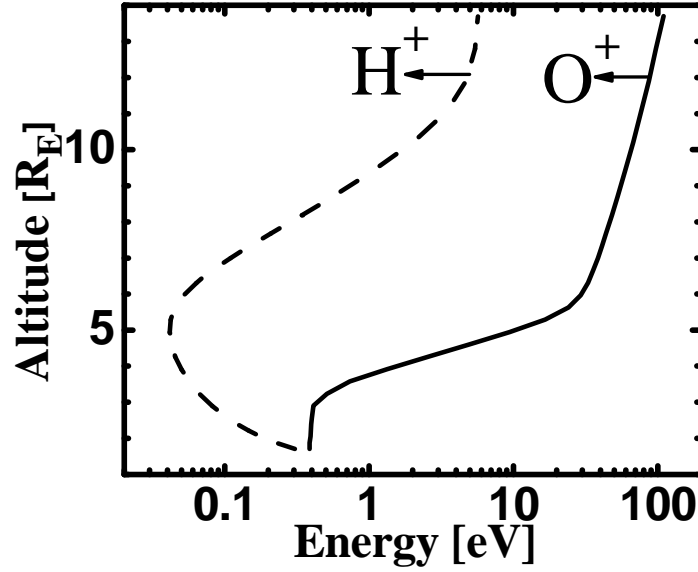


Figure 5.4: Altitude profile of ions energy for O^+ ions (solid line) and H^+ ions (dashed line), according to Barghouthi model and for the electromagnetic turbulence wavelength $\lambda_{\perp} = 8km$.

Finally, the polar wind ions consider supersonic if their thermal velocity greater than their velocity, were the thermal velocity for both O^+ and H^+ ions are given by:

$$\frac{1}{2}mv_{th}^2 = \frac{3}{2}kT \quad (5.3)$$

Therefore, the thermal velocity is given by:

$$v_{th} = \sqrt{\frac{3kT}{m}} \quad (5.4)$$

where m is the mass the ions, T is the temperature of the ions at the lower boundary (i.e. $1.7R_E$), and k is the Boltzmann's constant, Therefore, v_{th} reads

$$v_{th} = \begin{cases} 8.62km/s & \text{for } H^+ \\ 2.16km/s & \text{for } O^+ \end{cases} \quad (5.5)$$

On the other hand, the velocity of the polar wind ions can be obtained from Fig.(4.3) at any altitude in the simulation region, which extends from 1.7 to $13.7R_E$.

The qualitative comparisons between the simulation results of Barghouthi model and observations give evidences that Barghouthi model described in this thesis is appropriate to

be used when modeling the heating of ions through the wave particle interaction with electromagnetic turbulence in the polar wind region.

Experimental verification from different satellites and simulation results from different models that confirmed Barghouthi model predictions are given as follow: In the model of Lemaire and Scherer [1971], the potential difference between 1.32 and 4.15 R_E was about 1.7V. This resulted in the acceleration of the H^+ ions to above supersonic velocities, and the transition from O^+ ions dominant to H^+ ions dominant occurs above 1.87 R_E . This result is agreement with the simulation results from Barghouthi model as shown in Fig.(4.1), where the density for O^+ ions is smaller than that for H^+ ions above 1.7 R_E , where the density for both O^+ and H^+ ions at 1.87 R_E equals to 19 and 120 cm^{-3} , respectively. So the H^+ ion is the major species above 1.87 R_E .

After few years, Hoffman and Dobson [1980] concluded that the polar wind is composed primarily of electrons and ions (i.e. H^+ , He^+ and O^+), which varies with the solar cycle, and is dominated in density by O^+ ions up to at least 1.63 R_E and perhaps 1.95 –2.1 R_E . This result is agreement with the results of Barghouthi model, which produce the density of O^+ and H^+ ions at 1.95 R_E to be 20 and 110 cm^{-3} , respectively. Also, at 2.1 R_E the density of O^+ ions is 3.2 and that for H^+ ions is 79 cm^{-3} . Therefore, above 1.7 R_E the H^+ ions is the dominant, as shown in Fig.(4.1). After that, Abe et al. [1993a] concluded that, the transition from dominant O^+ ions at low altitudes to dominant H^+ ions at high altitudes is expected to occur between 1.63 R_E and 2.18 R_E , depending on the neutral hydrogen density, since the dominant source of polar wind H^+ ion is the accidental-resonant charge exchange reaction between hydrogen atoms and oxygen ions. This result agreement with the results of Barghouthi model, where H^+ is the major ion above 1.7 R_E , as shown in Fig.(4.1). The density of O^+ and H^+ ions at 2.18 R_E are 1.4 and 59 cm^{-3} , respectively, so above 2.18 R_E the H^+ is the dominant and the transition from dominant O^+ ions to dominant H^+ ions occurs below 1.7 R_E .

In the 16-moment model of Demars and Schunk [1994], which included H^+ , He^+ , and O^+ ions as major species and a number of other ions as minor species, in the supersonic case, the H^+ density decreasing with increasing altitude. To be specific, the simulation results from Barghouthi model is consistent with the results predicted from in the 16-moment model of Demars and Schunk [1994], where the density of H^+ ions decreasing almost

linearly with increasing altitude, which decreases from 180 to 25cm^{-3} when altitude increases from 1.7 to $3R_E$. Also, it decreases to 0.13 cm^{-3} at $13.7R_E$, as shown in Fig.(4.1). Furthermore, the H^+ ions are supersonic above $1.7R_E$.

In addition, observations from the POLAR satellite, especially near the POLAR satellite apogee (i.e. near $9R_E$), the density of the polar wind ions was very low (typically $< 10\text{cm}^{-3}$), Moore et al. [1995]. This result is consistent with the results obtained by Barghouthi model, where we obtained the density for both O^+ and H^+ ions at $9R_E$ equals to 6×10^{-5} and 0.7cm^{-3} , respectively, where the density for both ions is very low.

On the other hand, the composition ratio of the observed density and velocity between H^+ , O^+ provides interesting insight into the relative energy gains of the polar wind ion species. Su et al. [1998] found good correlation between the densities of the polar wind ion species and between their parallel velocities. On average, $n(H^+) : n(O^+) \sim 1 : 0.17$ and $v_{\parallel}(H^+) : v_{\parallel}(O^+) \sim 1 : 0.38$. The results from Barghouthi model for the density ratio between the H^+ and O^+ ions is $n(H^+) : n(O^+) \sim 1 : 0.1$ at $2R_E$, which is consistent with that result obtained by Su et al. [1998]. Also, the parallel velocity ratio between the H^+ and O^+ ions at $5R_E$, which is calculated by using Barghouthi model, is given as $v_{\parallel}(H^+) : v_{\parallel}(O^+) \sim 1 : 0.31$, which is very similar to the observation especially at $5R_E$.

Furthermore, Su et al. [1998] concluded that the observation from POLAR satellite near solar minimum shows that the polar wind is dominated by H^+ ions at $9R_E$, in terms of density and the He^+ ions are a minor constituent at this altitude. On the other hand, Barghouthi model simulation results obtained the densities of O^+ and H^+ ions at $9R_E$ to be 1.6×10^{-5} and 0.7cm^{-3} , respectively. So, at this altitude H^+ ion is the dominated species of the polar wind ions, as shown in Fig.(4.1), this result is consistent with observation. Moreover, the density of the O^+ polar wind ions was an order of magnitude smaller than of the H^+ polar wind ions in the geocentric altitude ($4.5 - 7.8R_E$), Elliott et al. [2001]. To be specific, this result is in a close agreement with the simulation result obtained from Barghouthi model, where the density for O^+ ions is smaller than that for H^+ ions in the altitude range ($4.5 - 7.8R_E$) as shown in Fig.(4.1). From Fig.(4.1) we note that the density for both O^+ and H^+ ions at $6R_E$ equals to 1.1×10^{-4} and 2.5cm^{-3} , respectively. Also, Yau et al. [2007] demonstrated from previous papers, at high altitude ($\sim 2 R_E$) outside the plasmasphere that the density of the polar wind ions was typically less than 10^3 cm^{-3} . This

result is consistent with the results of Barghouthi model, which produce the density of O^+ and H^+ ions at $2R_E$ to be about 13cm^{-3} and 100cm^{-3} respectively, which are less than 10^3cm^{-3} .

At high altitude, the median electron density follows a power law relationship with geocentric altitude with a power law index of -3.85 , (i.e., $n_e \propto R^\alpha$) where $\alpha = -3.85 \pm 0.32$, and the electron density ranges from ~ 35 to $\sim 1\text{ cm}^{-3}$ when altitude ranges from 2.1 to $4.66R_E$ altitude, which cause an approximately linear increase in the polar wind ion velocity with geocentric altitude over $(2.1 \text{ to } 4.66R_E)$ altitude range, Persoon et al. [1983]. On the other hand, Barghouthi model results show the increase of velocity for both O^+ and H^+ ions with geocentric altitude is approximately linear in the altitude range $(2.1 \text{ to } 4.66R_E)$, as shown in Fig.(4.3). This result is consistent with the observation obtained from different satellites.

The O^+ velocity increases from $<1\text{ km/s}$ to a few km/s at high altitudes, Barakat and Schunk [1983]. This is consistent with simulation result from Barghouthi model, where the O^+ velocity increases from 2.15 to 13km/s , when altitude varies from 1.7 to $5R_E$, owing to the effect of WPI and heating in the perpendicular directions.

Also, the 16-moment models of Ganguli et al. [1987] and Demars and Schunk [1989] predicted that the velocity of the H^+ polar wind ions was as large as $16 - 20\text{ km/s}$, at high altitudes. This result is agreement with the simulation results obtained from Barghouthi model, where the H^+ velocity varies from 15 to 23.7km/s , when altitude varies from 1.7 to $8R_E$, and it is equal to 18km/s at $2.89R_E$, as shown in Fig.(4.3).

Abe et al. [1993a] found that the observed ion velocity of all species of the polar wind to be highly variable in the altitude range $(1.16 - 2.58R_E)$, this consistent with Barghouthi model results, where the O^+ velocity varies from 2.2 to 2.3km/s , when altitude varies from 1.7 to $2.58R_E$. Also, the H^+ velocity varies from 15.5 to 18km/s , when altitude varies from 1.7 to $2.58R_E$. Therefore, this agreement with observation, where the velocity of the polar wind ions is highly variable. This suggested significant upward O^+ polar wind flow, contrary to classical polar wind theory predictions, and motivated the interest on the O^+ component of the polar wind in the subsequent studies of Chandler [1995] and of Su et al. [1998]. Also, Abe et al. [1993a] demonstrated that the velocity of polar wind ions increases

with altitude, and it is related with the electron temperature at a given altitude. The effect of electron temperature on O^+ polar wind flow studied by Barakat and Schunk [1983]. They assumed that the ambipolar electric field to be approximately proportional to the electron temperature (i.e. $E_{||} \propto -kT_e \propto n_e$, where T_e is electron temperature and n_e is electron density). As a result, they found that the O^+ velocity, at high altitudes, increases from <1 km/s to a few km/s. This demonstrates the relationship between the magnitude of polar wind ion acceleration and that of the ambipolar electric field responsible for the acceleration. On the other hand, the results of Barghouthi model produce the O^+ velocity increases almost monotonically with altitude as shown in Fig.(4.3), which increases from 2.2 to 58km/s, when altitude varies from 1.7 to $13.7R_E$. Also, the H^+ velocity increases almost linearly with altitude as shown in Fig.(4.3), which increases from 16 to 50km/s, when altitude varies from 1.7 to $13.7R_E$. So, the velocity of polar wind ions increases with altitude. On the other hand Barghouthi model explain the increases of the polar wind ions with altitude owing to the effect of WPI and heating in the perpendicular direction, especially for O^+ ions (i.e. acceleration of ions). Another result concluded by Abe et al. [1993a] is that the O^+ ions attain significant average upward velocity at higher altitudes compared with H^+ and He^+ ions. This results is excellent agreement with the simulation results obtained by Barghouthi model, where for example, the H^+ velocity equal 17km/s at $2R_E$, but the O^+ velocity equal 2.2km/s at this altitude and its velocity becomes equal to 17km/s at $\sim 5.3R_E$. Therefore, the O^+ ions attain significant average upward velocity at higher altitudes compared with H^+ ions at low altitude, as shown in Fig.(4.3).

In addition, Abe et al. [1993a] used the data collected from Akebono satellite to confirm that the velocity for both O^+ and H^+ ions is approximately monotonic increases with altitude and for both polar wind ion species. The velocity on the dayside was significantly larger than that on the nightside. On the dayside, the average O^+ velocity began to increase near $1.87R_E$, and reached a maximum of about 4 km/s near apogee. Comparing these results with the simulation results of Barghouthi model, Barghouthi model results are very close to these result as shown in Fig.(4.3), where the velocity of O^+ ions increases monotonically with altitude, which increases from 2.2 to 58km/s, when altitude varies from 1.7 to $13.7R_E$. Also, the velocity of H^+ ions increases monotonically with altitude, which increases from 15 to 50km/s, when altitude varies from 1.7 to $13.7R_E$. Also, the velocity of O^+ ions begins to increase monotonically with altitude around $2.3R_E$, as shown in Fig.(4.3). Further more, the O^+ ion velocity increases with altitude, Abe et al. [1993a, b, and 1996].

On the other hand, the simulation result from Barghouthi model produce the velocity of O^+ ions which increases monotonically with altitude as shown in Fig.(4.3), which increases from 2.2 to 58km/s, when altitude varies from 1.7 to 13.7 R_E . So, the velocity of O^+ polar wind ions increases with altitude.

The velocity of the polar wind ions (i.e. O^+ and H^+) increases with altitude, Drakou et al. [1997]. Also, the simulation result from Barghouthi model produce the velocity of O^+ ions increases monotonically with altitude as shown in Fig.(4.3), which increases from 2.2 to 58km/s, when altitude varies from 1.7 to 13.7 R_E . Also, the H^+ velocity increases almost linearly with altitude as shown in Fig.(4.3), which increases from 15 to 50km/s, when altitude varies from 1.7 to 13.7 R_E . So, the velocity of polar wind ions increases with altitude. The large velocities of the polar wind ions reflect to the continuous acceleration of the polar wind at very high altitudes due to a number of mechanisms, Su et al. [1998]. This agreement with the Barghouthi model results, where the velocity for both O^+ and H^+ ions is 38 and 26km/s respectively, at 9 R_E . Also, their velocities at 13.7 R_E are 58 and 50km/s, respectively, which are very large velocities. In addition, Barghouthi model says that the acceleration of the polar wind ions to large velocities, at high altitude, owing to the effect of WPI mechanism and heating in the perpendicular direction.

One of the important simulation results from Barghouthi model is the rate of increase of velocity larger at low altitudes and smaller at high altitudes. For example, the O^+ velocity increases from 2.2 to 2.3km/s, when altitude varies from 2 to 3 R_E (i.e. low altitude), but at high altitude the O^+ velocity increases from 26.9 to 30.9km/s, when altitude varies from 7 to 8 R_E , which means the rate of increase of velocity larger at low altitudes, similarly for H^+ ions, where the rate of increase of velocity larger at low altitudes, as shown in Fig.(4.3). This result of Barghouthi model is confirmed by Abe et al. [2004], where they concluded that the rate of increase of velocity larger at low altitudes and smaller at high altitudes for high the solar radio flux (i.e. in maximum solar activity). Also, Abe et al. [2004] presented that, the velocity of O^+ ions in the sunlit region remained below 1 km/s below 2.03 R_E but increased with altitude above this altitude. This result is consistent with the simulation results of Barghouthi model, where the velocity of O^+ ions at 2.03 R_E is 2.2km/s and it increases monotonically with altitude above 2.03 R_E , as shown in Fig.(4.3).

Yau et al. [2007] concluded that; as the polar wind ions flow upward along “open” magnetic field lines of the Earth in the polar cap and dayside cusp poleward of the plasmasphere, they increase in both drift speed and temperature. This result is consistent with the simulation results of Barghouthi model, where the drift velocity of O^+ ions increases with altitude as shown in Fig.(4.1), which increases from 6.5×10^{-4} to 45km/s, when altitude increases from 1.7 to 13.7 R_E . Also, the drift velocity of H^+ ions increases with altitude as shown in Fig.(4.1), which increases from 12 to 37km/s, when altitude increases from 1.7 to 13.7 R_E . On the other hand, the temperature of O^+ ions increases with altitude at all altitude, but for H^+ ions it increases with altitude at high altitude (i.e. above $\sim 5R_E$), as shown in Fig.(4.2).

From several observations obtained by many satellites such as POLAR, DE-1 and Akebono, Su et al. [1998] and Abe et al. [1993a], Yau et al. [2007] concluded that the velocity ratio between ion species of the polar wind spans a wide range of values, and on average lies between unity and the inverse square root mass ratio of the ions (i.e. $1 < v_{\parallel}(H^+)/v_{\parallel}(O^+) < [m(O^+)/m(H^+)]^{1/2} = 4$). This suggests that the total ion acceleration produces from a number of processes and factors of comparable energy gain probably. simulation results from Barghouthi model yields that the parallel velocity ratio between H^+ and O^+ , when altitude varies from 1.7 to 7.4 R_E as, $1 < v_{\parallel}(H^+) / v_{\parallel}(O^+) < 10$. This is agreement with the concluded result by Yau et al. [2007].

Nagai et al. [1984], Chandler et al. [1991], Abe et al. [1993a], and Drakou et al. [1997] concluded that the polar wind ions are supersonic by the time they reach 2.1 R_E , and we obtained the velocity for both O^+ and H^+ ions to be equals to 2.2 and 16.9km/s at 2.1 R_E . So, they are supersonic ions by the time they reach this altitude, since their velocities at 2.1 R_E greater than their thermal velocities, where the thermal velocity for both O^+ and H^+ ions are 2.16 and 8.62km/s, respectively. This explain, owing to several factors contribute in the increasing of the polar wind ions with altitude such as, WPI and heating the perpendicular direction.

In addition, Yasseen and Retterer [1991] model predicted the subsonic to supersonic transition altitude for the H^+ polar wind ions (i.e. the sonic point) is typically near 1.24 R_E , the sonic point corresponds to a singularity in a system of moment equations, making its numerical solution intrinsically difficult to obtain in moment based polar wind models.

Simulation results from Barghouthi model yields that the velocity of H^+ ions equals to 15km/s (i.e. supersonic, since the thermal velocity of H^+ ions is 8.62km/s) at $1.7R_E$, and above this altitude it increases with altitude, so the H^+ ions is supersonic above $1.7R_E$ and the sonic occur below $1.7R_E$, which consistent with Yasseen and Retterer [1991] model.

Furthermore, Su et al. [1998] calculated the Mach number (i.e. the ratio of ion drift velocity over ion thermal velocity) for the polar wind ions by using the data obtained from POLAR satellite. They found the Mach number of H^+ ranged from ~ 2 to 7, with an average of 4.6; and the Mach number of O^+ ranged from ~ 1 to 8, with an average of 3.5. As a result, polar wind ion species are supersonic at POLAR apogee (i.e. $9R_E$). To be specific, Barghouthi model produced similar results to the observations of Su et al. [1998], where the velocity of both O^+ and H^+ ions is 27.3 and 25.9km/s, respectively, at $9R_E$, so both ions are supersonic at this altitude, since the thermal velocity for both O^+ and H^+ ions are 2.16 and 8.62km/s, respectively.

Su et al. [1998] concluded that H^+ ion is supersonic, while O^+ ion is subsonic at $1.8R_E$; and for H^+ polar wind ion the perpendicular temperature exceeds the parallel temperature, this reflects to perpendicular ion heating of the polar wind plasma in the topside ionosphere. This is in a close agreement with the simulation results from Barghouthi model, where we calculated the velocity of both O^+ and H^+ ions at $1.8R_E$ equals to 2.15 and 16km/s, respectively. So, H^+ ions are supersonic, while O^+ ions are subsonic, since the thermal velocity for both O^+ and H^+ ions are 2.16 and 8.62km/s, respectively. In addition, we confirmed that the perpendicular temperature higher than parallel temperature for H^+ ions, where the parallel and perpendicular temperature of H^+ ions at $1.8R_E$ is 1100 and 3000k, respectively, owing to the WPI with the electromagnetic turbulence and heading in the perpendicular direction and this cause the acceleration of the polar wind ions to large velocities at high altitude. This mechanism (i.e. WPI) is suggested in Barghouthi model. Also, Su et al. [1998] demonstrated that the parallel to perpendicular temperature ratio is less than unity at low altitudes, which is equal to 0.52 for H^+ and 0.55 for O^+ at $1.8R_E$. On the other hand, at high altitude it more than unity. This results is consistent with the simulation results from Barghouthi model. We obtain the following results: the parallel to perpendicular temperature for both O^+ and H^+ ions equal to 0.8 at $2.5R_E$, were it is less than unity at low altitude for both ions. Another result is the parallel to perpendicular temperature ratio is about 0.37 for H^+ at $1.8R_E$, which agreement with the observation

results with the same scale. Also, for O^+ ions the parallel to perpendicular temperature ratio is about 0.95 for at $1.8R_E$, and this result is agreement with observation with the same scale. Finally, the parallel to perpendicular temperature ratio exceeds unity for H^+ ions between $2.7R_E$ and $6.6R_E$ (i.e. high altitude), which is equal to 4 at $4.9R_E$, as shown in Fig.(5.3), where this results consistent with observations.

The observed parallel to perpendicular temperature ratio from POLAR satellite of the polar wind ion species was significantly different at the perigee (i.e.5000km or $1.8R_E$) and apogee (i.e. 50500km or $9R_E$) of the POLAR satellite. Su et al. [1998] calculated the ratio of the averaged parallel to perpendicular temperature to be ~ 0.46 , and 0.58 for H^+ and O^+ , respectively, at POLAR perigee. Also, they concluded that the perpendicular to parallel temperature ratio for H^+ decreasing with altitude in the altitude range ($1.79 - 1.95R_E$) presumably reflects the conversion of perpendicular to parallel ion energy along the diverging magnetic field line owing to conservation of the first adiabatic invariant. These observations obtained from the POLAR satellite are agreement with the simulation results calculated by using Barghouthi model in polar wind region. These results include: First, the parallel to perpendicular temperature ratios for O^+ ions at $1.8R_E$ and $9R_E$ are 1 and 0.02, respectively. Also, for H^+ ions the ratios are 0.37 at $1.8R_E$ and 0.0625 at $9R_E$, therefore the ratio of both ions was significantly different at the two altitudes (i.e. at the POLAR apogee and perigee). Second, the parallel to perpendicular temperature ratio is about 0.37 for H^+ at $1.8R_E$. It is very consistent with the ratio obtained from observation, which equal to 0.37 at the same altitude. Third, the parallel to perpendicular temperature ratio is about 0.95 for O^+ at $1.8R_E$, which is with the same order with the ratio calculated from observation. Forth, the averaged perpendicular to parallel temperature ratio for H^+ decreasing with altitude in the altitude range ($1.7 - 5R_E$) as shown in Fig.(5.2), owing to the conservation of the first adiabatic invariant, which cause conversion of perpendicular to parallel ion energy along the diverging magnetic field line and additional ion acceleration or heating along the field line such as WPI and heating in the perpendicular directions, due the presence of the electromagnetic turbulence.

Moreover, the composition ratios of parallel and perpendicular temperatures between the polar wind ion species are of interest. Su et al. [1998] observed O^+/H^+ parallel temperature ratio to be about 4.6 at $1.87R_E$, while the corresponding perpendicular temperature ratio is about 3.4 at $1.87R_E$. Therefore, the O^+ ions have a higher temperature than the H^+ ions in

both the parallel and perpendicular directions. These observations are in close agreement with the simulation results of Barghouthi model, where we calculated the O^+/H^+ parallel temperature ratio at $1.87R_E$ to be ~ 3.52 and the O^+/H^+ perpendicular ratio at $1.87R_E$ is about ~ 2 and at $2.5R_E \sim 3.4$, which is very close to the corresponding value observation. This means that, the parallel and perpendicular temperature of O^+ ions greater than that of H^+ ions at all altitude as shown in Fig.(4.1).

In the 13-moment of Schunk and Watkins [1981,1982] model, the parallel H^+ ion temperature at high altitudes was greater than the perpendicular temperature. This is consistent with the results obtained from Barghouthi model, where the parallel to perpendicular temperature ratio exceeds unity for H^+ ions between $2.7R_E$ and $6.6R_E$ (i.e. high altitude), which is equal to 4 at $4.9R_E$. Also, Barghouthi result consistent with the 16-moment models of Ganguli et al. [1987] and Demars and Schunk [1989] resulting in, the parallel H^+ ion temperature was greater than the perpendicular temperature between 2.7 and $6.6R_E$ (i.e. above the collision dominated region; above $1.7R_E$).

In the Tam et al. [1995] model, they predicted that the perpendicular temperature comparable to the parallel temperature at high altitudes. This result consistent with the simulation results of Barghouthi model where the parallel to perpendicular temperature ratio is about one for O^+ at $1.7R_E$, but for H^+ ions the ratio is about one at $2.7R_E$ and at $6.6R_E$, (i.e. high altitude). So at these geocentric altitude Tam et al. [1995] model is consistent with Barghouthi model.

Schunk and Watkins [1982] and Demars and Schunk [1987a, 1995] models predicted that the temperature anisotropy increases with altitude at high altitudes for the polar wind ions. Also, Barghouthi model produces the same results, where the temperature anisotropy for O^+ ions increases with altitude. Also, for H^+ ions the anisotropy is increases with altitude, except at $2.7R_E$ and $6.6R_E$, where there is no anisotropy (i.e. the perpendicular temperature equal to the parallel temperature), as shown in Fig.(5.2).

Most models predict that the perpendicular temperature is decreasing with altitude, while the parallel temperature is less dependent on altitude, Drakou et al. [1997]. On the other hand, the simulation results of Barghouthi model are agreement with the above results, where the perpendicular temperature of H^+ ions decreases with altitude in the geocentric

altitude ($1.7R_E - 4.9R_E$) as shown in Fig.(4.1), and the parallel temperature of H^+ ions is not varying significantly with altitude, which varies from 0.07 to 0.05eV when altitude increases from $2R_E$ to $10R_E$ as shown in Fig.(4.1). In addition, for O^+ ions the parallel temperature varies from 0.95 to 1.9eV, when altitude increases from $6R_E$ to $13.7R_E$ as shown in Fig.(4.1). Therefore, the parallel temperature for both O^+ and H^+ ion is significantly variable with altitude. When plasma reached altitudes $5R_E$ or above, it developed large temperature anisotropy (i.e. the parallel temperature greater than the perpendicular temperature, Persoon et al. [1983] and Biddle et al. [1985]. Also, Barghouthi model produces results that agreement with these results such as, the parallel temperature exceeds the perpendicular temperature for H^+ ions between $2.7R_E$ and $6.6R_E$, where the parallel to perpendicular temperature ratio equal to 4 at $4.9R_E$, (i.e. it develops large temperature anisotropy).

Drakou et al. [1997] demonstrated that the parallel to perpendicular temperature ratio was in the range $(1/3 < T_{\parallel} / T_{\perp} < 3)$ by using data from Akebono. This result is consistent with the simulation result from Barghouthi model, where the parallel to perpendicular temperature ratio of H^+ ions is $(0.38 < T_{\parallel} / T_{\perp} < 4)$, when altitude changes from 1.7 to $4.9R_E$. In addition, Drakou et al. [1997] and Su et al. [1998] concluded that the temperature of polar wind ions is generally low, and is in the range of 0.05–0.35eV when altitude varies between 2.1 and $2.58R_E$, which consistent with the results of Barghouthi model, where the temperature of O^+ ions varies from 0.26 to 57eV, when the altitude changes from 1.7 to $13.7R_E$. Also, for H^+ ions the temperature varies from 0.2 to 3.9eV, when the altitude changes from $1.7R_E$ to $13.7R_E$ and the temperature at $5.3R_E$ equals 10 and 0.03 eV for O^+ and H^+ ions, respectively. Therefore, the polar wind ions temperature is generally low. In addition, the temperature of O^+ ions varies from 0.26 to 0.265eV, when the altitude changes from $2.1R_E$ to $2.58R_E$. Also, for the temperature of H^+ ions varies from 0.11 to 0.07eV, when the altitude changes from 2.1 to $2.58R_E$, which is in the observation range for temperature 0.05–0.35eV.

At the POLAR apogee (i.e. $9R_E$) and perigee (i.e. at $1.8R_E$), O^+ ions has a higher temperature than H^+ ions, and the observed temperature of both polar wind species is higher than that from polar wind model predictions, Su et al. [1998]. On the other hand, this result is consistent with the simulation results from Barghouthi model, where the temperature for both O^+ and H^+ ions at $1.8R_E$ equals to 0.26 and 0.18eV, respectively, and

at $9R_E$ it equal to 36eV for O^+ and 0.5eV for H^+ , as shown in Fig.(4.2). Therefore, the temperature of O^+ ions exceeds the temperature of H^+ ions at all altitudes.

Drakou et al. [1997], concluded that the temperature of the polar wind ions (i.e. O^+ and H^+) is little dependence on altitude. On the other hand, Barghouthi model produces the temperature of O^+ ions which varies from 0.26 to 0.265eV, when the altitude changes from 1.7 to $2.58R_E$. Also, for H^+ ions it varies from 0.2 to 0.08eV, when the altitude changes from 1.7 to $2.58R_E$. So, the polar wind ions temperature did not vary significantly with altitude.

Yau and André. [1997] classified outflows, which occur in the polar ionosphere into two groups: bulk ion flows with energies up to a few eV, such as the polar wind, and energetic ion outflows. The energy of the H^+ ions, which calculated from Barghouthi model varies from 0.3 to 6eV, when the altitude changes from 1.7 to $13.7R_E$. But for the O^+ ions it varies from (0.38 to 105eV), when the altitude changes from 1.7 to $13.7R_E$. From these results, we note that the energies are few eV for H^+ for all altitude, but the energies are few eV for O^+ ions at low altitude only.

In the model of Lemaire and Scherer [1972a], a monotonic potential energy altitude profile was assumed for each polar wind ion species. The species are divided into four trajectory types: ballistic, escaping, trapped, and incoming. All four trajectory types are allowed for particles such as O^+ ions that have positive potential energies (i.e. electric plus gravitational) above the baropause, but only escaping and incoming trajectories are possible for particles such as H^+ ions that have monotonically decreasing potential energies. To be specific, Barghouthi model produces simulation results which is consistent with the results obtained in the model of Lemaire and Scherer [1972a] as shown in Fig.(5.1) for both O^+ and H^+ ions. From this Fig.(5.1), we note that the potential energy of O^+ ions is positive and increasing with altitude. On the other hand, the potential energy for H^+ ions is negative and almost linearly decreasing with altitude.

Barghouthi model produces, the O^+ and H^+ ions distributions above $1.7R_E$, which is not Maxwellian, but they become conic distributions at some altitude and then they become toroidal distributions at higher altitude, this occur owing to temperature anisotropy, which results from different factors such as the effect of WPI and pressure cooker effect. These

results are agreement with the results obtained by Drakou et al. [1997]. They concluded that the actual ion distributions are not maxwellian due to higher energy tail component drifting at higher velocity.

Finally, the H^+ distribution close to Maxwellian distribution at low altitudes ($\sim 1.7R_E$) by using the semi-kinetic model, Barakat and Schunk [1983]. To be specific, the simulation results from Barghouthi model obtained consistent results, where the distribution of the H^+ ions is Maxwellian at low altitudes (i.e. $1.7R_E$) by using the Barghouthi model.

We can conclude that Barghouthi model is an excellent model in the polar wind region, since it produces acceptable simulation results when compared qualitatively to the corresponding observations. So far, Barghouthi model is the best model that produces simulation results when compared to the corresponding observations from different satellite.

We summarized the Barghouthi model predictions (i.e. the simulation results of Barghouthi model) and experimental verification (i.e. observations) in Tables (5.1-A, B, C, D, E, F) as shown below.

Table 5.1-A: Barghouthi Model Predictions and Experimental Verification

| Experimental Verifications | Barghouthi Model Predictions |
|--|---|
| 1. At high altitude ($\sim 2 R_E$) outside the plasmasphere, the plasma density is typically below 10^3cm^{-3} . [Yau et al., 2007] | The density of O^+ and H^+ ions at $2R_E$ are 13cm^{-3} and 100cm^{-3} respectively, which are less than 10^3cm^{-3} . |
| 2. The polar wind is dominated in density by O^+ ions up to at least $1.63R_E$ and perhaps $1.95 - 2.1R_E$. [Hoffman and Dobson, 1980] | The density of O^+ and H^+ ions at $1.95R_E$ are 20 and 110cm^{-3} , respectively. Also, at $2.1R_E$ the density are 3.2 and 79cm^{-3} respectively, and above $1.7R_E$ the H^+ ions is the dominant as shown in Fig.(4.1). |

Table 5.1-B: Barghouthi Model Predictions and Experimental Verification

| | |
|--|---|
| 3. The polar wind plasma density is very low (typically $<10\text{cm}^{-3}$) near $9R_E$. [Moore et al.,1995] | The density for both O^+ and H^+ ions at $9R_E$ equals to $6*10^{-5}$ and 0.7cm^{-3} , respectively. Therefore, the density for both ions is very low at this altitude. |
| 4. The correlation between the densities of the O^+ and H^+ ions on average are: $n(H^+) : n(O^+) \sim 1 : 0.17$ [Su et al.,1998] | The density ratio between the H^+ and O^+ ions at $2R_E$ is $n(H^+) : n(O^+) \sim 1 : 0.1$ |
| 5. The polar wind is dominated by H^+ ions at $9R_E$. [Su et al.,1998] | The densities of O^+ and H^+ ions at $9R_E$ are $1.6*10^{-5}$ and 0.7cm^{-3} , respectively. So, at this altitude H^+ ion is the dominated species, as shown in Fig.(4.1). |
| 6. O^+ density is an order of magnitude smaller than the H^+ density in the geocentric altitude ($4.5 - 7.8R_E$). [Elliott et al.,2001] | The density for O^+ ions is smaller than that for H^+ ions in the altitude range($4.5 - 7.8R_E$), as shown in Fig.(4.1). |
| 7. The transition from dominant O^+ at low altitudes to dominant H^+ at high altitudes is expected to occur between 1.63 and $2.18R_E$, depending on the neutral hydrogen density. [Abe et al., 1993a] | Above $1.7R_E$ H^+ is the major ion, as shown in Figure (4.1). The density of O^+ and H^+ ions at $2.18R_E$ is 1.4 and 59cm^{-3} , respectively. So, above $2.18R_E$ the H^+ is the dominant ion. |
| 8. The observed ion velocity of all polar wind species is highly variable in the altitude range ($1.16 - 2.58R_E$). [Abe et al., 1993a] | The O^+ velocity varies from 2.2 to 2.3km/s , when altitude varies from 1.7 to $2.58R_E$. Also, the H^+ velocity varies from 15.5 to 18km/s , when altitude varies from 1.7 to $2.58R_E$. Therefore, the velocity of the polar wind ions is highly variable in this altitude range. |
| 9. At very high altitudes (above $\sim 9R_E$), the polar wind ions have large velocities. [Su et al.,1998] | The velocity for both O^+ and H^+ ions is 38 and 26km/s respectively, at $9R_E$. Also, their velocities at $13.7R_E$ are 58 and 50km/s , respectively, which are very large velocities. |
| 10. As the polar wind ions flow upward, increase in drift speed of the polar wind ions. [Yau et al., 2007] | The drift velocity of O^+ ions increases with altitude as shown in Fig.(4.1), which increases from $6.5*10^{-4}$ to 45km/s , when altitude increases from 1.7 to $13.7R_E$. Also, the drift velocity of H^+ ions increases with altitude as shown in Fig.(4.1), which increases from 12 to 37km/s , when altitude increases from 1.7 to $13.7R_E$. |

Table 5.1-C: Barghouthi Model Predictions and Experimental Verification

| | |
|--|---|
| 11. On average, the velocity of polar wind ions increases with altitude. [Abe et al., 1993a] | The O^+ velocity increases almost monotonically with altitude as shown in Fig(4.3), which increases from 2.2 to 58km/s, when altitude varies from 1.7 to 13.7 R_E . Also, the H^+ velocity increases almost linearly with altitude as shown in Fig.(4.3), which increases from 16 to 50km/s, when altitude varies from 1.7 to 13.7 R_E . So, the velocity of polar wind ions increases with altitude. |
| 12. The rate of increase of velocity of polar wind ions larger at low altitudes and smaller at high altitudes. [Abe et al., 2004] | The O^+ velocity increases from 5 to 14km/s, when altitude varies from 4 to 5 R_E (i.e. low altitude), but at high altitude the O^+ velocity increases from 34.5 to 37.5km/s, when altitude varies from 8 to 9 R_E , which means the rate of increases of velocity larger at low altitudes, as shown in Fig.(4.3). |
| 13. O^+ ions attain significant average upward velocity at higher altitudes Compared with H^+ ions below 2.58 R_E . [Abe et al., 1993a] | The H^+ velocity equal 17km/s at 2 R_E , but the O^+ velocity equal 2.2km/s at this altitude and its velocity becomes equal to 17km/s at (~5.3 R_E). Therefore, the O^+ ions attain significant average upward velocity at higher altitudes Compared with H^+ ions at low altitude, as shown in Fig.(4.3). |
| 14. Linear increase in the polar wind ion velocity with geocentric distance over (2.1 to 4.66 R_E) altitude range. [Persoon et al., 1983] | The increase of velocity for both O^+ and H^+ ions with geocentric altitude is approximately linear in the altitude range (2.1 to 4.66 R_E), as shown in Fig.(4.3). |
| 15. The velocity for both O^+ and H^+ ions is (approximately) monotonic increases with altitude. [Abe et al., 1993a] | The velocity of O^+ increases monotonically with altitude as shown in Fig.(4.3), which increases from 2.2 to 58km/s, when altitude varies from 1.7 to 13.7 R_E . Also, the velocity of H^+ increases with altitude as shown in Fig.(4.3), which increases from 15 to 50km/s, when altitude varies from 1.7 to 13.7 R_E . |
| 16. The averaged O^+ velocity begins to increase near 1.8 R_E . [Abe et al., 1993a] | The velocity of O^+ begins to increase monotonically with altitude around 2.3 R_E as shown in Fig.(4.3). |
| 17. The velocity of O^+ ions is increasing with altitude above 2.03 R_E . [Abe et al., 2004] | The velocity of O^+ ions at 2.03 R_E is 2.2km/s and it increases monotonically with altitude above 2.03 R_E , as shown in Fig.(4.3). |

Table 5.1-D: Barghouthi Model Predictions and Experimental Verification

| | |
|---|---|
| 18. The velocity of the polar wind ions (i.e. O^+ and H^+) increases with altitude. [Drakou et al., 1997]. | The velocity of O^+ ions increases monotonically with altitude as shown in Fig.(4.3), which increases from 2.2 to 58km/s, when altitude varies from 1.7 to 13.7 R_E . Also, the H^+ velocity increases almost linearly with altitude as shown in Fig.(4.3), which increases from 15 to 50km/s, when altitude varies from 1.7 to 13.7 R_E . So, the velocity of polar wind ions increases with altitude. |
| 19. The O^+ ion velocity increases with altitude. [Abe et al.,1993a,b, and 1996] | The velocity of O^+ ions increases monotonically with altitude as shown in Fig.(4.3), which increases from 2.2 to 58km/s, when altitude varies from 1.7 to 13.7 R_E . So, the velocity of O^+ polar wind ions increases with altitude. |
| 20. The velocity ratio between ion species spans a wide range of values, and on average: $1 < v_{ }(H^+) / v_{ }(O^+) < [m(O^+)/m(H^+)]^{1/2} = 4$ [Su et al.,1998] and [Abe et al., 1993a] | The parallel velocity ratio between H^+ and O^+ ions, when altitude varies from 1.7 to 7.4 R_E . $1 < v_{ }(H^+) / v_{ }(O^+) < 10$. Therefore, this ratio spans wide range. |
| 21. The correlation between the parallel velocities of the O^+ and H^+ ions on average is $v_{ }(H^+) : v_{ }(O^+) \sim 1 : 0.38$ [Su et al.,1998] | The parallel velocity ratio between the H^+ and O^+ ions at 5 R_E is $v_{ }(H^+) : v_{ }(O^+) \sim 1 : 0.31$ |
| 22. The polar wind ions are supersonic by the time they reach 2.1 R_E . [Chandler et al., 1991] [Nagai et al.,1984] [Abe et al., 1993a]. | The velocity for both O^+ and H^+ ions equals to 2.2 and 16.9km/s at 2.1 R_E . So, they are supersonic ions by the time they reach this altitude, since the thermal velocity for both O^+ and H^+ ions are 2.16 and 8.62km/s, respectively. |
| 23. The polar wind ions are supersonic at 9 R_E . [Su et al.,1998] | The velocity of both O^+ and H^+ ions is 27.3 and 25.9km/s, respectively, at 9 R_E . So, they are supersonic at this altitude, since the thermal velocity for both O^+ and H^+ ions are 2.16 and 8.62km/s, respectively. |
| 24. At 1.8 R_E , H^+ ions are supersonic, while O^+ ions are subsonic. [Su et al.,1998] | The velocity of both O^+ and H^+ ions at 1.8 R_E equals to 2.15 and 16km/s, respectively. So, H^+ ions are supersonic, while O^+ ions are subsonic, since the thermal velocity for both O^+ and H^+ ions are 2.16 and 8.62km/s, respectively. |

Table 5.1-E: Barghouthi Model Predictions and Experimental Verification

| | |
|---|--|
| 25. The polar wind species are supersonic above $2.1R_E$. [Drakou et al., 1997] | The velocity for both O^+ and H^+ ions at $2.1R_E$ equals to 2.2 and 16.9km/s, respectively. In addition, the velocity for both ions increases with altitude. So, they are supersonic, since the thermal velocity for both O^+ and H^+ ions are 2.16 and 8.62km/s, respectively. |
| 26. The H^+ polar wind ion is supersonic at high altitude. [Nagai et al., 1984] | The velocity of H^+ ions equals to 15km/s at $1.7R_E$ and above this altitude its velocity increases with altitude. So the H^+ ions is supersonic above $1.7R_E$, since its thermal velocity equals to 8.62km/s. |
| 27. The parallel to perpendicular temperature ratio is less than unity at low altitudes for the polar wind ions. [Su et al., 1998] | The parallel to perpendicular temperature ratio for both O^+ and H^+ ions equal to 0.8 at $2.5R_E$, where the parallel to perpendicular temperature ratio for O^+ ions less than unity at all altitude, but for H^+ ions it is less than unity in the altitude ranges ($1.7 - 2.7R_E$) and ($6.6 - 13.7R_E$). Therefore at low altitude the parallel to perpendicular temperature ratio is less than unity. |
| 28. The parallel to perpendicular temperature ratio of the O^+ and H^+ ions is significantly different at two altitudes 9 and $1.8R_E$. [Su et al., 1998] | The parallel to perpendicular temperature ratios for O^+ ions at $1.8R_E$ and $9R_E$ are 1 and 0.02, respectively. Also, for H^+ ions the ratios are 0.37 at $1.8R_E$ and 0.0625 at $9R_E$. Therefore, the ratios of both ions are significantly different at the two altitudes. |
| 29. The averaged perpendicular to parallel temperature ratio for H^+ is decreasing with altitude in the altitude range ($1.79 - 1.95R_E$). [Su et al., 1998] | The perpendicular to parallel temperature ratio for H^+ is decreasing with altitude from 1.7 to $5R_E$ as shown in Fig.(5.2). |
| 30. The O^+/H^+ parallel temperature ratio, $\langle T_{//}(O^+) / T_{//}(H^+) \rangle \sim 4.6$ at $1.87R_E$. [Su et al., 1998] | The O^+/H^+ parallel temperature ratio at $1.87R_E$ is $\langle T_{//}(O^+) / T_{//}(H^+) \rangle \sim 3.52$ |
| 31. The O^+/H^+ perpendicular temperature ratio is $\langle T_{\perp}(O^+) / T_{\perp}(H^+) \rangle \sim 3.4$ at $1.87R_E$. [Su et al., 1998] | The O^+/H^+ perpendicular temperature ratio at $1.87R_E$ is $\langle T_{\perp}(O^+) / T_{\perp}(H^+) \rangle \sim 2$, and at $2.5R_E$ is $\langle T_{\perp}(O^+) / T_{\perp}(H^+) \rangle \sim 3.4$. |
| 32. The O^+ ions have a higher temperature than the H^+ ions in both the parallel and perpendicular directions. [Su et al., 1998] | The parallel and perpendicular temperature of O^+ ions are greater than that of H^+ ions at all altitudes, as shown in Fig.(4.1). |

Table 5.1-F: Barghouthi Model Predictions and Experimental Verification

| | |
|--|---|
| 33. The perpendicular temperature exceeds the parallel temperature for H^+ ions at $1.8R_E$. [Su et al.,1998] | The parallel and perpendicular temperature of H^+ ions at $1.8R_E$ is 1100 and 3000k, respectively, where the perpendicular temperature higher than parallel temperature for H^+ ions. |
| 34. The temperature of polar wind ions is generally low and it is in the range of 0.05 – 0.35 eV between $2.1R_E$ and $2.58R_E$. [Drakou et al.,1997] and [Su et al.,1998] | The temperature of O^+ ions varies from 0.26 to 0.265eV, when the altitude changes from $2.1R_E$ to $2.58R_E$. Also, for the temperature of H^+ ions varies from 0.11 to 0.07eV, when the altitude changes from $2.1R_E$ to $2.58R_E$. Therefore, the temperature of the polar wind ions is low in this altitude range. |
| 35. O^+ ions have a higher temperature than H^+ ions, at 1.8 and $9R_E$. [Su et al.,1998] | The temperature for both O^+ and H^+ ions at $1.8R_E$ equals to 0.26 and 0.18eV, respectively, and at $9R_E$ it equals to 36eV for O^+ and 0.5eV for H^+ . Therefore, the temperature of O^+ ions exceeds the temperature of H^+ ions at both altitudes, as shown in Fig.(4.2). |
| 36. The temperature of the polar wind ions (i.e. O^+ and H^+) is little dependence on altitude. [Drakou et al., 1997]. | The temperature of O^+ ions varies from 0.26 to 0.265eV, when the altitude changes from 1.7 to $2.58R_E$, also for H^+ ions it varies from 0.2 to 0.08eV, when the altitude changes from 1.7 to $2.58R_E$. So the polar wind ions temperature did not vary significantly with altitude. |
| 37. As the polar wind ions flow upward, increases in temperature of the polar wind ions. [Yau et al., 2007] | The temperature of O^+ ions increases with altitude at all altitude, but for H^+ ions it increases with altitude at high altitude (i.e. above $\sim 5R_E$), as shown in Fig.(4.2). |
| 38. Polar wind ion flows with energies up to a few eV. [Yau and André,1997] | The energy of the H^+ ions varies from 0.31 to 5.8eV, when the altitude changes from 1.7 to $13.7R_E$, but for the O^+ ions it varies from 0.39 to 105eV, when the altitude changes from 1.7 to $13.7R_E$. |

We also summarized the simulation results from different models that consistent with Barghouthi model predictions in Table (5.2-A, B, C) as shown below.

Table 5.2-A: Barghouthi Model Predictions and simulation results Verification

| Simulation result Verifications | Barghouthi Model Predictions |
|---|--|
| 1. The transition from O^+ to H^+ , as the major ion species, occurs above $1.87R_E$. [Lemaire and Scherer,1971] | The density for O^+ ions is smaller than that for H^+ ions above $1.7R_E$, where the density for both O^+ and H^+ ions at $1.87R_E$ equals to 19 and 120cm^{-3} , respectively. So, the H^+ ion is the major species above $1.87R_E$, as shown in Fig.(4.1). |
| 2. In the supersonic case, the H^+ density is decreasing with increasing altitude. [Demars and Schunk,1994] | The density of H^+ ions is decreasing almost linearly with increasing altitude as shown in Fig.(4.1), which decreases from 180 to 25cm^{-3} when altitude increases from 1.7 to $3R_E$. Also, it is decreased to 0.13 at $13.7R_E$, where the H^+ ions above $1.7R_E$ are supersonic, since the H^+ velocity greater than its thermal velocity above $1.7R_E$. |
| 3. The predict ions velocity is as large as 16 –20 km/s at high altitude ($\sim 2.89R_E$). [Ganguli et al, 1987] and [Demars and Schunk, 1989]. | The H^+ velocity varies from 15 to 23.7km/s, when altitude varies from 1.7 to $8R_E$, and it is equal to 18km/s at $2.89R_E$, as shown in Fig.(4.3). |
| 4. The O^+ velocity increases from <1 km/s to a few km/s at high altitudes. [Barakat and Schunk,1983] | The O^+ velocity increases from 2.15 to 13km/s, when altitude varies from 1.7 to $5R_E$. |
| 5. The subsonic to supersonic transition altitude for the H^+ polar wind (i.e. the sonic point) is typically near $1.24R_E$. [Yasseen and Retterer,1991] | The velocity of H^+ ions equals to 15km/s (i.e. supersonic) at $1.7R_E$ and above this altitude it increases with altitude. Since the thermal velocity of H^+ ions is 8.62km/s, so the H^+ ions is supersonic above $1.7R_E$. Therefore, the sonic point occurs below $1.7R_E$. |
| 6. The parallel H^+ ion temperature at high altitudes is greater than the perpendicular temperature. [Schunk and Watkins, 1981, 1982] | The parallel to perpendicular temperature ratio exceeds unity for H^+ ions between 2.7 and $6.6R_E$ (i.e. high altitude), which is equal to 4 at $4.9R_E$. |
| 7. The parallel H^+ ion temperature is greater than the perpendicular temperature above the collision dominated region. [Ganguli et al, 1987] and [Demars and Schunk, 1989]. | The parallel to perpendicular temperature ratio exceeds unity for H^+ ions between 2.7 and $6.6R_E$ (i.e. above the collision dominated region, were it is less than $1.7R_E$), where the ratio equal to 4 at $4.9R_E$. |
| 8. The perpendicular temperature comparable to the parallel temperature occurs at high altitudes. [Tam et al., 1995] | The parallel to perpendicular temperature ratio is about one for O^+ at $1.7R_E$, but for H^+ ions the ratio is about one at two altitudes 2.8 and $6.6R_E$, (i.e. high altitude). |

Table 5.2-B: Barghouthi Model Predictions and simulation results Verification

| | |
|---|--|
| 9. The temperature anisotropy increases with altitude at high altitudes. [Schunk and Watkins, 1982; Demars and Schunk, 1987a, 1995] | The temperature anisotropy for O^+ ions increases with altitude. Also, for H^+ ions the anisotropy increases with altitude, except at $2.8R_E$ and $6.6R_E$, where there is no anisotropy (i.e. The perpendicular temperature equal to the parallel temperature), as shown in Fig.(5.2). |
| 10. Most models predict that the perpendicular temperature is decreasing with altitude at low altitude. [Drakou et al., 1997] | The perpendicular temperature of H^+ ions decreases with altitude in the geocentric altitude ($1.7 - 4.9R_E$), where the effect of WPI is negligible and the ions in this range are dominated by the effect of the perpendicular adiabatic cooling. |
| 11. Most models predict that the parallel temperature is less dependent on altitude. [Drakou et al., 1997] | The parallel temperature of H^+ ions is not varying significantly with altitude, which varies from 0.07 to 0.05eV when altitude increases from 2 to $10R_E$. In addition, for O^+ ions it varies from 0.95 to 1.9eV, when altitude increases from 6 to $13.7R_E$. Therefore the parallel temperature for both O^+ and H^+ ion is significantly variable with altitude as shown in Fig.(4.1). |
| 12. When plasma reach altitudes $5R_E$ or above, it develop large temperature anisotropy (i.e. the parallel temperature greater than the perpendicular temperature). [Persoon et al., 1983; Biddle et al., 1985]. | The parallel temperature exceeds the perpendicular temperature for H^+ ions between 2.8 and $6.6R_E$, where the parallel to perpendicular temperature ratio equal to 4 at $4.9R_E$, (i.e. it develops large temperature anisotropy). |
| 13. O^+ ions have positive potential energies (i.e. electric plus gravitational) above the baropause. In contrast, H^+ ions have monotonically decreasing potential energies with altitude. [Lemaire and Scherer, 1972a] | The potential energy for O^+ ions is positive and increasing with altitude, but the potential energy of H^+ ions is negative and almost linearly decreasing with altitude as shown in Fig.(5.1). |

We can conclude that Barghouthi model is an excellent model in the polar wind region, since it produces acceptable simulation results when compared quantitatively and qualitatively to the corresponding observations. So far, Barghouthi model is the best model that produces simulation results when compared to the corresponding observations. In addition, Barghouthi model is also the best model that can be used in the aurora region, since it produces simulation results when compared to the corresponding observations, [Barghouthi, 2008]. This close agreement between the simulation results and observations

provides and evidence that Barghouthi model described in this thesis is appropriate to be used when modeling the heating of ions through the wave particle interaction in the polar wind region.

The most important result in this study is that the wavelength of the electromagnetic turbulence equals 8km, since the simulation results of Barghouthi model represent the closest results to the observations, which are obtained from different satellites. We can apply this model (i.e. Barghouthi model), that produces consistent simulation results when compared to the corresponding observations, on the solar wind, since it is "similar" to the polar wind with different boundary conditions.

5.2 Summary and conclusion

A Monte Carlo technique was used in order to study the effect of wave particle interaction (i.e. altitude and velocity dependent) on the H^+ and O^+ ions outflow at high altitudes and high latitudes in the polar wind region. This technique also includes the effects of body forces (i.e. gravity and polarization electrostatic field) and divergence of magnetic field of the Earth. The effects of wave particle interaction on the H^+ and O^+ ions outflows (i.e. the ions perpendicular heating and acceleration of the ions in the upward direction, owing to the conservation of the first adiabatic invariant) was modeled, developing a form for the perpendicular diffusion coefficient $D_{\perp}(r, v_{\perp})$ as a function of the position (r/R_E) along the magnetic field lines of the Earth and perpendicular velocity (v_{\perp}) . In this study, the Monte Carlo simulation was run for Barghouthi model, where the perpendicular diffusion coefficient $D_{\perp}(r, v_{\perp})$ is given in equation (2.26), and in each simulation we used 10^7 tested ions in order to compute the ion distribution function and also compute the profiles of its velocity moments (i.e. density, drift velocity, parallel temperature, and perpendicular temperature) for both H^+ and O^+ ions. The boundary conditions selected for polar wind region are similar to those of [Barghouthi et al., 1998], with the effect of body forces, divergence of magnetic field, and WPI.

As a result, we have found that:

- 1) The temperature anisotropy $(T_{\perp} / T_{\parallel})$ for H^+ ions was reduced at lower altitudes, but it is reversed $(T_{\perp}(H^+) > T_{\parallel}(H^+))$ at higher altitudes. On the other hand, the

temperature anisotropy ($T_{\perp} / T_{\parallel}$) for O^+ ions increases with altitude at low altitude, and at high altitude its average value is (~ 53), where ($T_{\perp}(O^+) > T_{\parallel}(O^+)$) for all altitudes.

- 2) The O^+ and H^+ velocity distribution functions [i.e. $f(O^+)$ and $f(H^+)$] develop conic features, owing to the effect of WPI (i.e. the ion perpendicular heating) and mirror force (i.e. diverging of the magnetic field), where the perpendicular temperature becomes greater than the parallel temperature. The O^+ ions develop conic features at ($\sim 4.27R_E$), while the H^+ ions develop the conic features at ($\sim 11.1R_E$), for the perpendicular electromagnetic turbulence ($\lambda_{\perp} = 8km$).
- 3) Above a certain point, called saturation point, the effect of altitude- and velocity-dependent WPI is the dominant and the ion heating becomes self-limiting. The saturation point for H^+ ions occurs at ($\sim 10.5R_E$), while for O^+ ions occurs at ($\sim 5.97R_E$), for the perpendicular electromagnetic turbulence ($\lambda_{\perp} = 8km$).
- 4) The O^+ ion is preferentially heated comparing with H^+ ion, where the temperature of O^+ ion higher than that of H^+ ion at all altitude. This is owing to the potential energy of the H^+ ions is negative and decreasing with altitude, while the potential energy for O^+ ions is positive and monotonically increasing with altitude, in addition, the diffusion coefficient of O^+ ions $D_{\perp}(O^+)$ greater than the diffusion coefficient of H^+ ions $D_{\perp}(H^+)$.
- 5) The O^+ ions are heated more efficiently than the H^+ ions at low altitudes due to pressure cooker effect.

As the polar wind ions heated in the perpendicular direction, they moved in the upward direction, and then their Larmor radius (a_L) increases (i.e. the ions Larmor radius (a_L) increasing rapidly with altitude), and may become comparable to or exceeds the wavelength of the electromagnetic turbulence (λ_{\perp}). The effect of this phenomenon was studied by assuming a wide range of the wavelength of the electromagnetic turbulence (λ_{\perp}), [i.e. $\lambda_{\perp} = \infty, 50, 20, 8$, and $1km$]. As a result, we conclude that:

- 1) At low altitudes, the wave length of the electromagnetic turbulence (λ_{\perp}) is much greater than the ions Larmor radius (a_L). Therefore, the simulation results of Barghouthi model are independent of the wavelength of the electromagnetic

turbulence (λ_{\perp}), but at high altitudes and above a certain point (called the saturation point) the ions Larmor radius (a_L) may become comparable to or even more than the perpendicular electromagnetic turbulence (λ_{\perp}). Consequently, the heating of the ions becomes self-limiting. The saturation point for H^+ ions occurs at ($\sim 10.5R_E$) for the perpendicular electromagnetic turbulence ($\lambda_{\perp} = 8km$). On the other hand, the saturation point for O^+ ions occurs at ($\sim 6.0R_E$) for the same perpendicular electromagnetic turbulence.

- 2) Above the saturation point, the ions velocity distribution function displays toroidal features, because the ions tend to move out of the region of large diffusion coefficient ($v_{\perp} \cong 0$) and accumulate in the region of relatively low diffusion coefficient (i.e. the ions tend to diffuse out of the heating zone in the velocity space). The velocity distribution function of H^+ ions displays toroidal features at ($\sim 12.8R_E$), but for O^+ ions the toroidal features appear at ($\sim 5.97R_E$), for the perpendicular electromagnetic turbulence ($\lambda_{\perp} = 8km$).
- 3) The ion heating is dramatically reduced above the saturation point, since the ions tend to move out of the region of large diffusion coefficient ($v_{\perp} \cong 0$) and accumulate in the region of relatively low diffusion coefficient (i.e. the ions tend to move out of the heating zone into a region of negligible WPI, and we explain this in the peaked nature of the diffusion coefficient). Therefore, the effect of WPI becomes negligible (i.e. the ion heating rate is reduced).
- 4) Since the ions Larmor radius (a_L) will be comparable to or exceeds the wavelength of the electromagnetic turbulence (λ_{\perp}) at high altitude, also as electromagnetic turbulence (λ_{\perp}) decreases, the argument ($\frac{a_L}{\lambda_{\perp}}$) approaches one at lower altitudes, then the saturation point occurred earlier, and consequently, the toroidal features appears at lower altitudes. For H^+ ions, namely for the case $\lambda_{\perp} = 8 km$ the toroidal features appear at $\sim 12.8R_E$, but for the case $\lambda_{\perp} = 20 km$ at geocentric altitude $\sim 13.7R_E$ the velocity distribution function begins to display toroidal features. In addition, for O^+ ions, namely, for the electromagnetic turbulence wavelength $\lambda_{\perp} = 20 km$, the toroidal features appears at altitude $\sim 6.66R_E$, but for the case

$\lambda_{\perp}=8km$, the toroidal appears at lower altitudes, where it starts to appear at geocentric altitude $\sim 5.97R_E$.

- 5) The toroidal features of O^+ ions appear at lower altitudes compared with H^+ ions (i.e. the saturation point of H^+ ions is occurred at higher altitudes than those for O^+ ions), where the toroidal features of H^+ ions appear at $\sim 12.8R_E$, but for O^+ ions the toroidal features appear at $\sim 5.97R_E$, for the perpendicular electromagnetic turbulence wavelength $\lambda_{\perp} = 8km$. This is owing to two reasons: First, the mass of O^+ ion is much large comparable to that of H^+ ion [$m(O^+) = 16 \times m(H^+)$]. Second, the potential energy of O^+ ions larger than that of H^+ ions, where the potential energy of the H^+ ions is negative and decreasing with altitude, while the potential energy for O^+ ions is positive and monotonically increasing with altitude.

From the comparison of the simulation results of Barghouthi model quantitatively and qualitatively with observations from different satellites, we confirm that the electromagnetic turbulence wavelength equals $8km$, (i.e. $\lambda_{\perp} = 8km$), since the simulation results of Barghouthi model represent the closest results to the observations when the electromagnetic turbulence wavelength $\lambda_{\perp} = 8km$, [Barghouthi, 2008], concluded that the wavelength of electromagnetic turbulence $\lambda_{\perp} = 8km$ in the aurora region. Therefore, our study confirmed that the wavelength of the electromagnetic turbulence equals to $8km$ (i.e. $\lambda_{\perp} = 8km$).

Finally, we can say, as an important result from this study, that Barghouthi model is an excellent model in the polar wind region, since it produces acceptable simulation results when compared quantitatively and qualitatively to the corresponding observations; and consequently, Barghouthi model so far, is the best model that produces simulation results when compared to the corresponding observations. In addition, Barghouthi model also the best model that can be used in the aurora region, since it produces simulation results which are compared with the obsevation, [Barghouthi, 2008].

References

- Abe, T., et al., Measurements of temperature and velocity distribution of thermal electrons by the Akebono (EXOS-D) satellite: Experimental setup and preliminary results, *J. Geomagn. Geoelectr.*, 42, 537-554, 1990.
- Abe, T., et al., Observations of polar wind and thermal ion outflow by Akebono/SMS, *J. Geomagn. Geoelectr.*, 48, 319-325, 1996.
- Abe, T., et al., Long-term variation of the polar winds velocity and its implication for the ion acceleration process: Akebono/suprathermal ion mass spectrometer observations, *J. Geophys. Res.*, 109, A09035, doi: 10.1029/2003JA010223, 2004.
- Abe, T., B. A. Whalen, A. W. Yau, R. E. Horita, S. Watanbe, and E. Sagawa, EXOS D (Akebono) Superthermal mass spectrometer observations of the polar wind, *J. Geophys. Res.*, 98, 11, 191, 1993a.
- Abe, T., B. A. Whalen, A. W. Yau, S. Watanbe, E. Sagawa, and K. I. Oyama, Altitude profile of the polar wind velocity and its relationship to ionospheric conditions, *Geophys. Res. Lett.*, 20, 2825, 1993b.
- Arvelius, S., Yamauchi, M., Nilsson, H., Lundin, R., Hobara, Y., Bavassano-Cattaneo, M.B., Paschmann, G., Korth, A., Kistler, L.M., and Parks, G.K.: Statistics of high-altitude and high-latitude O^+ ion outflows observed by Cluster/CIS, *Ann. Geophys.*, 23, 1909-1916, 2005.
- Axford, W. I., The polar wind and the terrestrial helium budget, *J. geophys. Res.*, 73, 6855, 1968.
- Axford, W. I., and C. O. Hines, A unifying theory of high-latitude geophysical phenomena and geomagnetic storms, *Can. J. phys.*, 39, 433, 1961.
- Banks, P. M., and T. E. Holzer, Features of plasma transport in the upper atmosphere, *J. Geophys. Res.*, 74, 6304-6316, 1969a.
- Banks, P. M., and T. E. Holzer, High- latitude plasma transport: The polar wind, *J. Geophys. Res.*, 74, 6317-6332, 1969b.
- Banks, P. M., and T. E. Holzer, The polar wind, *J. Geophys. Res.*, 73, 6846-6868, 1968.
- Barakat, A. R. and I. A. Barghouthi, The effects of wave-particle interactions on the polar wind O^+ , *Geophys. Res. Lett.*, 21 2279-2282. 1994a.
- Barakat, A. R. and I. A. Barghouthi, The effects of wave-particle interactions on the polar wind: Preliminary results, *Planet. Space Sci.*, 42, 987-992, 1994b.

- Barakat, A. R., and R. W. Schunk, Comparison of Maxwellian and bi-Maxwellian expansions with Monte Carlo simulations for anisotropic Plasmas, J. phys. D., 15, 2189,1982c.
- Barakat, A. R., and R. W. Schunk, O⁺ ions in the polar wind, J. Geophys. Res., 88, 7887-7894,1983.
- Barakat, A. R., and R. W. Schunk, Effect of hot electrons on the polar wind, J. Geophys. Res., 89, 9771-9783,1984.
- Barakat, A. R., and R. W. Schunk, Stability of polar wind, J. Geophys. Res., 92, 3409-3415,1987.
- Barakat, A. R., and R. W. Schunk, Stability of H⁺ beams in the polar wind, J. Geophys. Res., 94,1487-1494,1989.
- Barghouthi I. A., Effects of wave particle interactions on H⁺ and O⁺ outflow at high latitude; A comparative study, J. Geophys. Res., 102, 22. 062-22.075, 1997.
- Barghouthi I. A., A. R. Barakat, A. M. Persoon, The effects of altitude –dependent wave particle interactions on the polar wind plasma, Astrophysics and space sciences, 259, 117, 1998.
- Barghouthi I. A., N. A. Qatanani, M.S. Abu Issa, Toroidal distributions in the polar wind plasma; Indian j.phys, 77B (6), 621-625, 2003a.
- Barghouthi I. A., N. A. Qatanani, F. M. Allan, Monte Carlo simulation of Boltzmann equation in space plasma at high latitudes, Monte Carlo Methods and Appl., 9, 3, 201-216, 2003b.
- Barghouthi, I. A., and A. R. Barakat, Comparison between the wave-particle interaction in the polar wind and in the auroral region, Phys. Space Plasmas, 13, 445– 450.1993.
- Barghouthi, I. A., and M. A. Atout, Monte Carlo modeling of toroidal ion distributions and ion temperatures at high altitudes equatorward of the cusp: Effect of finite gyroradius, J. Geophys. Res., 111, A03202, 2006.
- Barghouthi, I. A., N. M. Doudin, A. A. Saleh, and V. Pierrard, High-altitude and high-latitude O⁺ and H⁺ outflows: the effect of finite electromagnetic turbulence wavelength , Ann. Geophys., 25, 2195-2202, 2007.
- Barghouthi, I. A., A Monte Carlo study for ion outflows at high altitude and high latitude: Barghouthi model, J. Geophys. Res., 113, A08209, 2008.
- Bauer, S. J., The structure of the topside ionosphere, Electron Density profiles in Ionosphere and Exosphere, edited by J. Frihagen, p. 387, North-Holland, New York, 1966.

- Belelly, P. L., A. R. Barakat, J. Fontari, D. Alcayde, M. Blancej. Wu, and C. Lathuillere, Observations of the structure and vertical transport of the polar of upper ionosphere with the EISCAT VHF radar, 1, Is EISCAT able to determine O^+ and H^+ polar wind characteristics? A simulation study, *Ann. Geophys.*, 10, 367-374, 1992.
- Belotserkovskii, O. M., and Yu. I. Khlopkov, Monte Carlo methods in applied mathematics and computational aerodynamics, computational mathematics and mathematical physics., Vol. 46, No.8, PP.1418-1441, 2006.
- Biddle, A. P., T. E. Moore, and C. R. Chppell, Evidence for ion heat flux in the light ion polar wind, *J. Geophys. Res.*, 90, 8552, 1985.
- Chandler, M.O., et al., Observations of polar ion outflows, *J. Geophys. Res.*, 96, 1421-1428, 1991.
- Chandler, M.O., Observations of downward moving O^+ in the polar topside ionosphere, *J. Geophys. Res.*, 100 (A4), 5795-5800, 1995.
- Chang, T., Lower Hybrid collapse, caviton turbulence, and charged particle energization in the topside auroral ionosphere and magnetosphere, *Phys. Fluids*, B 5(7), 2646-2656, 1993.
- Chang, T., Coppi, B.: Lower hybrid acceleration and ion evolution in the supraauroral region, *Geophys. Res. Lett.*, 8, 1253-1256, 1981.
- Chapell, C. R., T. E. Moore, and J. H. Waite Jr., The ionosphere as a fully adequate source of plasma for the earth's magnetosphere, *J. Geophys. Res.*, 92, 5896-5910, 1987.
- Chen, M. W., and M. Ashour-Abdalla, Heating of the polar wind due to ion-beam instabilities, *J. Geophys. Res.*, 95, 18, 949-18. 968, 1990.
- Crew, G.B., T. Chang.: Asymptotic theory of ion conic distributions. *Physics of fluids* 28(8), 2382-2394, 1985.
- Davies, Kenneth, *Ionospheric Radio*, Peter Peregrinus Ltd. London, 1990.
- Demars, H.G., Schunk, R.W., Comparison of semikinetic and generalized transport models of the polar wind, *Geophys. Res. Lett.*, 18, 713-716, 1991.
- Demars, H.G., Schunk, R.W., Semikinetic and generalized transport models of the polar and solar winds, *J. Geophys. Res.*, 97, 1581-1595, 1992.
- Dessler, A. J., and F. C. Michel, Plasma in the geomagnetic tail, *J. Geophys. Res.*, 71, 1421, 1966.
- Drakou, E., et al., Ion temperature measurements from the Akebono suprathermal mass spectrometer: Application to the polar wind, *J. Geophys. Res.*, 102, 17523-17539, 1997.

- Elliott, H.A., et al., Solar wind influence on the oxygen content of ion outflow in the high altitude polar cap during solar minimum conditions, *J. Geophys. Res.*, 106, 6067-6084, 2001.
- Ganguli, S.B., The polar wind, *Rev. Geophys.*, 34, 311-348, 1996.
- Ganguli, S. B., and P. J. Plamadesso, Plasma transport in the auroral return current region, *J. Geophys. Res.* 92, 8673-8690, 1987.
- Gurnett, D. A., and U. S. Inan, Plasma wave observations with the Dynamic explorer 1 spacecraft, *Rev. Geophys.*, 26, 285-316, 1988.
- Hoffman, J.H., et al., Initial ion composition results from the Isis 2 satellite, *J. Geophys. Res.*, 79, 4246-51, 1974.
- Hoffman, J.H., Dodson, W.H., Light ion concentrations and fluxes in the polar regions during magnetically quiet times, *J. Geophys. Res.*, 85, 626-632, 1980.
- Holzer, T. E., J. A. Fedder, and P. M. Banks, A comparison of kinetic and hydrodynamic models of an expanding ion-exosphere, *J. Geophys. Res.*, 76, 2453-2468, 1971.
- Huddleston, M. M., C. J. Pollock, M.P.Wuest, J. S. Pichett, T. E. Moore, and W. K. Peterson, Toroidal ion distributions observed at high altitudes equatorward of the cusp, *Geophysical Research Letters*, 27, 4, 469-472, 2000.
- Lemaire, J., O^+ , H^+ and He^+ ion distributions in a new polar wind model, *J. Atmos. Terr. Phys.*, 34, 1647-1658, 1972.
- Lemaire, J., and M. Scherer, Model of the polar ion-exosphere, *planet. Space Sci.*, 18, 103-120, 1970.
- Lemaire, J., and M. Scherer, Kinetic models of the solar and polar winds, *Rev. Geophys.*, 11, 427-468, 1973.
- Lemaire, J., and M. Scherer, Simple model for an ion-exosphere in an open magnetic field, *Phys. Fluids*, 14, 1683-1694, 1971.
- Li, P., G. R. Wilson, J. L. Horwitz, and T. E. Moore, Effect of mid-altitude ion heating on the ion outflow at polar latitudes, *Geophys. Res.*, 93, 9753-9763, 1988.
- Moore, T. E., C. R. Cahppell, M. Lockwood, and J. H. Waite Jr., Super thermal ion signature of auroral acceleration processes, *J. Geophys. Res.*, 90, 1611-1618, 1985.
- Moore, T. E., M. Lockwood, M. O. Chandler, J. H. Waite Jr., C. R. Chappell, A. Persoon, and M. Sugiura, Upwelling O^+ ion source characteristics, *J. Geophys. Res.*, 91, 7019, 1986b.
- Moore, T. E., and D. C. Delcourt, Transport and energization of ionospheric plasma (abstract), *Full Meet. Suppl., Eos Trans. AGU*, 73(43), 471, 1992.

- Nagai, T., J.H. Waite, J. L. Green, C. R. Chappel, First measurement of supersonic polar wind in the polar magnetosphere. *Geophysical Research Letters* 11, 669-672, 1984.
- Nilsson. H., M. Waara, O. Marghitu, M. Yamauchi, R. Lundin, H. Rème, J.-A. Sauvaud, I. Dandouras, E. Lucek, L. M. Kistler, B. Klecker, C. W. Carlson, M. B. Bavassano-Cattaneo, and A. Korth, An assessment of the role of the centrifugal acceleration mechanism in high altitude polar cap oxygen ion outflow, *Ann. Geophys.*, 26, 145-157, 2008.
- Nilsson. H., M. Waara, O. Marghitu, M. Yamauchi, R. Lundin, H. Rème, J.-A. Sauvaud, I. Dandouras, E. Lucek, L. M. Kistler, B. Klecker, C. W. Carlson, M. B. Bavassano-Cattaneo, and A. Korth, Transients in oxygen outflow above the polar cap as observed by the Cluster spacecraft, *Ann. Geophys.*, 26, 3365-3373, 2008.
- Nishida, A., Formation of plasmopause, or the magnetospheric plasma knee, by the combined action of magnetospheric convection and plasma escape from the tail, *J. Geophys. Res.*, 71, 5669-5679, 1966.
- Ogawa, Y., et al., Simultaneous EISCAT Svalbard and VHF radar observations of ion upflows at different aspect angles, *Geophys. Res. Lett.*, 27, 81-84, 2000.
- Persoon, A. M., D. A. Gurnett, and S. D Shawhan, polar cap electron densities from DE-1 plasma wave observations, *J. Geophys. Res.*, 88, 10, 123, 1983.
- Peterson, W.K., On the energy sources responsible for the escape of heavy ions from the ionosphere. *Physics of Space Plasma, SPI Conf. Proc. and Reprint Ser.*, Vol 14, edited by T. Chang and J. R. Jasperse, Scientific, Cambridge Mass, 1995.
- Pierrard, V., Lemaire, J., A collisional kinetic model of the polar wind, *J. Geophys. Res.*, 103, 11701-11709, 1998.
- Raitt, W.J., Schunk, R.W., Composition and characteristics of the polar wind, In: Johnson, R.G. (Ed.), *Energetic Ion Composition in the Earth's Magnetosphere*, pp. 99-141, Terra Scientific Publishing, Tokyo, 1983.
- Retterer, J. M., T. Chang, G. B., Crew, J. R. Jasperse, and J. D. Winningham, Monte Carlo modeling of oxygen ion conic acceleration by cyclotron resonance, *phys. Rev. Lett.*, 59, 148-151, 1987a.
- Retterer, J. M., T. Chang, G. B., Crew, J. R. Jasperse, and J. D. Winningham, Monte Carlo modeling of oxygen ion conic acceleration by cyclotron resonance with broadband electromagnetic turbulence, in *physics of space plasma, SPI Conf. Proc. and Reprint Ser.*, No. 6, edited by T. Chang, J. Belcher, J. R. Jasperse, and G. Crew, pp.97-111, Scientific, Cambridge, Mass., 1987b.

- Schunk, R.W., Time-dependent simulations of the global polar wind, *J. Atmos. Solar Terr. Phys.*, this issue, 2007.
- Schunk, R. W., Mathematical structure of transport equations for multispecies flows, *Rev. Geophys.*, 15, 429, 1977.
- Schunk, R. W. and A. F. Nagy, *Ionospheres: physics plasma physics, and chemistry*, First published, Cambridge, 2000.
- Schunk, R.W., Sojka, J.J., A three-dimensional time-dependent model of the polar wind, *J. Geophys. Res.*, 94, 8973-8991, 1989.
- Schunk, R.W., Sojka, J.J., Global ionosphere-polar wind system during changing magnetic activity, *J. Geophys. Res.*, 102, 11625–11651, 1997.
- Schunk, R.W. and D. S. Watkins, Electron temperature anisotropy in the polar wind, *J. Geophys. Res.*, 86, 91- 102, 1981.
- Schunk, R.W. and D. S. Watkins, Proton temperature anisotropy in the polar wind, *J. Geophys. Res.*, 87, 171-180, 1981.
- Schunk, R. W., The polar wind, in modeling Magnetospheric plasma, *Geophys. Monogr. Ser.*, Vol. 44, edited by T. E. Moore and J. H. Waite, P. 219, AGU, Washington, D. C., 1988.
- Shelley, E.G., et al., Satellite observations of energetic heavy ions during a geomagnetic storm, *J. Geophys. Res.*, 77, 6104-6110, 1972.
- Su, Y.J., et al., Polar wind survey with the Thermal Ion Dynamics Experiment/Plasma Source Instrument suite aboard POLAR, *J. Geophys. Res.*, 103, 29305-29337, 1988a.
- Su, Y.J., et al., Self-consistent simulation of the photoelectron-driven polar wind from 120 km to 9 RE altitude, *J. Geophys. Res.*, 103, 2279-2296, 1998b.
- Tam, S.W.Y., et al., Self-consistent kinetic photoelectron effects on the polar wind, *Geophys. Res. Lett.*, 22, 2107-2110, 1995a.
- Tam, S.W.Y., et al., Anisotropic kinetic effects of photoelectrons on polar wind transport, in *Cross-scale coupling in space plasmas*, Horwitz, J.L., Singh, N., Birch, J.L., Eds., *Geophys.*, 1995b.
- Tsurutani, B. T. and G. S. Lakhina, Some concepts of wave- particle interactions in the collisionless plasmas, *Reviews of Geophysics*, 35, 4, 491-502, 1997.
- Wilsson, G. R., C. W. Ho, J. L. Horwitz, N. Singh, and T. E. Moore, A new kinetic model for time-dependent polar plasma outflow: Initial results, *Geophys. Res. Lett.*, 17, 263, 1990.

- Wu, J., M. Blanc, D. Alcaide, A. R. Barakat, J. Fontanari, P. L. Beletly, and W. Kofman, Observations of the structure and vertical transport of the polar ionosphere with the EISCAT VHF radar, 2, First investigations of the topside O^+ and H^+ vertical ion flows, *Ann. Geophys.*, 10, 375-393, 1992.
- Yasseen, F., Retterer, J.M., Critical points in the 16-moment approximation, *J. Geophys. Res.*, 96, 1827–1830, 1991.
- Yasseen, F., et al., Monte-Carlo modeling of polar wind photoelectron distributions with anomalous heat flux, *Geophys. Res. Lett.*, 16, 1023-1026, 1989.
- Yau, A.W., et al., Minor ion composition in the polar ionosphere, *Geophys. Res. Lett.*, 18, 345-348, 1991.
- Yau, A. W., B. A. Whalen, T. Abe, T. Mukai, K. I. Oyama, and T. Chang, Akebono observations of electron temperature anisotropy in the polar wind, *J. Geophys. Res.*, 100, 17, 45, 1995.
- Yau, A. W., E. G. Shelley, W. K. Peterson, and L. Lenchysy, Energetic auroral and polar ion outflow at DE-1 altitude, magnitude, composition, magnetic activity dependence a long-term variations, *J. Geophys. Res.*, 90, 8417, 1985.
- Yau, A. W., Andre, M., Sources of ion outflow in the high latitude ionosphere, *Space Sci. Rev.*, 80 (1-2), 1-26, 1997.
- Yau, A. W., T. Abe, and W. K. Peterson, The Polar Wind: Recent Observations, *J. Geophys. Res.*, 90, 8417, 1985, 2007.

<http://www.albany.edu>

<http://ssdoo.gsfc.nasa.gov>

<http://www.phy6.org>

<http://www.uaf.edu>

<http://www.yahoo.com>

<http://www.google.com>

Appendices

Appendix A: Gravitational Force

Newton's law of gravity states that the mutual attractive force between two particles in the universe is directly proportional to the product of their masses and inversely proportional to the square of the distance between them, regardless of the medium that separates them. If an ion of mass (m) separated by a distance (r) from the Earth, then the ion will experience an attractive force (gravitational force) given by:

$$\mathbf{F}(\mathbf{r}) = -\frac{GM_E m}{r^2} \hat{\mathbf{r}} \quad (\text{A.1})$$

where G is the universal gravitational constant, M_E is the Earth mass, $\hat{\mathbf{r}}$ is a unit vector directed from the center of the Earth to the ion with mass (m), and the negative sign indicates that the gravitational force is attractive. Therefore, the ion is attracted to the Earth.

The acceleration of gravity commonly is denoted by (\mathbf{g}), which is produced by gravitational force from the Earth on the ion; \mathbf{g} is given by:

$$\mathbf{g} = \frac{\mathbf{F}}{m} = -\frac{GM_E}{r^2} \hat{\mathbf{r}} \quad (\text{A.2})$$

The gravitational potential energy $\phi_g(r)$ can be found from the definition of work done by the force:

$$W = -(\phi_g - \phi_{g_o}) = -\Delta\phi(r) = - \int_{1.7R_E}^r \mathbf{F}(\mathbf{r}) \cdot d\mathbf{r} \quad (\text{A.3})$$

where r and $1.7R_E$ are the geocentric distance to the location of the ion, ϕ_g and ϕ_{g_o} are the gravitational potential energy at altitudes r and $1.7R_E$, respectively. We can use the above equations to find the formula of gravitational potential energy as a function of r , which is the separated distance in the Earth-ion system, by substitute the gravitational force of equation (A.1) into equation (A.3) to obtain the following formula, [Barghouthi, 2008].

$$\Delta\phi_g(r) = -GM_E m \int_{1.7R_E}^r \frac{dr}{r^2} = GM_E m \left(\frac{1}{1.7R_E} - \frac{1}{r} \right) \quad (\text{A.4})$$

where r is the distance separated the Earth- ion system and provided that $r > 1.7R_E > R_E$.

Appendix B: Polarization Electrostatic Field

To describe the outflow of plasma under the effect of polarization electric field, many approximations are used. A diffusion approximation is one of these approximations, which we use it. In this approximation the wave phenomena are neglected and the flow of plasma is considered to be subsonic.

In addition, because the ions and electrons move with each other, a net zero current conditions prevail, also the heat flow can be ignored, for partially ionized plasma. Therefore, the momentum equation of electrons can be written as [Schunk and Nagy, 2000]:

$$\nabla_{\parallel} p_e + (\nabla \cdot \boldsymbol{\tau}_e)_{\parallel} + n_e e \mathbf{E}_{\parallel} - n_e m_e \mathbf{g}_{\parallel} = n_e m_e \nu_{ei} (\mathbf{u}_i - \mathbf{u}_e)_{\parallel} + n_e m_e \nu_{en} (\mathbf{u}_n - \mathbf{u}_e)_{\parallel} \quad (\text{B.1})$$

where p_e is electrons partial pressure, \mathbf{E}_{\parallel} is the polarization electrostatic field that develops due to the very slight charge separation, $\boldsymbol{\tau}_e$ is electrons stress tensor, n_e is electrons density, m_e is the mass of electron, \mathbf{g}_{\parallel} is the component of acceleration due to gravity along the geomagnetic field lines, ν is the collision frequency and, \mathbf{u}_i is the drift velocity of ions, and \mathbf{u}_e is the drift velocity of electrons.

However, in many applications it is needed to get the electrostatic potential (V_E), which can be obtained from an explicit expression for the electric field created owing to the movements of electrons. This electric field can be obtained from equation (B.1) under some conditions; which are the terms containing m_e is neglected, since the mass of electron is small. In addition, the electron-ion collision term is dropped. Therefore, equation (B.1) becomes as:

$$e \mathbf{E}_{\parallel} = -\frac{1}{n_e} \nabla p_e \quad (\text{B.2})$$

The expression is valid regardless of the number of ion species in the plasma.

For alternate form of isothermal electron gas, it is valid to write $\mathbf{E}_{\parallel} = -\nabla V_E(r)$, and letting $E = -\nabla \phi_p$, and $p_e = n_e k T_e$, where ϕ_p is the potential energy to the polarization electric field, k is the Boltzmann constant, and assuming that T_e is constant, which is the electron temperature. So equation (B.2) reads:

$$\frac{e}{kT_e} \frac{\partial V_E(r)}{\partial r} = \frac{1}{n_e} \frac{\partial n_e}{\partial r} \quad (\text{B.3})$$

where (r) is the spatial coordinate either along or perpendicular to magnetic field lines of the Earth (\mathbf{B}). To get the electrostatic potential (V_E) , we treat equation (B.3), by integration it, to get the well-known Boltzmann relation:

$$n_e = (n_e)_o e^{\frac{eV_E}{kT}} \quad (\text{B.4})$$

where $(n_e)_o$ is the equilibrium electron density that prevails when $V_E = 0$. We can now find the electrostatic potential (V_E) as:

$$V_E(r) = \frac{kT_e}{e} \ln \left(\frac{n_e}{(n_e)_o} \right) \quad (\text{B.5})$$

Therefore, the polarization electrostatic potential energy $\phi_E(r)$ is given by, [Barghouthi, 2008]

$$\phi_E(r) = kT_e \ln \left(\frac{n_e}{(n_e)_o} \right) \quad (\text{B.6})$$

Appendix C: Charged Particles in a Magnetic Field

It is known that when an ion of charge (q) and velocity (v) enters a uniform magnetic field, then it will be experienced by magnetic force, which is represented in Gaussian system of units as:

$$\mathbf{F} = \frac{q}{c} \mathbf{v} \times \mathbf{B} \quad (\text{C.1})$$

where c is the speed of light. When a positive ion moves perpendicular in a uniform magnetic field \mathbf{B}_o , the magnetic force (Lorentz force) can change only the direction of ion's velocity, with the same speed. Therefore, the ion will move in a circular motion about the magnetic field. The radius of the circular path is called Larmor radius (gyroradius) which it can be obtained by equating between the magnetic force and the centrifugal force to have:

$$a_L = \frac{mc}{q} \frac{v_{\perp}}{B} \quad (\text{C.2})$$

The quantity $\left(\frac{qB_o}{mc} \right)$ is called the Larmor frequency, which is denoted by:

$$\Omega_c = \frac{qB_0}{mc} \quad (C.3)$$

However, the path of positive ion in a uniform magnetic field can be represented by a spatial path as shown in Fig.(C.1).

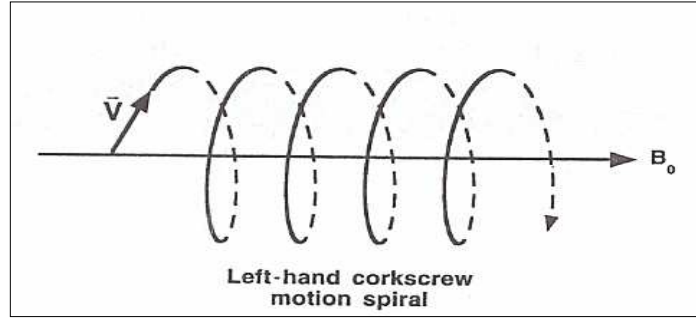


Figure C.1: Spiral motion of a charged particle in a uniform magnetic field [Tsurutani and Lakhina, 1997].

The ion velocity vector can be analyzed into two orthogonal components, with respect to the direction of the magnetic field (\mathbf{B}_0). These two components are: one parallel to \mathbf{B}_0 , which represented by \mathbf{v}_{\parallel} and the other perpendicular to \mathbf{B}_0 which represented by \mathbf{v}_{\perp} . Therefore, it is recommended to write:

$$\mathbf{v} = \mathbf{v}_{\parallel} + \mathbf{v}_{\perp} \quad (C.4)$$

Assume that there are no forces exerted on the ion in the parallel direction of the uniform magnetic field (\mathbf{B}_0); this implies that the ion moves unimpeded with a constant v_{\parallel} along the uniform magnetic field. This yields a cyclotron motion (as shown in the Fig.(C.1)), which is associated with the v_{\perp} velocity component and with larmor radius depends on the perpendicular velocity component.

In this cyclotron motion the magnitude of v_{\perp} remains constant (unchanged), but the direction of the perpendicular velocity v_{\perp} change continuously in a uniform magnetic field, as shown in Fig.(C.1). According to Lorentz force, the positive ions (i.e. O^+) gyrate in an opposite direction of gyration for negative ions (i.e. electrons), because the positive ions gyrate in a left-hand sense relative to the uniform magnetic field. The central field line about which the ions gyrate is called guiding center. When there is a strong magnetic field gradient in certain regions (i.e. non uniform magnetic field), the ion mirrored by Lorentz

force. At the moment in time when the ion is being mirrored, $v_{\perp} = v$ and $v_{\parallel} = 0$ (i.e. all velocity of the ion is in the perpendicular component), the ion accelerates in a direction anti parallel to the magnetic field, since the Lorentz force has a component toward the left. Since the Lorentz force operates in the direction perpendicular to velocity vector v_{\perp} , there is no work done on the ion, and the total energy of the ion remains constant:

$$E_T = \frac{1}{2}mv^2 = \frac{1}{2}mv_{\parallel}^2 + \frac{1}{2}mv_{\perp}^2 = E_{\parallel} + E_{\perp} \quad (C.5)$$

where E_T , E_{\parallel} and E_{\perp} are the total, parallel, and perpendicular kinetic energy of the ion respectively. However, for ion moves from left to right in magnetic field gradient as shown in Fig.(C.2), when E_{\parallel} decreases, and E_{\perp} increases, keeping E_T constant. The mirror point occurs when $E_{\perp} = E_T$ and $E_{\parallel} = 0$, then the ion starts to be mirrored and so E_{\parallel} begin to increase as E_{\perp} decreases. By the mirror force, the ion will be move in spiral motion a long the magnetic field lines and also bounce back and forth between mirror points [Tsurutani and Lakhina, 1997].

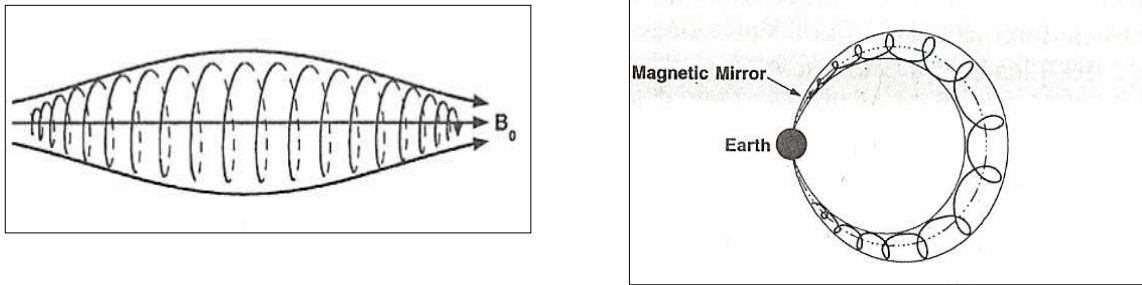


Figure C.2: Magnetic bottles for plasma particles [Tsurutani and Lakhina, 1997]

Appendix D: Wave Particle Interaction (WPI)

To include the effect of the WPI in a collisionless region, replace the binary collision term (i.e. right-hand side Boltzmann equation) by the term that is represent the interaction between ions and the electromagnetic turbulence, which is represented by particle diffusion in the velocity space such that [Retterer et al., 1987a]:

$$\left[\frac{\partial f_j}{\partial t} \right]_{WPI} = \left(\frac{1}{v_{\perp}} \right) \frac{\partial}{\partial v_{\perp}} \left[D_{\perp j} v_{\perp} \frac{\partial f_j}{\partial v_{\perp}} \right] \quad (D.1)$$

where D_{\perp} is the quasi-linear velocity diffusion coefficient rate perpendicular to geomagnetic field lines.

The influence of WPI on the ion species during Δt under the effect of the gravitational, electrostatic, and geomagnetic forces, is taking into consideration by incrementing the ions perpendicular velocity by randomly increment Δv_{\perp} such that:

$$\langle (\Delta v_{\perp})^2 \rangle = 4D_{\perp} \Delta t \quad (\text{D.2})$$

where Δt is the time interval chosen randomly and D_{\perp} is the perpendicular diffusion coefficient rate.

The perpendicular diffusion coefficient rate D_{\perp} is given by the following expression [Retterer et al., (1987b)]:

$$D_{\perp} = \frac{q^2}{m^2} \sum_{n=-\infty}^{\infty} \int \frac{d\omega}{2\pi} \int \frac{d^3 K}{(2\pi)^3} \left[\frac{n\Omega}{\omega} \right]^2 A_n \pi \delta(\omega - n\Omega - k_{\parallel} v_{\parallel}) \quad (\text{D.3})$$

with

$$A_n = \frac{1}{2} J_{n-1}^2 |E_L|^2(k, \omega) + \left[\frac{v_{\parallel} J_n^2}{v_{\perp}} \right]^2 |E_{\parallel}|^2(k, \omega) + \frac{1}{2} J_{n+1}^2 |E_R|^2(k, \omega) \quad (\text{D.4})$$

In the above equations, q is the ions charge, m is the ions mass, Ω is the ions gyrofrequency (i.e. larmor frequency), ω is the angular frequency of the electromagnetic turbulence, \mathbf{K} is the wave vector of the electromagnetic turbulence, $|E_L|^2$ and $|E_R|^2$ are the spectral densities of the electric field in the two perpendicular polarizations, $J_n = J_n\left(\frac{k_{\perp} v_{\perp}}{\Omega}\right)$ is the standard Bessel function.

[Retterer et al., 1987b], assumed the wavelength (λ_{\perp}) of the electromagnetic turbulence to be much greater than the ions Larmor radius (a_L), and assumed $(k_{\parallel} v_{\parallel} \ll \Omega)$, $n=1$ and $\left(\frac{k_{\perp} v_{\perp}}{\Omega} \ll 1\right)$, and found that D_{\perp} can be simplified as:

$$D_{\perp} = \frac{\eta q^2}{4 m^2} |E_x(\omega = \Omega)|^2 \quad (\text{D.5})$$

where $|E_L|^2(\omega) = \eta |E_x|^2(\omega)$, $|E_x|^2$ is the measured spectral density of the wave (electromagnetic turbulence), and η is the proportion of the measured spectral density by

plasma wave instrument (PWI) on board (DE-1) satellite that corresponds to a left-hand polarized wave.

However, the diffusion coefficient (D_{\perp}) given in equation (D.5) is independent of velocity, and it depends on position (altitude) through the variation of the ion gyrofrequency (Ω) along the magnetic field lines of the Earth, where the ion gyrofrequency depends on the magnetic field intensity, which is decreasing when the altitude is increasing.

To improve the altitude dependence of D_{\perp} [Barghouthi, 1997 and Barghouthi et al., 1998] computed the altitude dependence of D_{\perp} by analyzing experimental data obtained by PWI on board the DE-1 satellite. They obtained the following expressions for the perpendicular diffusion coefficient rate (D_{\perp}) in the polar wind plasma.

$$D_{\perp}(r) = \begin{cases} 5.77 \times 10^3 (r/R_E)^{7.95} \text{ cm}^2 \text{ sec}^{-3}, & \text{for } H^+ \\ 9.55 \times 10^2 (r/R_E)^{13.3} \text{ cm}^2 \text{ sec}^{-3}, & \text{for } O^+ \end{cases} \quad (\text{D.6})$$

However, this expression for the altitude dependent diffusion coefficient did not produced results that agree with the observations. To produce these observations requires a velocity dependent diffusion rate as suggested by [Retterer et al., 1994].

Appendix E: Barghouthi model

[Barghouthi, 1997 and Barghouthi et al., 1998] obtained a new forms for diffusion coefficient (D_{\perp}) for the case where the ions Larmor radius (a_L) is comparable or larger than the perpendicular electromagnetic turbulence (λ_{\perp}) by dividing the general form of the diffusion coefficient (D_{\perp}) giving in equation (D.3) by the simplified form of the diffusion coefficient (D_{\perp}) giving in equation (D.5) to get the following ratio, which denoted by R, [Barghouthi, 2008].

$$R = \frac{\frac{q^2}{m^2} \sum_{n=-\infty}^{\infty} \int \frac{d\omega}{2\pi} \int \frac{d^3k}{(2\pi)^3} \left[\frac{n\Omega}{\omega} \right]^2 A_n \pi \delta(\omega - n\Omega - k_{\parallel} v_{\parallel})}{\frac{\eta q^2}{4m^2} |E_x(\omega = \Omega)|^2} \quad (\text{E.1})$$

They plot the ratio R against the argument of Bessel function $k_{\perp} v_{\perp} / \Omega_i$ as shown in Fig.(2.5); they have two cases from the figure. First, when the argument $k_{\perp} v_{\perp} / \Omega_i$ is less than one, the ratio R is one, which means that the diffusion coefficient (D_{\perp}) is true. They reproduce [Retterer et al., 1987] simplified form for the diffusion coefficient (D_{\perp}), which given in equation (2.23) (i.e. the diffusion coefficient (D_{\perp}) is still velocity-independent). Second, the ratio R decreases as $(k_{\perp} v_{\perp} / \Omega_i)^{-3}$, when the argument $k_{\perp} v_{\perp} / \Omega_i$ becomes greater than one as shown in Fig.(E.1). In this case, the diffusion coefficient (D_{\perp}) giving in equation (D.5) needs modifications by multiply it by the quantity $(k_{\perp} v_{\perp} / \Omega_i)^{-3}$ (i.e. it becomes velocity dependent).

Finally, they obtained the following form for the diffusion coefficient (D_{\perp}), which is altitude and velocity dependent:

$$D_{\perp}(r, v_{\perp}) = D_{\perp}(r) \left\{ \begin{array}{ll} 1 & \text{for } \left(\frac{k_{\perp} v_{\perp}}{\Omega_i} \right) < 1 \\ \left(\frac{k_{\perp} v_{\perp}}{\Omega_i} \right)^{-3} & \text{for } \left(\frac{k_{\perp} v_{\perp}}{\Omega_i} \right) \geq 1 \end{array} \right\} \quad (\text{E.2})$$

where the diffusion coefficient $D_{\perp}(r)$ is given in equation (D.6).

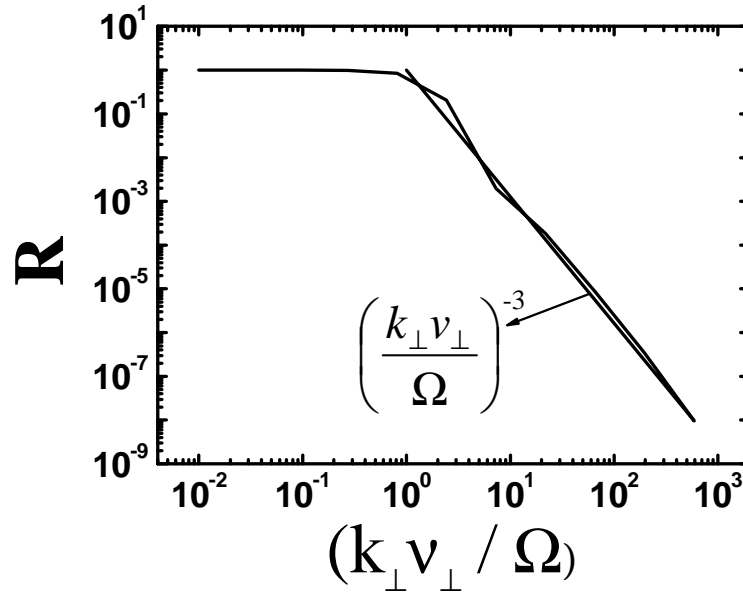


Figure E.1: The ratio R given in equation (E.1) versus the argument $k_{\perp}v_{\perp}/\Omega_i$. The straight line is the adopted dependence of the ratio R when the argument $k_{\perp}v_{\perp}/\Omega_i$ is greater than one, [Barghouthi, 2008].

Appendix F: Monte Carlo method

F.1 Generation of ions velocity

The starting point of most plasma simulations is the injection ion into the simulation region with a random initial velocity that corresponds to the ion distribution function at the injection point. Which in our study is the lower boundary (i.e. $r = 1.7R_E$), the ion velocity distribution functions assumed to be Maxwellian at the top of the barosphere (just below the exobase), [Barghouthi et al., 2003a, b], which written as:

$$f(\mathbf{v}) = n \left[\frac{m}{2\pi kT} \right]^{\frac{3}{2}} e^{-\frac{mv^2}{2kT}} \quad (\text{F.1})$$

where k is Boltzmann's constant, T is the temperature at the injection point (i.e. from boundary conditions), n is the number density, m is the mass of the ion, and \mathbf{v} is the velocity vector of the injected ion.

The ion velocity vector can be analyzed into two orthogonal components, with respect to the direction of the magnetic field (\mathbf{B}_0). These two components are: one parallel to \mathbf{B}_0 , which represented by \mathbf{v}_{\parallel} and the other perpendicular to \mathbf{B}_0 which represented by \mathbf{v}_{\perp} , therefore it is recommended to write as $\mathbf{v} = \mathbf{v}_{\parallel} + \mathbf{v}_{\perp}$. Therefore, it is recommended to write v^2 as $v^2 = v_{\parallel}^2 + v_{\perp}^2$. So, we can write the equation (F.1) as:

$$f(\mathbf{v}) = n \left[\frac{m}{2\pi kT} \right]^{\frac{3}{2}} e^{-\frac{m(v_{\parallel}^2 + v_{\perp}^2)}{2kT}} \quad (\text{F.2})$$

This can be written as:

$$\begin{aligned} f(\mathbf{v}) &= n \left[\left(\frac{m}{2\pi kT} \right)^{\frac{1}{2}} e^{-\frac{mv_{\parallel}^2}{2kT}} \right] \left[\left(\frac{m}{2\pi kT} \right)^{\frac{1}{2}} e^{-\frac{mv_{\perp}^2}{2kT}} \right] \\ &= n f(v_{\parallel}) f(v_{\perp}) \end{aligned}$$

With:

$$f(v_{\perp}) = \left(\frac{m}{2\pi kT} \right)^{\frac{1}{2}} e^{-\frac{mv_{\perp}^2}{2kT}} \quad (\text{F.3})$$

$$f(v_{\parallel}) = \left(\frac{m}{2\pi kT} \right)^{\frac{1}{2}} e^{-\frac{mv_{\parallel}^2}{2kT}} \quad (\text{F.4})$$

where $f(v_{\parallel})$ is the injected ions velocity distribution function parallel to the geomagnetic field lines and $f(v_{\perp})$ is the injected ions velocity distribution function perpendicular to the geomagnetic field lines. Using these distribution functions, parallel and perpendicular velocities to the geomagnetic field lines (i.e. $v_{\parallel s}$ and $v_{\perp s}$) of the injected ions can be generating.

F.2 Generation of $v_{\perp s}$

By using the probability density, we want to get the values for random variable of ions perpendicular velocity ($v_{\perp s}$) at the starting point (injection point) which is distributed over the interval $(0, \infty)$, [Aldrich, 1985], with probability density equal to one, which given by:

$$p(v_{\perp s}) = 2\pi v_{\perp s} f(v_{\perp s}) \quad (\text{F.5})$$

By taking the total probability from 0 to $v_{\perp s}$, that equal to a random number (G) which has values between (0,1) as in equation (F.6), which obtained by the substitute $f(v_{\perp})$ from equation (F.3) into equation (F.5) to obtain:

$$\int_0^{v_{\perp s}} P(v'_{\perp s}) dv'_{\perp s} = G \quad (F.6)$$

The value of ions perpendicular velocity ($v_{\perp s}$) can be obtained by solving equation (F.6), which is equal to:

$$v_{\perp s}^2 = -\left(\frac{2kT_s}{m_s}\right) \ln(1-G) \quad (F.7)$$

Therefore, the ion is injected or initiated with a random ions perpendicular velocity ($v_{\perp s}$) at the starting point or the exobase.

F.3 Generation of $v_{\parallel s}$

At this stage, we must differentiate between the local number of ions with $v_{\parallel s}$ and the actual number of those ions which can cross the lower boundary of the simulation region, which in the polar wind region is a geomagnetic tube extending from $r = 1.7R_E$ to $r = 13.7R_E$, (i.e. those ions with $v_{\parallel s} < 0$ will not cross the assumed injected boundary). The probability of finding an ion pass through the lower boundary (injection point) is proportional to the flux of those ions (i.e. the probability of those ions with $v_{\parallel s} > 0$, were they can reach and cross the lower boundary), which is given by:

$$p(v_{\parallel s}) = p(v_{\parallel s})_{local} \times v_{\parallel s} \times \alpha \quad (F.8)$$

where

$$p(v_{\parallel s})_{local} = f(v_{\parallel s}) = \left[\frac{m_s}{2\pi kT_s} \right]^{\frac{1}{2}} e^{\frac{-m_s}{2kT_s} v_{\parallel s}^2}$$

This is given from equation (F.4) and α is normalizing constant (i.e. $\int_0^{\infty} p(v_{\parallel s}) dv_{\parallel s} = 1$).

From the previous equations we obtain the formula for the probability density, which given by:

$$p(v_{\parallel s}) = 2\pi v_{\parallel s} \left[\frac{m_s}{2\pi k T_s} \right] e^{\frac{-m_s v_{\parallel s}^2}{2k T_s}} \quad (\text{F.9})$$

The value of ions parallel velocity ($v_{\parallel s}$) can be obtained by solving the above equation (i.e. equation (F.9)), same as we solved equation (F.6), which is equal to:

$$v_{\parallel s}^2 = - \left(\frac{2k T_s}{m_s} \right) \ln(1 - G) \quad (\text{F.10})$$

We must keep in mind that the formulas for ions perpendicular velocity ($v_{\perp s}$), which given in equation (F.7) and ions parallel velocity ($v_{\parallel s}$), which given in equation (F.10) are similar, but they have different numerical values owing to a random number (G) which has values between (0,1). This gives random generation of an ion from Maxwellian distribution at the boundary level.

F.4 Distribution Function

As we mentioned in the previous sections we need in the simulation process to inject 10^7 ions from the starting point ($r = 1.7R_E$). Where we deal with polar wind ions as a steady state flow of the three main component of the polar wind ions (i.e. H^+ , O^+ and electrons), these ions will be monitored until they escape from one ends of the simulation region, which is a geomagnetic tube extending from $r = 1.7R_E$ to $r = 13.7R_E$. At each altitude in the simulation region the behavior of these ions were monitored by a two dimensional grid in velocity space ($v_{\parallel s}, v_{\perp s}$), in order to compute the distribution function.

The velocities of the tested ions that they cross one of the monitoring altitude, can be used to compute the moments of the distribution function at that altitude. Also, the time that an ion spend in each bin divided by the bin's volume is taken to be proportional to the ion velocity distribution function at the center of that bin, [Barghouthi et al. 2003a].

To simplify the registration process, we use the symmetry in the azimuthal direction. Therefore, the bin's volume in velocity space can be represented as $\Delta^3 v = 2\pi v_{\perp} \Delta v_{\parallel} \Delta v_{\perp}$, and $f(v) d^3 v$ is equal to the number of test ions with velocities between v and $v + dv$.

From the above, if the width of the bin was chosen to be arbitrary constant such as c_1 , then the time needed for the ion to cross that bin is:

$$t = \frac{c_1}{|v_{\parallel s}|} \quad (\text{F.11})$$

$$\text{But } f_s(v) \propto \frac{\frac{c_1}{|v_{\parallel s}|}}{2\pi v_{\perp} \Delta v_{\parallel} \Delta v_{\perp}},$$

This can be written as

$$f_s = \frac{\frac{c_2}{|v_{\parallel s}|}}{2\pi v_{\perp} \Delta v_{\parallel} \Delta v_{\perp}} \quad (\text{F.12})$$

Let the width of the bin sides equals to $\frac{1}{3} \left(\frac{2kT_t}{m_t} \right)^{\frac{1}{2}}$ which is ($\frac{1}{3}$ of the thermal speed of the background ions).So,

$$\Delta v_{\parallel s} = \Delta v_{\perp s} = \frac{1}{3} \left(\frac{2kT_t}{m_t} \right)^{\frac{1}{2}} \quad (\text{F.13})$$

Keep in mind that the volume of the bin does not change, but these bins differ in volume, this makes that the distribution function to be written as:

$$f_s(v) = \frac{c}{|v_{\parallel}|} \quad (\text{F.14})$$

where c is constant.

At each predetermined altitude, we can determine the location of the tested ion by knowing the ion parallel velocity ($v_{\parallel s}$) and the ion perpendicular velocity ($v_{\perp s}$) of the tested ion, in order to make the registration process in the grid bins to be more easy.

The way of registration is described as the following; we use two integers such as J and I to determine the location of the ion where $J = INT(3v_{\perp s})$ and we take in consideration that ion parallel velocity ($v_{\parallel s}$) is symmetric around the ion perpendicular velocity ($v_{\perp s}$). Therefore, J takes integer from 0 to 10, the higher value for J was selected to be 10, because it corresponds to a velocity three times higher than the thermal velocity of the background ions, which is difficult for the tested ion to reach it. Therefore, we put a restriction on the values of J , such that $J = Min(J, 10)$ owing to make sure that the sorting is inside the array. On the other hand, we get the parallel direction (i.e. the value of I) by

considering the boundaries of the bins at $(-9.5, -8.5, \dots, 8.5, 9.5)$, since there is no azimuthal symmetry, where the value of I can be calculated by $I = NINT(3 \times v_{\parallel s})$, which take the values between $(-10, 10)$, after the above steps, every bin can be described by $(I, J$ and altitude). After we had determined the location of the test ions (i.e. the bin) and if the tested ion crossed through a certain bin, we can put the numerical value of $f_s(v_s)$ in that bin. after that, if another tested ion passed through the same bin we add its numerical value of $f_s(v_s)$ to the previous one. We repeat the above procedure until we finished all the ions. After we finished all the tested ions (i.e. after running the Barghouthi model), we get the numerical values for all bins. Finally, we get the graph of the distribution function of these ions at each altitude by connecting between the bins of the same numerical values of $f_s(v_s)$, [Barghouthi et al., 2003].

F.5 Moments of the distribution function

After we obtained the distribution function from the previous section, in this section we seek to obtain the moments of the ions (i.e. density n , drift velocity u , parallel temperature T_{\parallel} , and perpendicular temperature T_{\perp}).

The distribution function can be written as:

$$f(v_s) = 9c_2 \sum_i \frac{1}{|v_{\parallel s}^i|} \frac{\delta(v_{\parallel s} - v_{\parallel s}^i) \delta(v_{\perp s} - v_{\perp s}^i)}{2\pi v_{\perp s}^i} \quad (\text{F.15})$$

where $\delta(x)$ is the Dirac delta function [Barakat and Schunk 1982c], the superscript i denotes that the summation is over all continuous segments of the monitored ion trajectory in the velocity space.

We used the above distribution function to find the expression for the moments of the tested ions in the next subsections.

F.5.1. Density:

The number density n of the test ion s can be written as, [Barghouthi et al., 2003].

$$\begin{aligned}
n_s &= \int f_s(v_s) d^3v_s = 2\pi \int f_s(v_s) dv_{\parallel s} v_{\perp s} dv_{\perp s} \\
&= 9c_2 \sum_i 2\pi \int \frac{\delta(v_{\perp s} - v_{\perp s}^i) \delta(v_{\parallel s} - v_{\parallel s}^i) dv_{\parallel s} v_{\perp s} dv_{\perp s}}{2\pi |v_{\parallel s}^i| v_{\perp s}^i} \\
n_i &= 9c_2 \sum_i \frac{1}{|v_{\parallel s}^i|}
\end{aligned} \tag{F.16}$$

Therefore, after the calculating of the location of the test ion (i.e. the bin) we add the density store $\frac{1}{|v_{\parallel s}^i|}$.

F.5.2. Drift velocity:

The drift velocity u of the test ion s is equal to the expectation value of $v_{\parallel s}$ (i.e. $\langle v_{\parallel s} \rangle$):

$$\begin{aligned}
u_s &= \frac{\int v_{\parallel s} f_s(v_s) d^3v_s}{\int f_s(v_s) d^3v_s} = \frac{\int dv_{\parallel s} v_{\perp s} dv_{\perp s} 2\pi \sum_i \frac{\delta(v_{\perp s} - v_{\perp s}^i) \delta(v_{\parallel s} - v_{\parallel s}^i)}{2\pi |v_{\parallel s}^i| v_{\perp s}^i}}{\int dv_{\parallel s} v_{\perp s} dv_{\perp s} 2\pi \sum_i \frac{\delta(v_{\perp s} - v_{\perp s}^i) \delta(v_{\parallel s} - v_{\parallel s}^i)}{2\pi |v_{\parallel s}^i| v_{\perp s}^i}} \\
u_s &= \frac{\sum_i \frac{v_{\parallel s}^i}{|v_{\parallel s}^i|}}{\sum_i \frac{1}{|v_{\parallel s}^i|}} = \frac{\sum_i \text{sign}(v_{\parallel s}^i)}{\sum_i \frac{1}{|v_{\parallel s}^i|}}
\end{aligned} \tag{F.17}$$

where sign means (+) or (-).

F.5.3. Perpendicular temperature:

The random thermal velocity is defined as $\mathbf{c}_s = \mathbf{v}_s - \mathbf{u}_s$. From the expectation value of the kinetic energy ($\frac{1}{2} m c_s^2$), we can obtained the thermal energy ($\frac{3}{2} k T_s$), which is given by

$$\frac{3}{2} k T_s = \frac{\int \frac{1}{2} m_s [(v_{\parallel s} - u_s)^2 + v_{\perp s}^2] f_s(v_s) d^3v_s}{\int f_s(v_s) d^3v_s}$$

$$\frac{1}{2}kT_{\parallel s} + kT_{\perp s} = \frac{\int \frac{1}{2}m_s (v_{\parallel s} - u_s)^2 f_s(v_s) d^3 v_s}{\int f_s(v_s) d^3 v_s} + \frac{\int \frac{1}{2}m_s v_{\perp s}^2 f_s(v_s) d^3 v_s}{\int f_s(v_s) d^3 v_s} \quad (\text{F.18})$$

The perpendicular temperature is given by the expectation value of $T_{\perp s} = \frac{1}{k} \left\langle \left(\frac{1}{2} m_s v_{\perp s}^2 \right) \right\rangle$,

i.e. which is the second term of the above equation, therefore $T_{\perp s}$ can be represented by:

$$T_{\perp s} = \frac{m_s}{2k} \frac{\sum_i (v_{\perp s}^i)^2 / |v_{\parallel s}^i|}{\sum_i \frac{1}{|v_{\parallel s}^i|}} \quad (\text{F.19})$$

F.5.4. Parallel temperature:

From equation (F.18), the parallel temperature is defined as:

$$T_{\parallel s} = \frac{\frac{m_s}{k} \int (v_{\parallel s} - u_s)^2 f_s(v_s) d^3 v_s}{\int f_s(v_s) d^3 v_s}$$

$$T_{\parallel s} = \frac{\frac{m_s}{k} \left[\int v_{\parallel s}^2 f_s(v_s) d^3 v_s - 2u_s \int v_{\parallel s} f_s(v_s) d^3 v_s + u_s^2 \right]}{\int f_s(v_s) d^3 v_s}$$

and so, it is can be written as:

$$T_{\parallel s} = \frac{m_s}{k} \left[\frac{\sum_i (v_{\parallel s}^i)^2 / |v_{\parallel s}^i|}{\sum_i \frac{1}{|v_{\parallel s}^i|}} - \left(\frac{\sum_i \text{sign}(v_{\parallel s}^i)}{\sum_i \frac{1}{|v_{\parallel s}^i|}} \right)^2 \right] \quad (\text{F.20})$$

where sign means (+) or (-).

Therefore, we found the solution of Boltzmann's equation i.e. the distribution function $f_s(v_s)$ and the moments of the distribution function by using the Monte Carlo Simulation.

دراسة مقارنة بين المشاهدات العملية والنتائج الحاسوبية لنموذج البرغوثي المستخدم في تفسير كيفية هروب ايونات الاكسجين وايونات الهيدروجين من ارتفاعات منخفضة الى ارتفاعات عالية في منطقتي القطب الشمالي والقطب الجنوبي للارض.

اعداد: شريف حسن محمود غيطان

اشراف: أ. عماد احمد البرغوثي

ملخص:

تسمى عملية هروب بلازما الرياح القطبية من طبقة الايونسفير الى طبقة المغنتوسفير في منطقة دوائر العرض العليا مع خطوط المجال المغناطيسي الارضي شبه المفتوحة بالرياح القطبية (Polar Wind)، والتي تشكل عنصرا مهما في الربط ما بين طبقتي الايونسفير والمغنتوسفير.

إن عملية تسخين ايونات الهيدروجين (H^+) وايونات الأكسجين (O^+) ناتجة عن تفاعل هذه الايونات مع الاضطراب الكهرومغناطيسي (Wave Particle Interaction)، والتي لها تأثير مباشر على انتشار البلازما في منطقة الرياح القطبية، لقد تم دراسة اثر تفاعل ايونات الهيدروجين (H^+) وايونات الأكسجين (O^+) مع الامواج الكهرومغناطيسية باستخدام طريقة محاكاة مونت كارلو. لقد احتوى النموذج الحاسوبي (Monte Carlo Simulation) على تأثير تسارع الجاذبية الارضية، المجال الكهربائي المستقطب، وانحدار المجال المغناطيسي الارضي، بالإضافة الى تأثير تفاعل الموجة والايون (WPI)، ضمن منطقة المحاكاة والتي تقع (1.7-13.7) أضعاف نصف قطر الارض).

من خلال هذه الدراسة، تبين أن النسبة ($T_{\perp} / T_{\parallel}$) لايونات الهيدروجين (H^+) تقل تدريجيا عند الارتفاعات المنخفضة وهي اقل من واحد، ولكن هذه النسبة تنعكس اذ تصبح ($T_{\perp}(H^+) > T_{\parallel}(H^+)$) عند الارتفاعات العالية، وذلك نتيجة التسخين بالاتجاه المتعامد مع خطوط المجال المغناطيسي الأرضي (WPI). اما بالنسبة لايونات الاكسجين (O^+) فان النسبة ($T_{\perp} / T_{\parallel}$) تزيد تدريجيا مع الارتفاع عند الارتفاعات المنخفضة، ولكنها عند الارتفاعات العالية تصبح ثابتة تقريبا وقيمتها المتوسطة حوالي 53، اذ ان ($T_{\perp}(O^+) > T_{\parallel}(O^+)$) عند كل الارتفاعات ويتبع ذلك

أن التوزيع لايونات الأكسجين (O^+) وايونات الهيدروجين (H^+) في فضاء السرعة يأخذ شكلا مخروطيا.

كما تبين انه نتيجة للتسخين العمودي لايونات الهيدروجين (H^+) وايونات الأكسجين (O^+) الناتج عن تفاعل هذه الايونات مع الاضطراب الكهرومغناطيسي، فان الايونات تكسب طاقة وتهرب الى ارتفاعات عالية وباستخدام اثر تفاعل الموجات الكهرومغناطيسية المعتمدة على سرعة الايونات فان قوى التسخين تصبح محدودة ذاتيا (self-limiting heating)، وبالتالي يظهر الشكل الحلقي لتوزيع الايونات في فضاء السرعة. يظهر الشكل الحلقي لايونات الأكسجين (O^+) عند ارتفاعات اقل من تلك التي يظهر عندها لايونات الهيدروجين (H^+)، وذلك لان تأثير التفاعل بين الأمواج الكهرومغناطيسية وايونات الأكسجين له اثر أكبر مما هو عليه بالنسبة لايونات الهيدروجين، حيث تكون عملية التسخين لايونات الأكسجين أكثر فاعلية منها في حالة ايونات الهيدروجين.

ان اهم نتيجة تم الحصول عليها من هذه الدراسة، هو ان طول موجة الاضطراب الكهرومغناطيسي تساوي 8 كم ($\lambda_{\perp} = 8km$)، وذلك لان النتائج الحاسوبية التي تم الحصول عليها من نموذج البرغوثي تتوافق بشكل كبير مع المشاهدات التي تم الحصول عليها من الاقمار الاصطناعية.

اخيرا، نستطيع القول ان نموذج البرغوثي يعد انسب نموذج لدراسة تفاعل ايونات الهيدروجين (H^+) وايونات الأكسجين (O^+) مع الاضطراب الكهرومغناطيسي في منطقة الرياح القطبية، وذلك بسبب التقارب الكبير بين النتائج الحاسوبية التي تم الحصول عليها من نموذج البرغوثي مع المشاهدات.